T.R.
ERCIYES UNIVERSITY
GRADUATE SCHOOL OF NATURAL AND APPLIED SCIENCE
MECHANICAL ENGINEERING DEPARTMENT

BALLISTIC IMPACT BEHAVIOUR OF THICK AND THIN COMPOSITES

Prepared by
DAWOOD SALEEM HUWIASH AL BEHADILI

Supervisor
Prof. Dr. Recep GÜNEŞ

M. Sc. Thesis

December 2017
KAYSERI

T. R.
ERCIYES UNIVERSITY
GRADUATE SCHOOL OF NATURAL AND APPLIED SCIENCE
MECHANICAL ENGINEERING DEPARTMENT

BALLISTIC IMPACT BEHAVIOUR OF THICK AND THIN COMPOSITES

(M. Sc. Thesis)

Prepared by
DAWOOD SALEEM HUWIASH AL BEHADILI

Supervisor
Prof. Dr. Recep GÜNEŞ

This study was supported by the Scientific Research Projects Unit of Erciyes University (ERU/BAP) under the research Grant No. FYL-2017-7738

December 2017
KAYSERI

COMPLIANCE WITH SCIENTIFIC ETHICS

I hereby declare that all information in this document has been obtained and presented in accordance with academic rules and ethics conduct. I also declare that, as required by these rules and conduct, I have fully cited and referenced all material and results that are not original to this work.

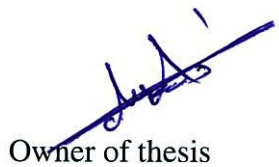

Owner of thesis

DAWOOD SALEEM HUWAISH AL-BEHADILI

COMPLIANCE WITH GUIDELINES

The M.Sc. thesis entitled **"Ballistic Impact Behaviour of Thick and Thin Composites."** has been prepared in accordance with Erciyes University Graduate Education and Teaching Institute Thesis Preparation and Writing Guide.

Owner of thesis

DAWOOD SALEEM HUWAISH AL-BEHADILI

Supervisor

Prof. Dr. Recep GÜNEŞ

Head of Department

Prof. Dr. Necdet ALTUNTOP

ACCEPTANCE AND APPROVAL PAGE

The study called **"Ballistic Impact Behaviour of Thick and Thin Composites"** has been prepared by **DAWOOD SALEEM HUWIASH AL BEHADILI** supervised by **Prof. Dr. Recep GÜNEŞ,** is accepted as a M.Sc. Thesis in Erciyes University Graduate School of Natural and Applied Science Department of Mechanical Engineering by the jury.

……/……/……

JURY:

Head of the Jury	: Prof Dr. Recep GÜNEŞ	……
Juror	: Assoc. Prof. Dr. Ahmet ERKLİĞ	……
Juror	: Assoc. Prof. Dr. Recep EKİCİ	……

APPROVAL:

That the acceptance of this thesis has been approved by the Institute Board with the decision number 02/01/2018.. and the date of ..2018/..01–24

02../01../2018

Director of the Institute
Prof. Dr. Mehmet AKKURT

ACKNOWLEDGMENTS

In the name Allah, the most Merciful and Beneficent. I am grateful to my Lord who has given me strength and wisdom to complete this thesis.

I want to express my deep gratitude to my supervisors Prof. Dr. Recep GÜNEŞ for his ongoing guidance, helping, encouragement, patience, and valuable advices throughout my study.

I would also like to express deep gratitude to every member of my committee, Assoc Prof. Dr. Recep EKİCİ and Assoc. Prof. Dr. Ahmet ERKLİĞ, for their invaluable service.

Thanks are also due to Dr. Murat Aydan, Umut ÇALIŞKAN, Assoc. Prof. Dr. Fehmi NAIR, and Mevlüt HAKAN.

Special thanks as well to the Republic of Turkey and the academic staff in Erciyes University especially the Scientific Research Projects Coordination Unit (BAPSIS).

There are no words which can express my thanks and appreciation to my all family who continues to support, pray, and have patience until I reached this moment.

I am also lucky to be surrounded by colleagues with high scientific and ethical values who provided their continuous support and friendship. I am also grateful to my children, wife, parents, and my entire family who supported me during my studies.

Finally, I would like to thank my sponsor, the Iraqi government and the Ministry of Higher Education, as well as my employer the Municipality of Baghdad, for supporting me giving me this opportunity to pursue my studies.

Last but not least, I dedicate this thesis, my studies, and my career to the one who gave us everything so that we can live with dignity. The one I love and the one whom Allah loves, our Prophet Muhammad (Peace Be Upon Him, His Family, Companions, and those who follow him). In conclusion, I Thank You All.

Dawood Saleem AL-BEHADILI

Kayseri, December 2017

BALLISTIC IMPACT BEHAVIOUR OF THICK AND THIN COMPOSITES

DAWOOD SALEEM HUWAISH AL-BEHADILI

Erciyes University - Graduate School of Natural and Applied Sciences
M.Sc. Thesis, December 2017
Thesis Supervisor: Prof. Dr. Recep GÜNEŞ

ABSTRACT

Composite material usage is becoming more popular in the fields such as automotive, aviation, marine, military application, transportation industry, space application, body armor, armored vehicles and essential equipment due to less weight, more resistance, and better handling fatigue than metals. Even though there are obvious benefits of composite materials, there are drawbacks as well, especially in handling impact. Researchers have tried to solve the impact damage from low velocities for some time, but high velocity impact damage is still quite new. This research compares the effect of ballistic impact on composites that are both thin and thick through the various stages of the impacts. Using experiments, high-velocity impact was tested to understand the sequence of damage. We used laminated composites (E-Glass /Epoxy) for two types of samples a thin composite plate consists of 16 unidirectional layers and a thick composite plate consists of 50 unidirectional layers at the end of the manufacturing process. The thin and thick composite plates have been produced anti-symmetric layer stacking sequenced and three different fiber orientations such as $[0^o/90^o]_A$, $[-45^o/+45^o]_A$ and $[30^o/60^o]_A$, which carried out this tests by a single stage gas gun (gas gun ballistic) system at velocity range from 447 m/s to 861 m/s. It was observed that the thin plates to be more damaged than the thick plates at the same velocity tests. Also at the first velocity all thick specimens have in case of rebounding of the bullet which causes relatively small deformations, at the second velocity all thick specimens are in case of penetration with delamination and the area surrounding the bullet damaged and a burn in the area from which the bullet ent**e**red, at the third velocity all thick specimens are in case of perforation and it is observed bullet debris except $[-45^o/+45^o]_{A25}$, is penetration case with delamination and swelling look like in the second velocity cases. And another side, all thin specimens were perforated at the velocities tests for all stacking sequences. Therefore, the experiments also showed an increase in inter-laminar shear stress (that depends on the sequence of stacking) and a decrease in the effectiveness of the laminates, with increasing bullet velocity.

Keywords: Ballistic impact, high-velocity impact, laminated composite, thin and thick composites, single-stage gas-gun, Fragment Simulating Projectiles (FSPs).

KALIN VE İNCE KOMPOZİTLERİN BALİSTİK DARBE DAVRANIŞI
DAWOOD SALEEM HUWAISH AL-BEHADILI

Erciyes Üniversitesi - Fen Bilimleri Enstitüsü
Yüksek Lisans Tez, Aralık 2017
Tez Danışmanı: Prof. Dr. Recep GÜNEŞ

ÖZET

Kompozit malzeme kullanımı, daha az ağırlık, daha fazla direnç ve daha iyi taşıma yorulması sağlaması nedeniyle özellikle otomotiv, havacılık, denizcilik, askeri uygulamar, nakliye endüstrisi, uzay uygulamaları, vücut zırhı, zırhlı araçlar ve gerekli ekipmanlar gibi alanlarda metallerden daha popüler hale gelmektedir. Kompozit malzemelerin belirgin yararları olmasına rağmen, özellikle de darbe etkilerinde dezavantajları bulunmaktadır. Araştırmacılar, düşük hızlardan gelen darbe hasarını bir süredir çözmeye çalıştı, ancak yüksek hız hasarı hala oldukça yenidir. Bu tez çalışması, darbelerin çeşitli aşamalarında balistik etkinin hem ince hem de kalın olan kompozitler üzerindeki etkisini araştırmaktadır. Deneyler kullanarak hasarın oluşumunu anlamak için yüksek hızlı darbe etkisi test edildi. İki farklı kalınlıkta üretilen E-cam/Epoksi kompozitlerden ince kompozit plakalar 16 katmanlı tek yönlü tabakadan oluşurken, kalın kompozit plakalar 50 katmanlı tek yönlü tabakadan oluşmuştur. İnce ve kalın kompozit plakalar $[0º/90º]_A$, $[-45º/+45º]_A$ ve $[30º/60º]_A$ gibi üç farklı lif oryantasyonu dizisi ile istiflenmiş antisimetrik tabakalar olarak üretilmiştir. Balistik testler 447 m/s ile 861 m/s hızlar aralığında tek aşamalı bir gaz tabancasıyla gerçekleştirilmiştir. Burada ince levhalar aynı hız testlerinde kalın plakalara göre daha fazla hasara uğramıştır. Ayrıca birinci hızda yapılan testlerde tüm kalın numunelerde mermi geri teperken, nispeten küçük deformasyonlar gözlenmiştir. İkinci hızlarda tüm kalın numunelerde delaminasyon hasarı gözlenirken mermiyi çevreleyen alanın zarar gördüğü tespit edilmiştir. Üçüncü hızlarda, $[-45º/+45º]_{A25}$ istiflemeye sahip plakalar haricinde, tüm kalın numunelerde delinme izlenmiştir. İkinci hızlarda numunelerde delaminasyon ve şişme deformasyonları gözlenmiştir. Diğer taraftan, tüm ince numuneler ile yapılan testlerde delinme meydana gelmiştir. Bu nedenle deneyler, mermi hızının artmasıyla, tabakalar arası kayma gerilmesinin arttığını ve katmanların etkinliğinde bir azalma olduğunu göstermiştir.

Anahtar Kelimeler: Balistik darbe, yüksek hızlı darbe, katmanlı kompozit, ince ve kalın kompozitler, tek-kademeli gaz-silahı, parçacık simülasyon mermileri.

CONTENTS

BALLISTIC IMPACT BEHAVIOUR OF THICK AND THIN COMPOSITES

CHAPTER TWO

MATERIALS AND METHODS

CHAPTER THREE

EXPERIMENTAL RESULTS AND DISCUSSIONS

CHAPTER FOUR

CONCLUSIONS AND FUTURE WORKS

LIST OF ABBREVIATION

$\overline{Q_{ij}}$	matrix denotes transformed reduced stiffness, Q_{ij}
$\eta_{i,ij}$	coefficient of mutual influence of the first kind that characterizes stretching in the i – direction
$\eta_{ij,i}$	coefficient of mutual influence of the second kind that characterizing shearing in the ij – plane.
E_K	Kintic Energy of projecile
E_T	The total energy
E_{abs}	Energy absorption of the laminate
E_{rot}	rotation Enegy of projecile
V_{imp}	The collision velocity (the impact velocity)
V_{res}	The residual velocity
v_i	Striking velocity
v_r	residual velocity
ε_1	applies for both fibers and matrix ,
σ_f	acts on the cross-section area of the fibers A_f , and
σ_m	acts on the cross-section area of the matrix A_m
A_{df} , A_{db},	the damage area on the front face and back face
E_1	The first modulus of the composite material in the 1-direction, in the fiber direction
E_2	The apparent young's modulus to both the fiber and the matrix
FSP	Fragment Simulated Projectile
G_{12}	The shear modulus of a lamina
MIL	military specification
ν	Poisson's ratio
V_1	The first velocity
V_2	The second velocity

$\mathbf{V_3}$	The third velocity
VARI	Vacuum Assisted Resin Injection
$\mathbf{V_{BL}}$,$\mathbf{V_{50}}$	The ballistic limit velocity
F	Force
m	Mass
a	Acceleration

LIST OF FIGURES

LIST OF TABLES

INTRODUCTION

I.1. Overview

A **composite material** is a material system composed of a mixture or combination of two or extra macro-constituents that differ in form and (or) material composition and are essentially insoluble in one another to achieve properties (chemical, physical, etc.) that are superior to those of the constituent's original materials. The main component of composite materials is the matrix and the reinforcement. The most common reinforcements are fibers, which provide most of the stiffness and strength. The matrix binds the fibers together providing load transfer between fibers and between the composite and the external loads and supports [1].

Aluminum, steel, and other traditional materials used by engineers can be impure and this can influence different qualities of the same material. They are considered composite by definition, but aren't true composites because the impurity found in them gives them the same qualities of the natural material. As such, one can adjust the definition of composites based on certain parameters [2].

There are four categories of composite materials according to the matrix:

Polymer matrix composites (PCM) are either thermoset or thermoplastic. The thermoset types include: polyester, polyimide, and epoxy. Thermoplastics are poly-sulfone and polyether-ether-ketone. PCMs are resins made from either type that use glass, carbon, boron, or aramid fibers to add reinforcement and are made for use in low temperatures.

Metal matrix composites (MMC) are metals or alloys that use ceramic, boron, or carbon fibers for reinforcement. Alloys used in MMCs can be copper, titanium, magnesium, or aluminum. The metal matrix can become soft or even melt, which limits the maximum usable MMC temperature. They were made primarily to make metallic

components more efficient and have the same benefits such as use in high temperatures, strong shear strength, and high chemical inertness.

Ceramic matrix composites (CMC) are used in high temperature situations. They are made with ceramic matrices and fibers. The matrices can be silicon nitride, glass-ceramic, aluminum oxide, or silicon carbide.

Carbon/carbon composites (CCC) can used at high temperatures and have minimal density and thermal expansion. They are made from carbon or granite matrices with fabric or yarn for support [3-4].

The categories of composite materials according to reinforce composite, Mentioned in the following points:

A. Unidirectional Fiber-Reinforced Composites

The unidirectional fiber-reinforced composite is a two-phase material. It has parallel agreement between the fibers and filaments, both of which are aligned randomly opposite of the fiber axis plane. Fibers can be continuous or not; straight or woven.

Whiskers and fibers are different. What defines a fiber is the geometry: a high ratio or length to diameter, with the diameter being almost crystalline. On the other hand, whiskers have the same style diameter, but they are short with a much lower ratio of length to diameter.

Hooke's law defines the equation related to these composites, where the coefficients of the materials are functions of the material and parameters of the basic components [5-6].

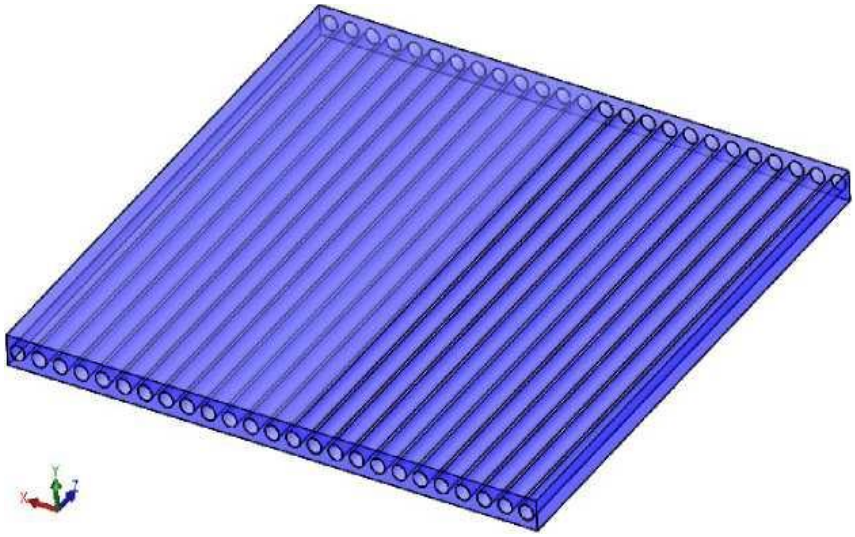

Figure I.1. A lamina with longitudinal fibers [2].

B. Laminated Composites Consisting of Unidirectional Composites

Laminated composites are formed when unidirectional layers that have the same properties are bonded together. Cross-ply refers to adjacent layers being orthogonal. Angle-ply means they are symmetric compared to an axis.

The governing constitutive equation is the relation between the in-plane stress and moment and the in-plane strain and curvature. The material coefficients of this equation are expressed as functions of the properties of the unidirectional composite and lamination parameters [5-6].

The composite material is treated as a heterogeneous anisotropic continuum. Therefore, the structural behavior of the composite material is described by the mechanical constitutive equation of the composite. The material coefficients of this equation describe the extent of mechanical response of the composite under the impact of external loads [5-6].

Structural composites can be classified basically into two classes: multiphase and laminated. These are discussed in the following paragraphs.

1. Multiphase Composites

The multiphase composite consists of two or more constituent phases, although most available composites contain only two phases. Examples of two- phase composites include cement aggregate, tungsten carbide in cobalt, alumina whiskers in metal, silica fiber phenolic, Teflon fiber in plastics, and glass - reinforced plastics. As a mathematical approximation, two-phase materials can be represented by a quasi-homogeneous continuum, i.e. locally heterogeneous but grossly homogeneous. Of the two phases, the stronger, or reinforcing phase, can be approximated as spherical or cylindrical inclusions dispersed in the matrix phase. For example, the aggregates can be regarded as spherical inclusions; the whiskers, fibers, and filaments as cylindrical inclusions. The type of symmetry of a grossly anisotropic composite depends on the packing arrangement of the inclusions, e.g., tetragonal or orthotropic symmetry for square packing and transversely isotropic for hexagonal packing [5].

2. Laminated Composites

The laminated composite consists of many layers of multiphase or homogeneous materials bonded together. Examples of laminated composites include plywood, sandwich construction, and reinforced plastics. As a mathematical approximation, laminated composites can be represented by an in-plane homogeneous and transversely heterogeneous continuum. The transverse heterogeneity has a step-wise variation in material properties between layers (composite layers are bonded together two or more) as shown in Figure I.2. Lamination achieves the mechanical properties in the composite. Mechanical properties can be changed with the fibers angle in laminate [5].

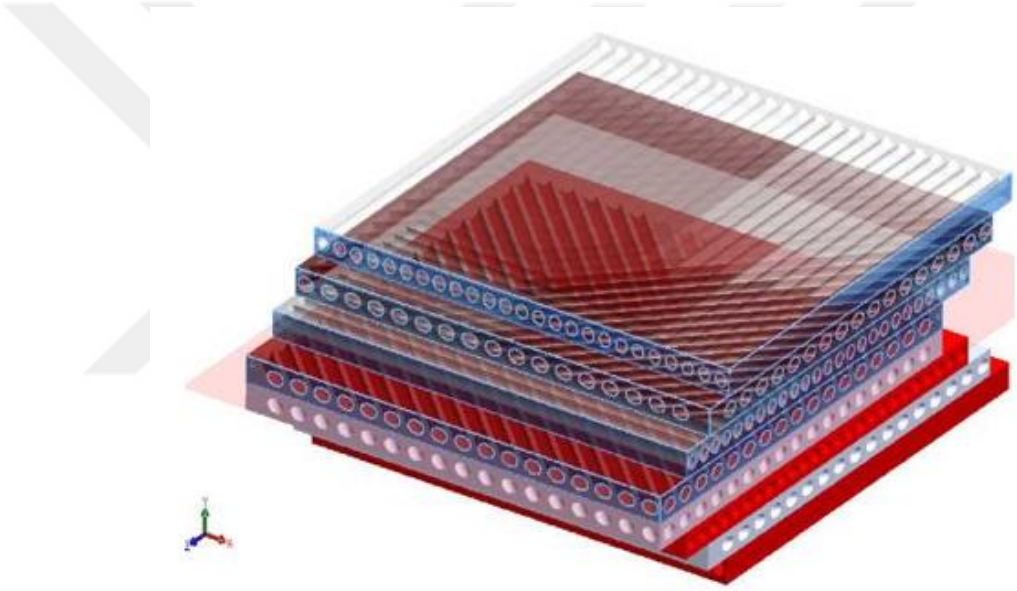

Figure I.2. A laminated composite with the fiber angle of $[90^{\circ}/+45^{\circ}/0^{\circ}/-45^{\circ}]_s$ [2]

Fiber Types

Many types of fibers are used to reinforce structures. They are distinguished by length (short, long, continuous), strength (low, medium, high, ultra-high), or chemical composition (organic, inorganic). The most used inorganic fibers used in composites are carbon, mineral, glass, boron, ceramic, and metallic. Polymeric fibers are used for organic fibers. Choosing a fiber type involves a trade off among mechanical and environmental properties and cost.

there are many types of fibers such as Silica and Quartz Fibers, Carbon Fibers, Carbon Nanotubes, Organic Fibers, Boron Fibers, Ceramic Fibers, Basalt Fibers, Metallic Fibers, and Glass Fibers [7].

Glass fibers

Glass fibers are processed from bulk glass an amorphous material fabricated from a mixture of sand, limestone, and other oxidic compounds. One can yield many different glass fibers (used for different purposes) by controlling the chemical composition and manufacturing process. Regardless, these fibers will still have normal glass characteristics, including inertness, hardness, and resistance to corrosion. These properties make glass fibers the most common kind of fiber utilized in low-cost industrial applications. The high strength of glass fibers is attributed to the low number and size of defects on the surface of the fiber. All glass fibers have similar stiffness but different strength values and different resistance to environmental degradation. The reduction of fiber strength in the composite with respect to the strength of the virgin reinforcement is also caused by residual stresses and secondary loads (shear and transverse to fiber direction), among other factors. The tensile strength of glass fibers decreases at elevated temperature, with S- and R-glass having better strength retention at elevated temperatures. The operating temperature limitations of polymer matrix composites is controlled by the matrix, which can resist up to 275°C depending on the matrix type, and to a lesser extent by the reduction in strength fibers at high temperatures. Fiber tensile strength also decreases with chemical corrosion, since glass fibers are susceptible to chemicals such as alkalis, while humidity enables those chemicals to reach the surface of the fiber. Chemical corrosion and dissolution influence the growth and propagation of surface micro cracks that are inherent to glass fibers. Also, tensile strength reduces with time under sustained loads. This effect is called static fatigue or stress corrosion. Mainly to account for this effect, a stress ratio (similar to a safety factor) of 3.5 is used in the design of glass reinforced composites for pressure vessels subject to permanent load [7].

Epoxy

Epoxy is a general term that refers to a wide assortment of polymers built with molecules from epoxide groups. Epoxide groups are oxirane structures (three atom rings).

Epoxies are found in resins for prepregs and structural adhesives. They make great adhesives, are resistant to chemicals, don't shrink much, are quite strong, and are easy to make. They are also cheaper than polymers. Pultrusion, filament winding, press molding, autoclave molding, and vacuum bag molding are all methods to produce them. Although the most frequent temperatures used for curing are from 120 to 180°C, the curing can begin even at room temperature. The curing process will determine how the materials can be used. Curing at higher temperatures will make the material more resistant to higher temperatures [8].

I.2. Scope of Study and Motivation

The use of composite materials ranges from the transportation, automobiles, marine, and aerospace sectors. Because these materials are easier to maintain, costs are lessened, Also, they have good ratios of strength to weight and resistance to corrosion. Because of these advantages, militaries have taken an interest in composite materials for ships, submarines, and even land vehicles. Because of the potential use in combat, it is imperative that composite materials can handle the impact of missiles and other ballistic events. As it is stands, researchers understand the response of these materials at static, quasi-static loading rates and ballistic impact. However, we must delve deeper into understanding the response at the high strain rates from shock and ballistic events [9].

I.3. Aim of thesis (Objective)

The purpose of this study is to experimentally investigate the behavior laminates composite (E-Glass /Epoxy) for two types of samples a thin composite plate consists of 16 unidirectional layers and a thick composite plate consists of 50 unidirectional layers at the end of the manufacturing process, the final thickness of the composite plate will be measured. The thin and thick composite plates will be produced antisymmetric layer stacking sequenced and three different fiber orientations such as 0/90, -45/+45 and 30/60. Impact tests will be carried out in the mechanic's Laboratory of Erciyes University by using single-stage gas gun system at velocity range from 447 m/s to 861 m/s.

I.4. Outline of thesis

This thesis consists of four parts in the general frame in addition, an introduction. General information about composite materials is given in introduction chapter, In Chapter one, general information about impact loading and others topic in this thesis, literature research. laminate behavior theory, the tools and methods used in the work done in Chapter two have explained. In chapter three are the results discussed and the conclusion and recommendations in chapter four are given.

CHAPTER ONE

GENERAL INFORMATION

1.1. Introduction

Impact is a very wide research area. Various industries are involved such as the automotive, aviation and military industry. In general, the possibility of impact on a structure, system or component requires additional specifications for a product on top of the conventional ones. Vehicles of automotive are nowadays designed to guarantee good crashworthiness capabilities for passengers. Aircrafts are not supposed to crash because of the consequences of a bird impact. In military service, helicopters, vehicles and personal armor (for instance, helmets and bullet-proof vests) are exposed to several types of ammunition, causing typical high velocity impact problems. Impact problems in the automotive and aviation industry as mentioned above are low velocity impact problems. All these impact problems have one aspect in common, viz. protected structures should be as light as possible to avoid loss of mobility. For this reason, impact resistance of materials is always defined by comparing achieved protection versus structural weight [10-11].

Impact behavior of materials is mainly categorized by the low and high velocity impact regime. These regimes are characterized by either the projectile velocity (kinetic energy) or the duration of the impact event. In the low velocity regime less than 10 m/s the whole impacted structure experiences the impact. Kinetic energy of the projectile is mainly absorbed by elastic deformation of the target. Boundary conditions and geometry of the target have a significant influence on the, more or less, quasi-static behavior of the target. At high velocity impact more than 300 m/s, due to the much shorter duration of the event, only material in the vicinity of the projectile experiences deformation. Inertial effects and wave propagation phenomena control the transient dynamic behavior of the target. Geometry and boundary conditions are less important as

long as the generated longitudinal strain waves are not reflected from the edges of the target. Kinetic energy of the projectile is absorbed by the local deformation and destruction of the target material, deformation of the projectile and local acceleration of the target. No clear boundary between both velocity regimes exists, since there is a transition which is target material dependent [12-14]. There is another important difference between the impact regimes. In many low velocity impact problems structures should still be capable of bearing stresses after impact, i.e. bird-impact of an aircraft. Whereas, at high velocity impact, a structural element gives a requested protection level and is replaced after impact, because of irreversible damage, i.e. ballistic impact of armored car door. Traditionally steel armor is widely used for high velocity impact problems. However, in recent years, steel armor has been successfully replaced by composites to achieve weight advantages. Energy dissipation mechanisms are quite different for various materials [15-17].

Composite materials are suitable for use in problems involving high velocity impact because they combine lightness with high mechanical strength. However, impact of composite materials is a very complex process. The impact resistance of a composite depends on several aspects such as: fiber properties (elastic moduli, failure strain and viscoelastic properties), fiber architecture (unidirectional lamina, woven fabrics), matrix properties, composite areal density etc. Many failure phenomena occur during impact such as: fiber and matrix breakage, delamination and fiber pull-out. These failure processes interact very strong and are strain rate dependent, which makes it difficult to determine which mechanism is predominant. At high loading frequencies or impact rates, material properties are different from those observed at normal loading conditions as a result of viscoelastic properties. As a consequence of this the amount of energy absorbed by these separate failure mechanisms depends on the velocity of the projectile. Furthermore, many of these failure processes are strongly dependent on environmental effects such as temperature and moisture. Therefore, fiber, matrix and interface properties are still optimized by trial and error using ballistic experiments [18-19].

1.2. Classification of Impacts

There are quite a number of reasons to use composite materials. The most common of which is when impact damage is to be expected, such as from gunfire. This research will cover the best impact measuring methodology, as well as how to understand where and when impact damage will occur.

Impact testing fits into two main parts: **(a)** low-velocity impact, and **(b)** high-velocity impact. These two main categories lead to three main types of impact testing. Charpy impact testing and drop weight impact testing fall into the category of low-velocity impact testing. Ballistics impact testing falls into the category of high-velocity impact testing. Technology has increased to the point that there are now advanced measuring devices for instrumented impact testing such as single-stage gas-gun system for measure ballistic impact tests [20].

1.2.1. Ballistics Impact Testing

Ballistic impact is a excessive velocity influence by a small mass object, analogous to runway debris or small arms fire. The simulation of ballistic impacts can be achieved with a light-gas gun or other ballistic launcher. It is important to study the reaction of materials to ballistic impact loads. Protection against high-velocity impact from objects such as projectiles is of main concern for both military and civilian purposes. Lightweight body armour systems for ballistic protection of personnel can be designed by combining dissimilar materials with diverse properties. Applications in research include body armor, armored vehicles and fortified buildings, as well as the protection of essential equipment, such as the jet engines of an airliner.

Forces of inertia have a strong effect on the high-velocity impact, as do changes in strength, variations of stiffness, and wave production. All of these are caused by high strain. Quite a number of parameters affect fiber composite response time under the high-velocity impact, such as: mass, projective geometry, type, thickness, and more. Composites of woven fabric are tougher at handling this impact [21].

Test Setup and Procedure

Ballistics testing is very complex, which means the setup is crucial. The figure below shows a typical arrangement:

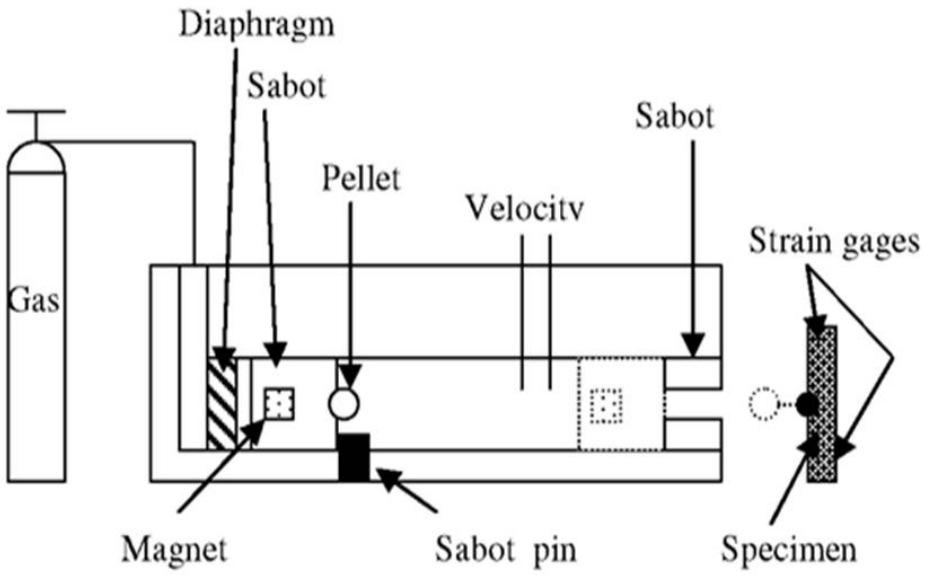

Figure 1.1. Apparatus for ballistic impact testing [20].

The Figure 1.1 shows a test apparatus called the gas-gun impact test machine. It operates with gas being forced into the diaphragm's back end that causes expansion and pressure sent to the sabot. At this, the pin of the sabot is released and the sabot itself is forced through the barrel. The pins here measure how long it takes for the sabot to move between them, and they output velocity. The sabot is prevented from further movement by the stops, and the pellet (usually steel or zirconia) then moves to cause an impact. Strain gages measure the strain this process causes. [21].

Table 1.1 displays an important database regarding the different velocity regimes and their corresponding application and test method [21].

Table 1.1. Provides the different velocity regimes [21].

Velocity regime	Impact test equipment	Material test method	Typical applications
Low velocity 0-50 m/s	-Drop hammer -Pneumatic accelerator	Quasi-static testing machines: - -Hydraulic -Servo-hydraulic -Screw-driven	-Dropped objects -Vehicle impact/ ship collision -Crash-worthiness of -Containers for hazardous materials
Sub-ordnance 50-500 m/s	-Compressed air gun -Gas gun	-Pneumatic -Hydraulic -Taylor impact tests -Split Hopkinson: - Pressure bar (SHPB) or Tension bar (SHTB)	-Design of nuclear containment -Free-falling bombs & missiles Fragments due to accidental explosions
Ordnance 500-1300 m/s	Compressed air gun gas gun	Taylor tests SHPB SHTB	Military
Ultra-ordnance 1300-3000 m/s	-Powder gun - Two-stage light gas gun	Taylor impact test	Military
Hypervelocity >3000 m/s	Two-stage light gas gun	Taylor impact test	-Space vessels - Exposed to meteoroid impact & space debris

1.2.2. Failure Modes

The fiber, interphase, and matrix properties will impact the threshold energies or necessary stresses that are needed to cause failure from impact. Different impacts are classified according to the level of damage. High velocity impacts will cause penetration that breaks the fibers. Low velocity impacts will crack the matrix and produce delamination.

There are different ways that projectiles will impact the target. The various ways to absorb energy are:

- Kinetic energy absorbed by the moving cone formed on the back face of the target.
- Shear plugging of the projectile into the target.
- Energy absorbed due to the tensile failure of the primary yarns.
- Energy absorbed due to elastic-deformation of the secondary yarns.

- Energy absorbed due to delamination, matrix cracking, and frictional energy absorbed during penetration.

Perforation may occur is there is failure in various modes. The target's modes are different depending on the properties of the materials used, the velocity of impact, the shape of the projectile and target, support, masses, and more. This is shown in Figure 1.2 [21].

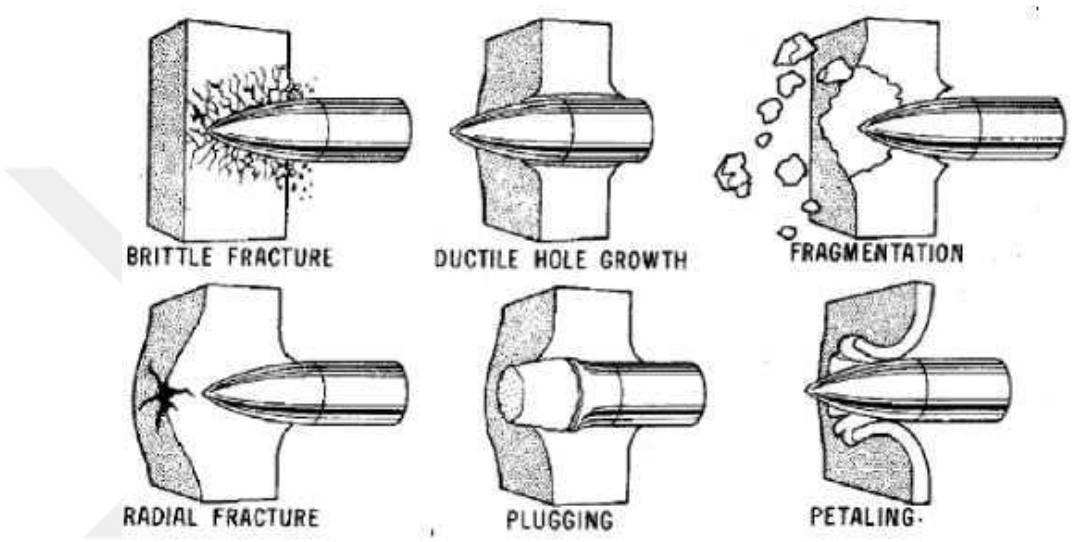

Figure 1.2. Common failure modes of target [21].

1.2.3. Acceleration Devices of Projectile

For speeds in excess of 330 m/s, projectiles are sent through a device with a cylinder that has a diameter slightly larger than its own diameter, using some sort of propellant.

Gas guns can fire projectiles because of a pressurized chamber with a plastic diaphragm that limits the flow of gas into the barrel. After reaching a specific pressure, the projectile accelerates through the barrel when the diaphragm bursts from heat. These guns are used to test high velocity impact from speeds between 75 and 270 m/s. That said, using complex systems, speeds up to 800 m/s are possible. For speeds of 350 m/s, a burning powder gun is often used. In these guns, the bullets are shot out because of a reaction of explosive powder within the barrel. The highest velocity that can be tested is 3000 m/s [22].

1.2.4. Types of Projectiles

Results of testing will vary based on the type of projectiles used. The most common projectiles in these tests are spheres or cylinders made from steel. Common ammunition is also used, as are projectiles fragmented for testing purposes.

The spheres and cylinders of steel are used for testing gas guns because they are easily bought or made to fit the test barrel dimensions. They also showcase similar results in the low velocity testing, which makes their usage perfect for comparing and contrasting results. However, they are often a poor representation of the projectiles one may face in the field, such as those from enemy fire.

FSPs, or fragmented simulated projectiles, were designed by the American Army for the purpose of representing projectiles one may encounter in combat. They are cylindrical and made in accordance to a specific military condition (MIL-P-46593A). They also feature a blunt nose shaped as a chisel and a base with a raised flange. Figure 1.3 shows their design. Projectiles similar to FSPs are shot from a powder burning gun. As such, various militaries use FSPs for their testing of armor [22].

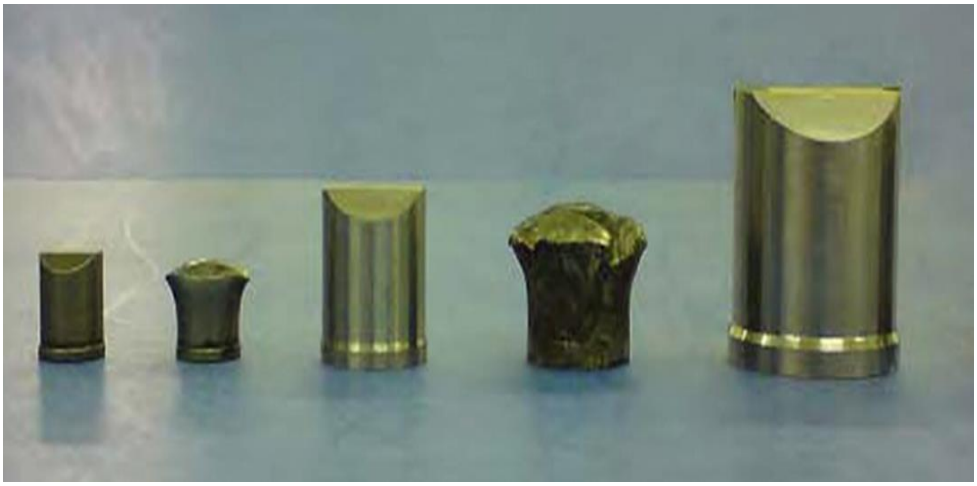

Figure 1.3. FSPs (Fragment Simulating Projectiles) [22].

Common ammunition is useful in ballistic velocity testing and are fired from a burning powder gun. They are cheap and easily purchased from any weapon shop. They are also useful because testing is based around common weapon fire. However, because of the lead used to make ammo, the bullets can become deformed or break, which raises a disadvantage in testing [22].

1.3. Literature Review

The issue of damage in composites because of an effect is a serious issue for researchers and has been for quite some time. Composite parts can be damaged in several ways during use when they are impacted by an outside object. There are two types of damage: low and high velocity effect damage.

Although the effect of low velocity damage has had vast research dedicated to it, high velocity has been neglected by researchers. This is because the problem is complicated and the information is inadequate.

Damage occurs when an object collides with the test components. In actual scenarios, it is hard to know the severity of the impact, the approach velocity, duration and rate of deformation of the velocity. This study focuses on high-velocity impact, specifically as it relates to aircraft. Aircraft vehicles can have such an impact in numerous ways, such as a bird colliding with the vehicle or a truck crashing into an engine on the runway. There is also much debris in space that can negatively impact spacecraft and satellites. NASA is focused on this issue, as debris can cause serious damage to extremely fast-moving vehicles.

As such, engineers must consider every possibility and plan against failures due to collision. Repair engineers must also develop schemes to quickly handle serious damage in such situations, such as fast repair or replacement of the damaged parts.

The below studies focus on impact damage in composite materials.

Kazemahvazi [23] investigated in the active loading of composite and sandwich structures for the laminates with a lot of fibers in the loading direction very little difference in residual net-section strength was observed between laminates with drilled circular holes and laminates with holes generated from fragment simulating projectile (FSPs) and It was found that unidirectional laminates with holes predominantly fail through three failure modes: local shear failure, local net-section failure, and global net-section failure. Also, it was found that cores with low relative density (slender core members) show very large inertial stabilization effects and have a dynamic strength that can be more than seven times higher than the quasi-static strength.

Menna *et al* [24] dealt with study the numerical simulation of low-velocity impact tests through the LS-DYNA Finite Element (FE) code which was carried out on glass fabric/epoxy laminates, adopting two-panel thicknesses and various impact energies.

Tanay Topac *et al* [25] investigated in the dynamic failure process of composite laminates under low-velocity impact for Carbon Fiber Reinforced Polymer beam laminate and damage in angle 0^0, 90^0 using a united experimental and numerical approach by 3D finite element analysis is performed using ABAQUS/Explicit to simulate the experiments and Digital Image Correlation analysis.

Hassan *et al* [26] studied experimentally to investigate the behavior of woven fabric composite laminates under low-velocity impact. Simulated the impact mechanics of fiberglass/epoxy composite using MSC.MARC, MENTAT. They noticed the damage process by the F-d graph for a thicknesses range of 2, 3 and 4 mm and impact energy levels ranging from 9.8 J to 29.4 J. Variations in maximum influence force and bending stiffness were used to evaluate the damage of the glass fiber reinforced plastic laminates (GFRPs).

Guneş *et al* [27] introduced an experimental and numerical study on aluminum honeycomb sandwich structures under low-velocity impact loadings in order to investigate the behavior of honeycomb sandwich constructions, which is consisted of two identical aluminum face sheets and an aluminum honeycomb core, was carried out the experimental study by using a drop-weight impact test system. by this technique, were measured the contact forces and absorbed energies to determine the influence of impact energy for one configuration of the sandwich structure. Based on these results, was developed a numerical model by finite element method for sandwich structures.

The answer to the impact problem is approachable from three methodologies:

A. Empirically by collecting and analyzing a high quantity of data.
B. Making models that emulate real-life events.
C. Discretization that breaks down structures into the smallest parts and analyzes each based on the laws of physics.

Impact dynamics is based on the laws of mass, momentum conversion, and energy conservation. Impact on a composite plate is dissipated by either material deformation

or the making of new surfaces.

Deformation is first and can create cracks is there is enough impact energy. Then propagation occurs, which leads to the creation of new surfaces [28].

Numerous specialists and investigators have utilized software programs in order to predict the failure modes and damages, particularly in composite structures which subjected to low-speed, high-speed affect harm and quasi-static loads etc., which concentrated on the studied of experimental and numerical, for example, ABAQUS/Explicit, LS-Dyna, MSC. Dytran, DYNA3D, and 3DIMPACT [29]. Also, there are many researchers and investigators who have provided analytical studies to a number of researchers who have studied the composite materials under ballistic impact and high-speed projectiles effects such as:

Feli *et al* **[**30] investigated and developed the analytical model for perforation process of composite sandwich boards with honeycomb center subjected to high-speed effect of the barrel shaped shot. Impacts of composite skins and aluminum honeycomb center on aperture resistance and ballistic execution of sandwich boards. As indicated by the model outcomes, they got the following conclusions:

– The front and move down composite skins are the principle consider in charge of the vitality ingestion, while the vitality consumed by the honeycomb center is exceptionally lower.

– Using the Twaron filaments, rather than carbon strands AS4-6 k as a front and move down skins, case as far as possible speed of sandwich board increments by 100%.

Fras *et al* [31] researched the ballistic effect execution of 40 mm thick an Al composite AA7020-T651 against non-axisymmetric shots, 20 mm distance across piece recreating shots (FSPs) at effect speeds between 900m/s and 1500m/s, in the test conditions (thick target, penetrator of a particular shape, high-speed impacts), utilizing numerical model (MAT-107) for the Lagrangian approach and presented actualized in LS-DYNA.

Pandya *et al* [32] studied four types of symmetric hybrid composites made using plain weave E-glass fabric and 8-harness satin weave (T300) Toray carbon fabric with epoxy resin. It is watched that ballistic limit of confinement speed, V_{50} can be expanded for the composites by adding E-glass layers to T300 carbon layers contrasted and just carbon

composites for a similar overlay thickness. Putting E-glass layers in the outside and carbon layers in the inside gives higher ballistic breaking point speed than setting carbon layers in the outside and E-glass layers in the inside, where they found a decent match between the tentatively acquired ballistic cutoff speed, V_{50} and the logically created ballistic limit velocity, V_{BL}.

Buitrago *et al* [33] analyzed the puncture of composite sandwich structures subjected to high-velocity impact. Sandwich boards with carbon/epoxy skins and an aluminum honeycomb center were displayed by a three-dimensional limited component demonstrate actualized in Abaqus/Explicit. The model was approved with trial tests by looking at numerical and test remaining speed, ballistic point of confinement, and contact time. They found in the effect speeds over 250 m/s, around 45% of the effect vitality was consumed by the front skin and 40% by the back skin. For effect speeds near a ballistic utmost, the front skin consumed practically the 60% of the vitality. On the contrariwise, the honeycomb core absorbed between 10 and 20% of the impact energy by plastic strain, at all the impact velocities analyzed. Also, they studied the energy absorption mechanisms in both skins and the core.

Ivañez *et al* [34] studied response the behavior of composite sandwich plates with E-glass fiber/polyester face-sheets and foam core which subjected to high-velocity impact by performing a 3D finite-element model in Abaqus/Explicit. They found on the back face sheet, the damaged zone was greater in the sandwich model than in the spaced plates because the impact velocity over the back face sheet was lesser in the sandwich structure and the damaged zone increased when the impact velocity was reduced. Where the contribution of the foam core on the impact behavior was evaluated by the analysis of the residual velocity, ballistic limit, and damaged area.

Hazell *et al* [35] studied an experimentally on two 6-mm thick Carbon Fiber Reinforced Polymer (CFRP) laminates have been joined together to evaluate the ballistic performance of such a system when subjected to impact and penetration by fully annealed stainless steel sphere projectile (Ø11.97 mm ± 0.01 mm; mass = 7.165 g ± 0.001 g; VHN = 127 hardness). The balls (AISI 304) velocities ranging from 187 m/s to 1219 m/s. Targets were placed at normal incidence to the axis of projectile flight and angled at 45°. It was observed that the ballistic performance of the two-part system was

improved compared with similar thin CFRP laminates over the impact energy range of interest.

Hani *et al* [36] investigated the effects of different laminated hybrid composites stacking arrangement subjected to ballistic impact. The hybrid composites consist of laminated woven coir (C) and woven Kevlar (K) layers laminated together. The results obtained had with energy absorption of 435.6 kJ and 412.2 kJ under the projectile speed of between 330 m/s and 321 m/s respectively. Samples that achieved partial penetration during projectile impact where proposed the best stacking sequence is KKCC-KKCC-KKCC with the ballistic limit of 348 m/s.

Terra *et al* [37] presented an analytical formulation to model high-velocity impacts on thin woven fabric composite target. They didn't found on any dissipation of energy due to primary yarn failure for carbon/epoxy targets, as the impact duration were found to be too small in comparison with the time necessary to load the yarns until failure.

Chen *et al* [38] researched and discuss the engineering design and evaluation of 2D and 3D fabrics on the influence of construction of fabrics on ballistic performance. They found the hybrid design of ballistic panels from the used woven and uniform distribution (UD) fabrics indicated that it is possible to improve its the ballistic performance by using layer materials according to the impact mechanism.

Shanazari *et al* [39] developed a modified analytical model for hybrid woven/unidirectional panel subjected to ballistic impact.

Yen [40] developed a ply-level material constitutive model for plain weave composite laminates to enable computational analyses of progressive damage and failure in the laminates under ballistic impact conditions were added the major fiber failure modes (tensile, compressive, punch shear and crush loading) and implemented within LS-DYNA.

Feli *et al* [41] introduced a new technique of FE simulation, based on LS-Dyna FE code, for normal penetration of cylindrical projectiles onto the ceramic–composite armor with the total thickness of 40 mm targets under high-velocity impact. When the cylindrical tungsten projectile impacted the ceramic front plate a fragmented ceramic conoid breaks from ceramic tile and the semi-angle of ceramic conoid with increasing projectile, initial velocity decreases, where were the initial velocities between 470 and

500 m/s. They observed an incremental jump in the computed residual velocity of the projectile, near the ballistic limit velocity the projectile remained in the fragmented ceramic tile for more time and the dishing of composite layers' increases, also with increasing projectile initial velocity, the delamination of upper layers of composite plate decreases.

García-Castillo *et al* [42] presented a study to analyze the parameters that affect the ballistic behavior of woven laminate plates of E-glass fibers, and to determine their influence on the ballistic limit, contact time, and the energy absorption mechanisms. A formulation in non-dimensional variables of the model proposed regardless of the ratio, they found the main energy absorption mechanism was the fiber failure at velocities under the ballistic limit and the cone movement for impact velocities over the ballistic limit. They found linear relation between the ballistic limit and geometry ratio, and a power law between the ballistic limit and density ratio.

Sudhir Sastry *et al* **[**43] studied the ballistic impact on the composite materials, the CFRP, the E-glass/epoxy and the Kevlar/Epoxy for six different ply stacking sequences. They found the Kevlar/ epoxy absorbs a maximum kinetic energy of 43.8 kJ, compared to the other the two materials. The E- glass/epoxy shows better impact characteristics when stacked in the sequence [0/90/+45/-45/0/90/+45/-45]. The Kevlar/epoxy material displays better impact features when arranged with $\pm 45^0$ in the symmetrically stacked sequence of [+45/-45/+45/ -45/-45/+45/-45/+ 45].

Wang *et al* [44] used the projectiles with 7.62 mm, 12.7mm and 20.0mm calibers in the ballistic testing with relatively low and high impact velocities between 200 m/s and 1000 m/s. In order to estimate the extent of damage caused by ballistic impact on the specimens by examining ultrasonic A-scan and flash thermography non-destructive inspection techniques. FEM analysis indicated that the shear stress in the laminate away from the center of the specimen is significantly lower than at the center where used fiber-reinforced polymer composite materials.

Luan *et al* [45] introduced a transversely isotropic nonlinear viscoelastic model to estimate the mechanical behaviors of (poly-para-phenylene terepthal amide PPTA) fiber tow. The FEM (LS-DYNA) strategy presented herein, combined with the user defined material model of the PPTA fiber tows and the micro- structural model of the three-

dimensional angle-interlock woven composite 3DAWC panel, is found to make accurate predictions for the simulation of ballistic properties of 3DAWC. They found the ballistic penetration damage features of the 3DAWC panel, which reveal that the stress propagation in 3D textile structural composite can be divided into three stages:

(1) Initial impact through the projectile.

(2) Perforation after the shear wave reaching to rear surface of the target.

(3) The internal energy absorbed by wefts and warps of FEM were compared and it is found that the woven structure parameters of 3DAWF play an important role in energy absorption of ballistic penetration.

Mohan *et al* [46] developed a modified analytical model for unidirectional composites laminate which subjected to ballistic impact. They have been used the analytical formulation to determine the ballistic limit, energy absorption, and the damaged area to expected unidirectional cross-ply laminates.

Tasdemirci *et al* **[**47] investigated experimentally and numerically the effect of rubber, Teflon and aluminum foam inter-layer material on the ballistic performance of composite armor.

Chi *et al* [48] presented a semi-analytical model approach on the performance of ceramic/metal armor under ballistic impact.

Alankaya *et al* [49] studied the effects of impactor velocity to penetration mechanism, and investigated the ballistic damage of Ultra-high-molecular-weight polyethylene (Dyneema) plates under different velocities.

Omidvar *et al* [50] used the experimental method of Taguchi design in order to found a correlation between the penetrating effects with different parameters. From during the gained results show that the best property combination between penetrating impact and impact resistance have been obtained by the layering ratio of 0.6, filling materials weight percentage of 50% and thickness of 6 mm, respectively, for the composite of Kevlar 49 fibers in the epoxy matrix.

Reddy *et al* [51**]** described ballistic performance of E-glass/phenolic laminated composite having different impacts velocities by 7.62 mm mild steel core projectile. They found a nonlinear correlation between energy absorption and laminate thickness.

Long [52] investigated the ballistic impact behavior in polymer composite panels by the numerical simulation using explicit dynamic finite element analysis technique. 3D failure criteria and damage constitutive including strain rate effects were used to simulate the damage of composite laminates. The contact and penetration process, as well as damage evolution mechanisms. The results indicated that the dimension or initial velocity of the projectile, layup of laminated panel, and selective failure criterion of composite materials have significant influences on the dynamic response and failure behavior of laminated composite panel upon ballistic impact.

Zhang *et al* [53] presented the influence of fabric structure impact and thickness on the ballistic impact behavior of Ultra-high molecular weight polyethylene (UHMWPE) composite laminate (at the striking velocity of about 700 m/s), they found a bilinear relationship between specimen thickness and the ballistic limit velocity, as such unidirectional composite laminates exhibit higher ballistic impact velocity and absorbed energy capacity compared to other. Therefore, the dominant failure mechanisms of unidirectional composite laminates were identified to be plugging and hole friction for thin laminates; whereas delamination, fiber tension and bulging for thick ones.

McWilliams *et al* [54] developed a numerical modeling for elastic-plastic orthotropic material model with hydrostatic pressure dependent yield surface, which used to model the pressure dependent response for the woven fabric metal matrix composites (MMC) during impact to predict the ballistic limit and occurring during dynamic loading of woven fabric reinforced (MMC). The finite element modeling framework to offer insight into the progression of damage mechanisms through the impact event. They noticed that 3D woven MMC is 13 % and 40 % lower in terms of ballistic limit and through thickness shear strength respectively than its 2D counterpart. Moreover, the numerical results successfully predict the ballistic limit of a 2D fabric reinforced MMC within 6% of the experiment.

Aydin *et al* [55] investigated experimentally deformation and damage states of Al/SiC functionally graded sandwich plates under ballistic impact loadings and the effect of material composition variation through the thickness. The relationship between the ballistic performance and the composition variation by using a 9 mm Parabellum bullets on the functionally graded sandwich plates (FGSPs) manufactured with powder stacking hot pressing method. They found the response of the functionally graded sandwich

plates to the ballistic impact loadings as well as their damage mechanism exhibits a strong dependency on the definition of material composition variation of the core region between two upper and lower aluminum layers.

Guneş *et al* investigated damage mechanisms and deformation of honeycomb sandwich structures reinforced by the functionally graded face sheets consist of ceramic (SiC) and aluminum (Al 6061) phases under ballistic impact by finite element method using explicit dynamic analysis ANSYS LS-DYNA. In the first study [56] the effect of the material composition of functionally graded face sheets on the ballistic performance of honeycomb sandwich structures and the penetration and perforation threshold energy values on ballistic performance and ballistic limit of the sandwich structures were determined. **In the second study [57],** they investigated by numerically on honeycomb sandwich structures reinforced by FG face sheets including three types of material composition (n = 0.1, 1.0 and 10.0) under ballistic impact. They found that the projectile's initial velocity is equal to the ballistic limit when the total energy absorbed by sandwich structure is equal to the initial kinetic energy of the projectile.

Sharma *et al* [58] introduced experimental and numerical study to investigate the ballistic resistance of AA2014-T652 forged plates in the velocity region from 800 m/s to 1300 m/s against rigid and deformable projectiles (Spherical projectiles 10 mm diameter). All ballistic impact of finite element simulations of tests had carried out using the calibrated Johnson-Cook models. Ballistic impact tests on 15 mm thick target plates revealed the quasi-brittle fracture behavior of the material, which resulted in extensive fragmentation and conical crater formation on the rear side of the target. Numerical results overestimated the ballistic limit velocities as the quasi-brittle fracture of a target could not be captured using Johnson-Cook failure model.

Pach *et al* [59] presented the study about ballistic resistance of hybrid composite shields for the analysis of the damage caused by a ballistic impact, further compared to the results of computer simulations conducted using the finite element method (FEM). The (5.56 x 45) mm ammunition with the bullet of (SS109) (MESCO) type has used. They recommended in further works that the parameters of molding composites should be modified in order to improve the saturation of the weft and warp threads of the aramid fabric with the polymer.

Holmen *et al* [60] presented ballistic impact simulations with varying yield surfaces, initial velocities, and projectile nose shape, and concluded that the shape of the yield surface affects the results of ballistic impact simulations. A high-exponent yield criterion was applied in 3D nonlinear finite element simulations of ballistic impact. The effect of the yield surface shape was compared to the effects of changing the parameters controlling friction, rate sensitivity, adiabatic heating, and temperature softening. The numerical simulations were conducted to explain the yield surface shape influences the results of ballistic impact simulations of steel plates. Although the residual velocity close to the ballistic limit velocity is influenced by the yield surface indicator, the results suggest determine the ballistic limit or to predict residual velocities far from the ballistic limit, a von Mises yield surface gives enough results.

Yang *et al* [61] researched ballistic characteristics of Ultra-High Molecular Weight Polyethylene (UHMWPE) unidirectional (UD) laminate, including failure modes of UHMWPE fibers through ballistic impact and its impact on the ballistic performance of UD laminate. Finite Element (FE) results displayed when material properties degradation of Dyneema UD induced by thermal damage was taken into account, stress wave propagation and transverse deflection of Dyneema UD was highly constrained, which leads to quick perforation. Ballistic test results showed that performance of UHMWPE UD laminate was degraded during ballistic impact when Dyneema UD sheets are placed on the striking face before Twaron woven fabrics. Also investigated that the failure modes of UHMWPE fibers and its influence on ballistic performance of UHMWPE UD laminate. According to photographic examinations of post-impact Dyneema UD panels, thermal damage of Dyneema UD laminate during ballistic influence can be obviously observed from the typical globular and be melting appearance of fractured UHMWPE fibers. For back layers, tensile failure is also dominant.

There are three phases to ballistic effect events. The first is when the projectile contacts the target and its face compresses into it. During compression, the material flows into the thickness of the target. It is also possible that the material flows towards the target’s face. The compression stage proceeds until the through-the-thickness compressive wave spreads to the target’s back end. Stress from compression are made

under the region the projectile connects with and causes tension around the radial direction.

The projectile then moves further within the target due to layer compression that may cause failure at various modes. This produces a bulge at the back end and moves to impact's second phase. Failure can occur at various components of the upper layer and the projectile continues forward movement. A plug formation can occur before the projectile and tension will continue at the back of the target because of the bulge. At this stage, cracking also occurs between layers.

The third stage is when the projectile moves ahead until it and the plug exit the target at the back end. During the motion, forces of friction occur between the projectile and target and produce heat [62].

CHAPTER TWO

MATERIALS AND METHODS

2.1. Introduction

This section deals with laminate theory, ballistic impact mechanics in which ballistic science is generally in three subcategories: internal ballistic, external ballistic and terminal ballistic, penetration mechanism and the ballistic limit. In the thesis, vacuum Assisted Resin Injection (VARI) Method has been used to produce the specimens in experimental. In the investigation of high-velocity impact behavior of thin and thick laminated composites, the conservation of energy is the primary point of departure for the formation of physical equations. The kinetic energy possessed by a bullet is transferred to the target as a large amount of deformation energy in the later stages of the impact. In this regard, energy damping behaviors are shown to be an important part of the work performed under the target impact loads.

2.2. Laminate Theory

A common sheet of composite material is known as a lamina or ply and acts as a building block. Laminas are reinforced with many fibers embedded into the matrix, either woven, continuous (or not), uni or bidirectional, or random. The matrix is either metal or thermoplastic (or another non-metal material). Of all matrixes, unidirectional laminas are the strongest in the fiber direction, but very weak in the opposite direction. An example is shown in Figure 2.1. On the other hand, anisotropic are different material properties at a point in all direction depend on the orientation of reference axes.

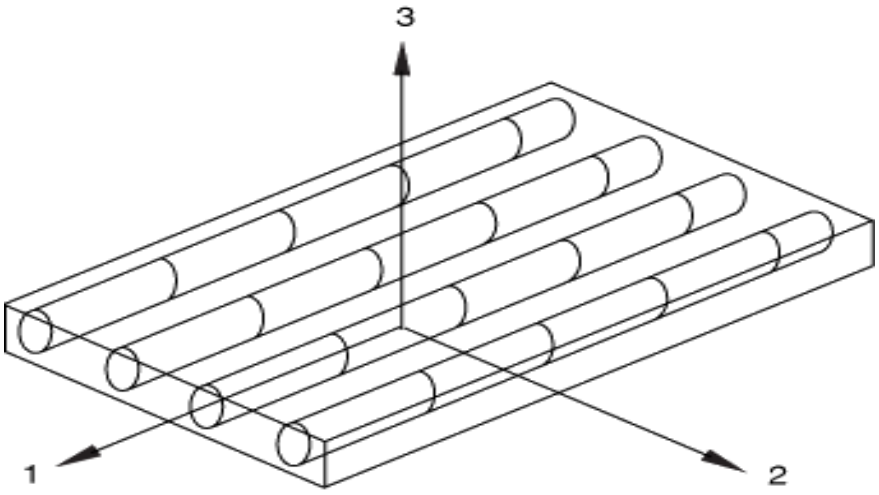

Figure 2.1. Type of lamina with unidirectional fiber [4].

It is impossible to use one lamina because it will be thin and very weak. As such, laminas are stacked in layers to create stiffness needed for the application. It is also possible to stack layers in opposite directions. This is known as the stacking sequence. Laminas are dependent on the direction of stacking, so the information below covers the various elasticity characteristics.

Laminate dimensions are usually much more bigger than the thickness. This is because their usage requires bending. As such, they are used as plate elements. According to references of 4, 63,64 , following topics are presented in this chapter:

- Constitutive Relations for a Laminae
- Mechanics of Materials Approach to Stiffness
- The Physics Theory of Ballistic Impact

2.2.1. Constitutive Relations for a Laminae

The in-plane linear constitutive relations for the orthotropic lamina in the principal material coordinates of a lamina are:

$$\begin{Bmatrix}\sigma_1\\ \sigma_2\\ \sigma_6\end{Bmatrix} = \begin{bmatrix}Q_{11} Q_{12} & 0\\ Q_{12} Q_{22} & 0\\ 0 & 0 & Q_{66}\end{bmatrix} \begin{Bmatrix}\epsilon_1\\ \epsilon_2\\ \epsilon_6\end{Bmatrix} \quad (2.1)$$

The above relation holds for material coordinates of 1,2,3 . Here, 1 is fiber direction, 2 is in the transverse direction and 3 is out of plane direction as shown in Figure 2.2. The Q_{ij} terms in Equation 2.1 are related to engineering constants as:

$$Q_{ij} = C_{ij} - \frac{C_{i3}C_{j3}}{C_{33}} \quad \text{where} , \quad (ij = 1, 2 , \ldots, 6) \tag{2.2}$$

$$Q_{11} = \frac{E_1}{1 - V_{12}V_{21}}$$

$$Q_{12} = \frac{V_{12}E_2}{1 - V_{12}V_{21}} = \frac{V_{21}E_1}{1 - V_{12}V_{21}}$$

$$Q_{22} = \frac{V_{12}E_2}{1 - V_{12}V_{21}} \quad , \; Q_{66} = G_{12}$$

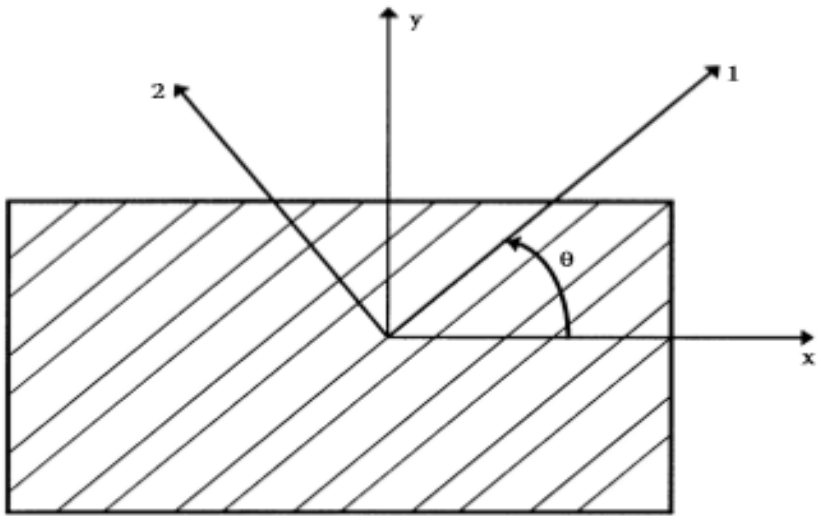

Figure 2.2. Local and global axes of angle laminae [4]

Because laminates are made from stacking different elements in various coordinates, one must use the (x, y, z) coordinates to make the constitutive equations for the various layers. The following obtains material coordinate stress from global coordinates.

$$\begin{pmatrix} \sigma_1 \\ \sigma_2 \\ \sigma_6 \end{pmatrix} = \begin{pmatrix} \mathrm{Cos}^2\theta & \mathrm{Sin}^2\theta & 2\mathrm{Cos}\theta\mathrm{Sin}\theta \\ \mathrm{Sin}^2\theta & \mathrm{Cos}^2\theta & -2\mathrm{Cos}\theta\mathrm{Sin}\theta \\ -\mathrm{Cos}\theta\mathrm{Sin}\theta & \mathrm{Cos}\theta\mathrm{Sin}\theta & \mathrm{Cos}^2\theta - \mathrm{Sin}^2\theta \end{pmatrix} \begin{pmatrix} \sigma_x \\ \sigma_y \\ \sigma_{xy} \end{pmatrix}$$

or

$$\begin{pmatrix}\sigma_x\\ \sigma_y\\ \sigma_{xy}\end{pmatrix}=\begin{pmatrix}\mathrm{Cos}^2\theta & \mathrm{Sin}^2\theta & -2\mathrm{Sin}\theta\mathrm{Cos}\theta\\ \mathrm{Sin}^2\theta & \mathrm{Cos}^2\theta & 2\mathrm{Sin}\theta\mathrm{Cos}\theta\\ \mathrm{Sin}\theta\mathrm{Cos}\theta & -\mathrm{Sin}\theta\mathrm{Cos}\theta & \mathrm{Cos}^2\theta-\mathrm{Sin}^2\theta\end{pmatrix}\begin{pmatrix}\sigma_1\\ \sigma_2\\ \sigma_6\end{pmatrix} \tag{2.3}$$

where θ is the angle from the x-axis to the 1-axis.

It is worth noting that this transformation is not related to the material properties but rather a rotation of the directions of stress. This makes rotational direction critical. As such the equations for strain-transformation are as follows:

$$\begin{pmatrix}\epsilon_x\\ \epsilon_y\\ \frac{\epsilon_{xy}}{2}\end{pmatrix}=\begin{pmatrix}\mathrm{Cos}^2\theta & \mathrm{Sin}^2\theta & -2\mathrm{Sin}\theta\mathrm{Cos}\theta\\ \mathrm{Sin}^2\theta & \mathrm{Cos}^2\theta & 2\mathrm{Sin}\theta\mathrm{Cos}\theta\\ \mathrm{Sin}\theta\mathrm{Cos}\theta & -\mathrm{Sin}\theta\mathrm{Cos}\theta & \mathrm{Cos}^2\theta-\mathrm{Sin}^2\theta\end{pmatrix}\begin{pmatrix}\epsilon_1\\ \epsilon_2\\ \frac{\epsilon_{12}}{2}\end{pmatrix} \tag{2.4}$$

A so-called especially orthotropic lamina is an orthotropic lamina whose principal material axes are aligned with the natural body axes:

$$\begin{Bmatrix}\sigma_x\\ \sigma_y\\ \sigma_{xy}\end{Bmatrix}=\begin{Bmatrix}\sigma_1\\ \sigma_2\\ \sigma_{12}\end{Bmatrix}=\begin{bmatrix}Q_{11}Q_{12} & 0\\ Q_{12}Q_{22} & 0\\ 0 \quad 0 & Q_{66}\end{bmatrix}\begin{Bmatrix}\epsilon_1\\ \epsilon_2\\ \epsilon_{12}\end{Bmatrix} \tag{2.5}$$

The stress and strain transformation of eq.2.1 with Reuters' matrix, eq.2.2, after abbreviating eq.2.5 as;

$$\begin{Bmatrix}\sigma_1\\ \sigma_2\\ \sigma_{12}\end{Bmatrix}=[Q]\begin{Bmatrix}\epsilon_1\\ \epsilon_2\\ \epsilon_{12}\end{Bmatrix}$$

to obtain $$\begin{Bmatrix}\sigma_x\\ \sigma_y\\ \sigma_{xy}\end{Bmatrix}=[T]^{-1}\begin{Bmatrix}\sigma_1\\ \sigma_2\\ \sigma_{12}\end{Bmatrix}=[T]^{-1}[Q][H]\,[T][H]^{-1}\begin{Bmatrix}\epsilon_x\\ \epsilon_y\\ \epsilon_{xy}\end{Bmatrix} \tag{2.6}$$

$[H]\,[T][H]^{-1}$ can be shown to be $[T]^{-T}$ where the superscript T denotes the matrix transpose . Where $[\overline{Q}] = [T]^{-1}[Q][T]^{-1}$ following equation gives stress – strain relation in x – y coordinates for an orthotropic lamina

$$\begin{Bmatrix}\sigma_x\\ \sigma_y\\ \sigma_{xy}\end{Bmatrix}=[\overline{Q}]\begin{Bmatrix}\epsilon_x\\ \epsilon_y\\ \epsilon_{xy}\end{Bmatrix}=\begin{pmatrix}\overline{Q_{11}} & \overline{Q_{12}} & \overline{Q_{16}}\\ \overline{Q_{12}} & \overline{Q_{22}} & \overline{Q_{26}}\\ \overline{Q_{16}} & \overline{Q_{26}} & \overline{Q_{66}}\end{pmatrix}\begin{Bmatrix}\epsilon_x\\ \epsilon_y\\ \epsilon_{xy}\end{Bmatrix} \tag{2.7}$$

in which,

$$\overline{Q_{11}} = Q_{11}\text{Cos}^4\theta + 2\,(\,Q_{12} + 2\,Q_{66}\,)\,\text{Sin}^2\,\theta\,\text{Cos}^{\,2}\,\theta + Q_{22}\,\text{Sin}^4\,\theta$$

$$\overline{Q_{12}} = (\,Q_{11} + Q_{22} - 4\,Q_{66}\,)\,\text{Sin}^2\,\theta\,\text{Cos}^2\,\theta + Q_{12}\,(\,\text{Sin}^4\,\theta + \text{Cos}^4\,\theta\,)$$

$$\overline{Q_{22}} = Q_{11}\text{Sin}^4\theta + 2\,(\,Q_{12} + 2\,Q_{66}\,)\,\text{Sin}^2\,\theta\,\text{Cos}^{\,2}\,\theta + Q_{22}\,\text{Cos}^4\,\theta$$

$$\overline{Q_{16}} = (\,Q_{11} - Q_{12} - 2\,Q_{66}\,)\,\text{Sin}\,\theta\,\text{Cos}^3\,\theta + (\,Q_{12} - Q_{22} + 2\,Q_{66}\,)\,\text{Sin}^3\,\theta\,\text{Cos}\,\theta$$

$$\overline{Q_{26}} = (\,Q_{11} - Q_{12} - 2\,Q_{66}\,)\,\text{Sin}^3\,\theta\,\text{Cos}\,\theta + (\,Q_{12} - Q_{22} + 2\,Q_{66}\,)\,\text{Sin}\,\theta\,\text{Cos}^3\,\theta$$

$$\overline{Q_{66}} = (Q_{11}+Q_{22} - 2\,Q_{12}-2\,Q_{66}\,)\,\text{Sin}^2\theta\,\text{Cos}^{\,2}\,\theta + Q_{66}\,(\,\text{Sin}^4\,\theta + \text{Cos}^4\,\theta\,) \qquad (2.8)$$

where $\overline{Q_{ij}}$ matrix denotes transformed reduced stiffness , Q_{ij}.

The following equation to express the strain in term of the stresses by inversion of the stress – strain or transformation of strain – stress relation as:

$$\begin{Bmatrix}\epsilon_1\\ \epsilon_2\\ \epsilon_{12}\end{Bmatrix} = \begin{bmatrix}S_{11}S_{12} & 0\\ S_{12}S_{22} & 0\\ 0 \quad 0 & S_{66}\end{bmatrix}\begin{Bmatrix}\sigma_1\\ \sigma_2\\ \sigma_{12}\end{Bmatrix} \qquad (2.9)$$

$$\begin{Bmatrix}\epsilon_x\\ \epsilon_y\\ \epsilon_{xy}\end{Bmatrix} = [T]^T[S][T]\begin{Bmatrix}\sigma_x\\ \sigma_y\\ \sigma_{xy}\end{Bmatrix} = \begin{pmatrix}\overline{S_{11}} & \overline{S_{12}} & \overline{S_{16}}\\ \overline{S_{12}} & \overline{S_{22}} & \overline{S_{26}}\\ \overline{S_{16}} & \overline{S_{26}} & \overline{S_{66}}\end{pmatrix}\begin{Bmatrix}\sigma_x\\ \sigma_y\\ \sigma_{xy}\end{Bmatrix} \qquad (2.10)$$

where $[H][T]^{-1}[H]^{-1}$ was found to be $[T]^T$ and ;

$$\overline{S_{11}} = S_{11}\text{Cos}^4\theta + (2\,S_{12} + S_{66}\,)\,\text{Sin}^2\,\theta\,\text{Cos}^{\,2}\,\theta + S_{22}\,\text{Sin}^4\,\theta$$

$$\overline{S_{12}} = S_{12}\,(\,\text{Sin}^4\,\theta + \text{Cos}^4\,\theta\,) + (\,S_{11} + S_{22} - S_{66}\,)\,\text{Sin}^2\,\theta\,\text{Cos}^2\,\theta$$

$$\overline{S_{22}} = S_{11}\text{Sin}^4\theta + (\,2S_{12} + S_{66}\,)\,\text{Sin}^2\,\theta\,\text{Cos}^{\,2}\,\theta + S_{22}\,\text{Cos}^4\,\theta$$

$$\overline{S_{16}} = (\,2S_{11} - 2S_{12} - S_{66}\,)\,\text{Sin}\,\theta\,\text{Cos}^3\,\theta - (\,2S_{22} - 2S_{12} - S_{66}\,)\,\text{Sin}^3\,\theta\,\text{Cos}\,\theta$$

$$\overline{S_{26}} = (\,2S_{11} - 2S_{12} - S_{66}\,)\,\text{Sin}^3\,\theta\,\text{Cos}\,\theta - (\,2S_{22} - 2S_{12} - S_{66}\,)\,\text{Sin}\,\theta\,\text{Cos}^3\,\theta$$

$$\overline{S_{66}} = 2\,(2S_{11} + 2S_{22} - 2S_{12} - S_{66})\,\text{Sin}^2\,\theta\,\text{Cos}^{\,2}\,\theta + S_{66}\,(\text{Sin}^4\,\theta + \text{Cos}^4\,\theta) \qquad (2.11)$$

Under condition of plane stress, written as:

$$\begin{Bmatrix}\sigma_1\\ \sigma_2\\ \sigma_{12}\end{Bmatrix} = \begin{bmatrix}Q_{11}Q_{12}Q_{16}\\ Q_{12}Q_{22}Q_{26}\\ Q_{16}Q_{26}Q_{66}\end{bmatrix}\begin{Bmatrix}\epsilon_1\\ \epsilon_2\\ \epsilon_{12}\end{Bmatrix} \tag{2.12}$$

or inverted form as;

$$\begin{Bmatrix}\epsilon_1\\ \epsilon_2\\ \gamma_{12}\end{Bmatrix} = \begin{bmatrix}S_{11}S_{12}S_{16}\\ S_{12}S_{22}S_{26}\\ S_{16}S_{26}S_{66}\end{bmatrix}\begin{Bmatrix}\sigma_1\\ \sigma_2\\ \tau_{12}\end{Bmatrix} \tag{2.13}$$

where; $S_{11}=\frac{1}{E_1}$, $S_{22}=\frac{1}{E_2}$, $S_{16}=\frac{\eta_{12,1}}{E_1}=\frac{\eta_{1,12}}{G_{12}}$, $S_{12}=-\frac{V_{12}}{E_1}=-\frac{V_{21}}{E_2}$

$S_{66}=\frac{1}{G_{12}}$, $S_{26}=\frac{\eta_{12,2}}{E_2}=\frac{\eta_{2,12}}{G_{12}}$

so, $\eta_{i,ij}=\frac{\varepsilon_j}{\gamma_{ij}}$ for $\tau_{ij}=\tau$ and all other stresses = 0 .

therefor $\eta_{ij,i}=\frac{\gamma_{ij}}{\varepsilon_i}$ for $\sigma_i=\sigma$ and all other stresses = 0 .

The current stiffness matrix is only applicable for the analysis of an on-axis arrangement as shown in Figure 2.3(a). A new matrix, $[\overline{Q}]$ is required in the analysis of an θ angle lamina with an off-axis arrangement shown in Figure 2.3(b).

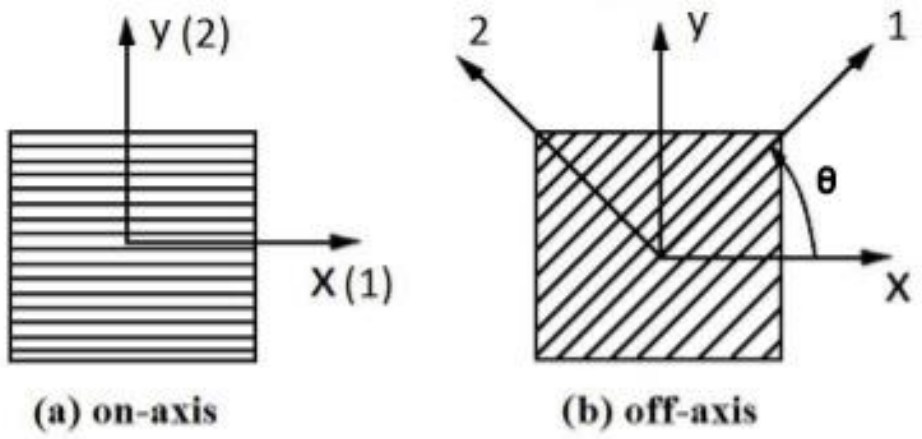

Figure 2.3. On and off-axis configurations [63].

It is possible to assume composite laminate performance after finding the stiffness and compliance matrices of the unidimensional lamina. A reference number and (z) coordinate are given to each of the lamina to find the coordinate system location. (Figure 2.4).

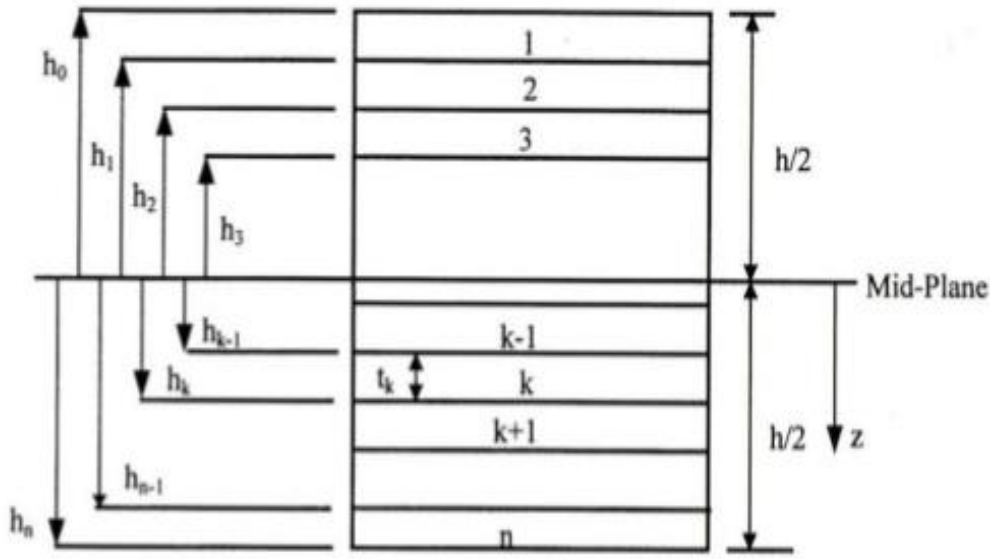

Figure 2.4. Stacking Sequence Nomenclature of Laminate [4].

Thus, the stress for k^{th} lamina can be determined by following relation:

$$\begin{Bmatrix} \sigma_x \\ \sigma_y \\ \sigma_{xy} \end{Bmatrix}_k = \left(\begin{pmatrix} \overline{Q_{11}} & \overline{Q_{12}} & \overline{Q_{16}} \\ \overline{Q_{12}} & \overline{Q_{22}} & \overline{Q_{26}} \\ \overline{Q_{16}} & \overline{Q_{26}} & \overline{Q_{66}} \end{pmatrix} \right)_k \begin{Bmatrix} \epsilon_x^0 \\ \epsilon_y^0 \\ \epsilon_{xy}^0 \end{Bmatrix} + Z \begin{Bmatrix} k_x \\ k_y \\ k_{xy} \end{Bmatrix}$$

2.2.2. Mechanical Approach of Materials to Stiffness

Most researchers assume that fiber direction strains are the same as those in the matrix for unidimensional composite materials (Figure 2.5). If the stresses are different, then one could expect a break between the fibers and matrix.

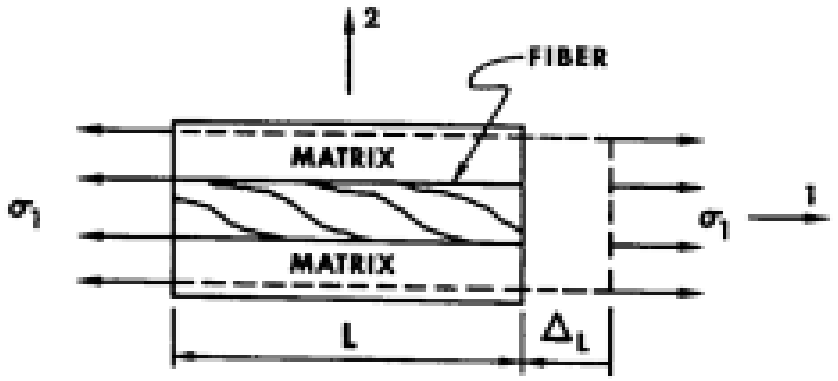

Figure 2.5. Loaded of volume element in 1-D [64].

2.2.2.1. Determination of E1

The first modulus to be determined is that of the composite material in the 1-direction, in the fiber direction as:

$\varepsilon_1 = \frac{\Delta L}{L}$, $\sigma_f = E_f \varepsilon_f$ for fiber , $\sigma_m = E_m \varepsilon_m$ for matrix

where ; ε_1 applies for both fibers and matrix , σ_f acts on the cross-section area of the fibers A_f , and σ_m acts on the cross-section area of the matrix A_m , the resultant force on the volume element is

$P = \sigma_1 A = \sigma_f A_f + \sigma_m A_m$

After substitution , and $V_f = \frac{A_f}{A}$, $V_m = \frac{A_m}{A}$ then : for determine E_1 is

$$E_1 = E_f V_f + E_m V_m \quad (2.14)$$

2.2.2.2. Determination of E_2

The apparent young's modulus , E_2 , in the mechanics of lamina approach the same transverse stress σ_2 is assumed to be applied to both the fiber and the matrix

The strains in fiber and matrix are found from the stresses:

$$\varepsilon_f = \frac{\sigma_2}{E_f} \quad , \quad \varepsilon_m = \frac{\sigma_2}{E_m} \quad (2.15)$$

where $\varepsilon_f \cong V_f W$, $\varepsilon_m \cong V_m W$, the total transverse deformation is :

$$\Delta W = \varepsilon_2 W = V_f W_{\varepsilon_f} + V_m W_{\varepsilon_m} \text{ , Also } \varepsilon_2 = V_f \varepsilon_f + V_m \varepsilon_m \quad (2.16)$$

After sub. eq.2.15 of the strains from eq 2.16 and simplified these equations have gotten:

$$E_2 = \frac{E_f E_m}{V_m E_f + V_f E_m} \quad (2.17)$$

2.2.2.3. Determination of Poisson's ratio ν_{12}

Poisson's ratio is obtained by method similar to the analysis for E_1, as

$\nu_{12} = \frac{\varepsilon_2}{\varepsilon_1}$, for the stress state $\sigma_1 = \sigma$ and all other stresses are zero .

The transverse deformation Δw is :

$$\Delta_w = -W_{\varepsilon 2} = W_{V12\,\varepsilon_1} \text{ , Also } (\Delta_w = \Delta_{mw} + \Delta_{fw}) \quad (2.18)$$

the analysis for the transverse E_2, the transverse deformations are:

$$\Delta_{mw} = W V_{mVm\varepsilon 1} , \Delta_{fw} = W V_{fVf\varepsilon 1} \quad (2.19)$$

Combine eq. 2.18 , 2.19 and divide by $\varepsilon_1 W$ to get :

$$\nu_{12} = \nu_m V_m + \nu_f V_f \quad (2.20)$$

2.2.2.4. Determination of G_{12}

The shear modulus of a lamina, is determined shearing stresses on the fiber and the matrix as:

$$\gamma_m = \frac{\tau}{G_m} , \quad \gamma_f = \frac{\tau}{G_f} \quad (2.21)$$

The total shearing deformation is:

$\Delta = \gamma W$, $\Delta_m = V_m W_{\gamma m}$, $\Delta_f = V_f W_{\gamma f}$, because ($\Delta = \Delta_m + \Delta_f$) , divide by W :

$$\gamma = V_m \gamma_m + V_f \gamma_f \quad (2.22)$$

and after sub. in eq. 2.21 and rewrite eq. 2.22 to get finally equation,

$$G_{12} = \frac{G_m G_f}{V_m G_f + V_f G_m} \quad (2.23)$$

2.2.3. The Physics Theory of Ballistic Impact

Based on the theory of Aristotle 2000 years ago, in the case of throwing an arrow or body or the like that, the penetration of the body to the air opened his way through the momentum and the body falls after the end of its energy because of friction with air. Many theories have emerged in the sixteenth century AD, in 1686, Sir Isaac Newton presented his laws of motion in the "Principia Mathematica Philosophiae Naturalis".The laws are shown below, and the application of these laws to aerodynamics also.

Newton's laws; three laws of mechanics describing the motion of a body are as followed:

Newton's first law is that all objects in motion stay in motion and objects at rest will stay at rest unless an outside force changes their trajectory. This law explains inertia. This means that is there is no net force, then the object remains at a steady velocity. With a velocity of zero, the object remains still. The velocity changes because of force applied to it.

Newton's second law regards the velocity of an object that changes after a force is acted upon it. This force is the same as momentum (mass multiplied by velocity) for time. Newton's calculus is important to explain this law, as he showed the changes by differentials. Objects have a constant mass (m) that dictates the force (F) comes from multiplying mass times acceleration (a: $F = m.a$).

$$\sum F = m.a \quad (2.24)$$

where , $a = \frac{d}{dt} v$

Newton's third law states that when a force acts on a body due to another body, then an equal and opposite force acts simultaneously on that body.

Impulse-Momentum-Impacts

Momentum: "quantity of motion" – Any object which has both mass and a velocity is said to have momentum, if , $a = \frac{d}{dt} v$ based on Newton's laws of motion as:

$$F = m.a \ , \ \sum F = m.a \tag{2.25}$$

This can be rewritten with acceleration as the derivate of velocity with respect to time:

$$F = m.\frac{d}{dt} v \tag{2.26}$$

If this is integrated from time t_1 to t_2 , $F\,dt = d(m.v)$

$$\int_{t_1}^{t_2} F\,dt = m.v_2 - m.v_1 \tag{2.27}$$

An impulsive force is one that acts on a particle for a limited time. When there is a momentum change from this force, it is called impulsive motion. When different particles interact with one another, it is shown as:

$$\sum m.v_1 + \sum F.\Delta t = \sum m.v_2$$

When two particles collide and there are no external impulsive forces acting on them, total momentum is conserved. The equation becomes:

$$\sum m.v_0 = \sum m.v_1 \tag{2.28}$$

Conservation of Momentum

The total momentum of any given system will remain constant unless acted upon by an external force. The momentum before a collision is equal to the momentum after a collision.

$$mV = Mv \tag{2.29}$$

where, v the velocity of the gun reaction.

Conservation of Energy

In order to calculating kinetic energy and rotation energy of projectile the following equations are used :

$$E_K = \frac{1}{2} m.v^2 \quad (2.30)$$

$$E_{rot} = \frac{1}{2} m.I\omega^2 \quad (2.31)$$

where, I moment of inertia ($kg.m^2$) , ω angular velocity (rad/sec) , the projecite with the total energy value of :

$$E_T = E_K + E_{rot} \quad (2.32)$$

for Energy absorption of the laminate are calculated using equation :

$$E_{abs} = \frac{1}{2} m (v_i^2 - v_r^2) \quad (2.33)$$

where , m mass of the projecitle , v_i striking velocity , v_r residual velocity

where in 1960 which the first studies and theories on the ballistic impact are created. The first thing to be clear is that for a fabric to resist the impact of a projectile, it must absorb all the kinetic energy of the last one. As it has been studied throughout the race, the kinetic energy depends on the mass and the velocity of the projectile, so that the ballistic impact will depend to a great extent on these two parameters.

2.4. Impact Mechanism

In general, the impact is examined in two groups of thin and thick specimens under ballistic impact test. Impact mechanics examine the dynamic response of these bodies to collisions with reaction forces generated at the moment of a collision. It also examines the physical phenomena that occur in colliding bodies during impact, depending on the type of impact.

2.4.1. Ballistic Impact and Low Velocity Impact Mechanism

Ballistics is a branch of mechanics that focuses on acceleration of bullets (and other projectiles) from a gun barrel. It also covers how the projectile behaves at the muzzle, as it moves, and how it effects the target. There are three focuses: interior, exterior, and terminal ballistics. This reseach deals with terminal, or how projectiles and targets interact. Terminal ballistics covers the strike angle and velocity, as well as the different targets and projectile types.

Situations, where the target collides with the bullet, may be the result; the impact of the bullet to the target, the impact angle, the material, the tip geometry and weight, the mechanical properties of the target material, the thickness and the number of layers. There are several definitions in the literature regarding ballistic impact. When the bullet penetrates the target completely, that is, when the impacts that result in perforation are defined as ballistic impacts, the impacts where penetration does not occur are examined within the low-speed impact concept. It is a very important issue to determine the final speed of the bullet in studies related to ballistic impacts. This account is particularly difficult in experimental investigations. Because of a large number of particles belonging to the projectile and the target are scattered during the impact and penetration. These particles can act on sensory devices related to speed measurement and cause errors in calculation. Special measurement systems have been developed to remove this difficulty. The solution methods for the collision problems can be shaped in three different ways: These are the approach in which a large number of experimental information is acquired and related to each other. While this method is useful for solving problems with certain conditions, trying to use them on problem areas outside the conditions in which existing experimental information is obtained is very difficult and makes the solution impossible. The second method is to develop and use engineering models for numerical simulation of the impact. This approach can be applied in various fields ranging from simple functioning one-dimensional problems to complex, two or three-dimensional crash problems with different damage patterns.The last method is the discretization method, which is based on dividing the structure into small elements and applying the basic equations separately for each element. The use of the appropriate numerical solution technique - for example, end-of-line elements or finite difference method - is time-consuming, as well as providing convergent solutions

[65-66]. The most common method used to develop a model for penetration is the iterations made with experimental and analytical results. An experimental study is an important influence shaping the model. In an analytical work on an armor subject to high-speed impact, the first thing to do in order to understand the problem is to develop a model that can determine the loads that impact the target during impact. Thus, the dynamic behavior of the target can be defined with accuracy. Today, there are a variety of test assemblies that can be used to simulate different types of impacts. For high-speed crashes, a low-weight body is used with the aid of air-operated "gas gun" Measuring systems to ensure that the changes in the parameters that make up the focal point of the work are to be considered as a whole in the test set-ups. It is important to select the appropriate test/test system in order to be able to test the correctness of the approach used in the model. These methods should be checked against the actual situation in nature, as well as the scientific work must be complete. On other hands, the two colliding of the body surfaces come together at a relative velocity in a given instantaneous domain. Then interference or interpenetration occurs between these objects. It is not the interference or penetration due to the interface pressure that occurs due to the small contact area between the two body surfaces, but the local deformation and the subsequent indentation that occur during the contact period. If the colliding bodies are not deformation, the amount of sinking is equal to the penetration between the surfaces. The resistance of the interface between the bodies is formed by the interface or contact pressure of each impact during impact, which has the effect or reaction force acting on the two colliding bodies in opposite directions. In the event of a collision between rigid bodies, the contact force acting during the collision is a consequence of the local deformations required to create a contact area of the two body surfaces The regional deformations that occur during the impact vary depending on the stiffness of the colliding bodies as well as on the relative impact velocity at the beginning of contact. In low-speed collisions, contact pressures occur, which cause only small deformations; they are important only in a small area near the contact area. At higher speeds, large deformations (unit shape changes) occur due to plastic flow near the contact area. These large regional deformations are of great significance in the form of cratering or penetration and can be easily detected [65-66].

2.4.2. Terminal Ballistics

Terminal ballistics is of particular interest to engineers who craft armor and anti-armor. It is a science that begins with the bombardment of the target and the events that occur between the bullet and the target during the duration of the crash, the effects of the projectile and the target on each other. Relevant impact is usually in the ordance velocity range (0.5 - 2 km/s). This the velocity of rifle and gun fire sent to buildings and armored vehicled. Jet impact velocity is especially focused on by engineers, and it falls in the range between 2 and 8 km/s. Before World War 2, termial ballistics was built around the relationship between depth of penetration and impact. After this, American and British scientists focused on the penetration of jets with armor plates and built models to analyze the situation thoroughly. The mechanical phenomena that occur during the target penetration of the bullet, the effect of the bullet and the target without colliding, if any, the behavior of the jumping particles and the fatal or injurious effects of the shot are revealed by the terminal ballistics [67-68].

2.4.3. Internal Ballistics

Beginning with the insertion of the bullet into the cartridge bed, it examines the mechanical structure of the firearm, its operation, the formation of the explosion, the effect on the cartridge, and the movements of the bullet core until it leaves the gun. In fact, when gunpowder is fired, a fire does not come on and an increasing amount of gas is brought to the square. This, in turn, pushes the bullet forward. But as the area of influence of the gases expands, the pressure falls in the same area. Therefore, it is tried to keep the pressure constant by using heavy burnt guns and long barrels. By prolonging the effect of these long barrels, high initial velocities are achieved without overturning the barrels. The internal ballistic event starts with the trigger being pulled, until the moment the barrel leaves the barrel. Internal ballistic calculations can be reliably predicted mathematically when bullets are large in size. It is quite difficult when it is small size. In the past, ballistic data were determined by velocity and pressure test methods or empirical methods instead of computation for small bullets. Performance values were obtained by shooting tests of small size bullets containing a large number of core / gun combinations. Sufficient data was extracted from these tests and acceptable results were obtained for small bullets by evaluating them together with sound ballistics

information. When the known kinetic energy equation ($E_k = 1/2\ mv^2$) equals the amount of energy released from the barrier, the projectile speed can be calculated with acceptable accuracy. Only a small fraction of the actual energy [69].

2.4.4. External Ballistic

If the aerodynamic forces influenced by the inertia, gravity, and air acting on the projectile or fuze are known, the account of the orbits does not present any significant difficulty. However, it is difficult to know the aerodynamic forces. A bullet must travel in the first exit position toward the target point during a flight to defeat air resistance and make a stable flight. If the bullet changes its position or even rolls, it causes the flight to not come to an end and fall into its intended range. There are two methods to achieve flight stabilization. These are fin stabilization and spin, rotation stabilization. In the flap stabilization, the flaps mounted on the bullet allow the bullet to go round in its own axis. This is ensured by aerodynamic forces on the fins. As a consequence of the gyroscopic rotational motion of a spin-stabilized bomb, motion always continues along the first target direction. The inertia of this rotational motion does not allow deviations to be the correct axis [69].

2.5. Penetration Mechanism

The study of plate penetration and perforation covers a diverse range of problems and applications. Penetration is the impact of projectiles into a target. Perforation is a type of penetration when the projectile completely passes through its target. Conversely, embedment is when the projectile remains lodged inside the target after impact [66].

Kinetic energy penetration is a subject that is generally studied in high-speed pulse applications. Particularly in ballistic impact analysis, the events occurring during the impact between the bullet and the target are examined.

Conceptually, penetration penetrates the target partly, that is, it stays in the target. This is also the basic fulcrum of a work aimed at achieving an appropriate armor design. Perforation (puncture) is the progression of the bulge during the thickness of the target, that is to say the bullet completely penetrates the target. It is caused by the kinetic energy which is caused by the penetration of the bullet with the target or the movement of the perforation. This point distinguishes kinetic energy collisions from chemical

energy discharges. The development of kinetic energy penetration is shown in Figure 2.6.[65,70]

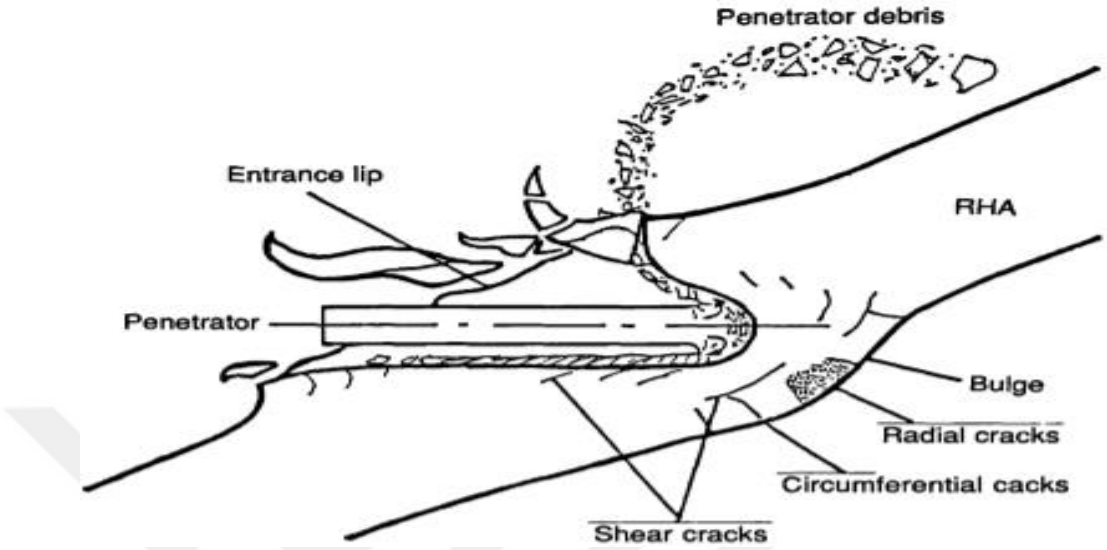

Figure 2.6. Kinetic energy penetration [70].

As soon as the bullet hit the target, tension waves occur in both the bullet and the target body. Depending on the impact speed and material properties, these tensile waves travel at or above the speed of the sound in the material. These are followed by slippery waves with slower speeds. At high impact velocities, the bullet forms relief waves that create a three dimensional stress state in two-dimensional, angular impacts in vertical impacts due to free surface. As a result, due to the boundary conditions, the tension waves in the push direction are turned in the pull direction. At higher speeds, the effect of these waves is greater than at lower speeds [65,70].

If a long, cylindrical object begins to bend at a speed below the ballistic limit (the minimum speed required for perforation), hit the target surface. As the impact speed increases, the plastic deformation concentrates in a certain region and the fuselage deforms without the tip of the cylinder dipping the target. If the impact occurs at a higher speed, in addition to plastic deformation, the cylinder is buried in the target. This situation is shown in Figure 2.7 [65,70].

Penetration at impacts over the ballistic limit begins simultaneously with the impact. (Figure 2.8) At the first moment of impact, the pressure between the surfaces is higher than both the target and the material strength of the bullet, so that the remaining part of

the bullet leads to a deformed crater while penetration with erosion occurs at the end of the bullet.

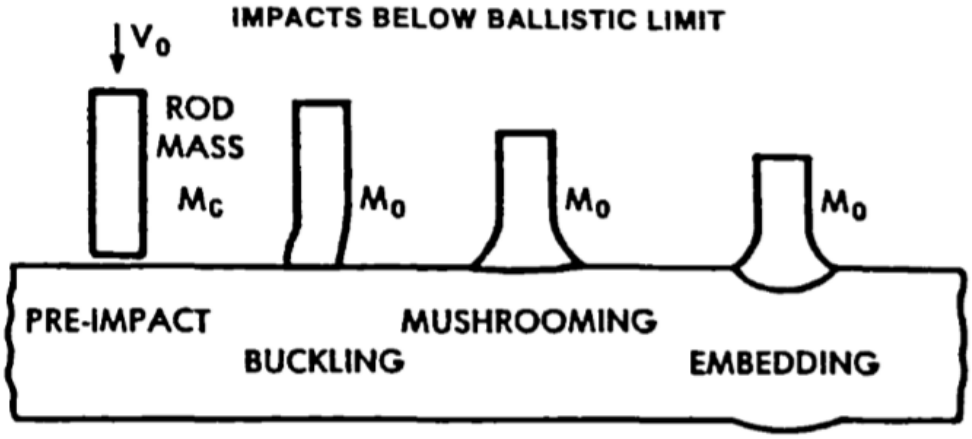

Figure 2.7. Impact behavior below the ballistic limit [70].

As the crater progresses deeper, the bottom expands in a manner appropriate to the deformation of the end of the barrel, and high shear stresses occur at the contact surface. Depending on the material properties, the impact speed and the thickness of the target after a certain period of time, the shape changes in the form of bulging and spreading on the back surface of the target. During ballistic penetration and puncture, the bullet and target are exposed to equal and opposite forces to start from the contact surfaces. Waves emanating from the interface form bullets and stresses and displacements within the target and cause changes in their condition. Bullet; it may lose some of its weight, it may change its orbit, it may become deformed, it may lose some of its weight due to erosion, it may cause particles to break away at different sizes [65,70].

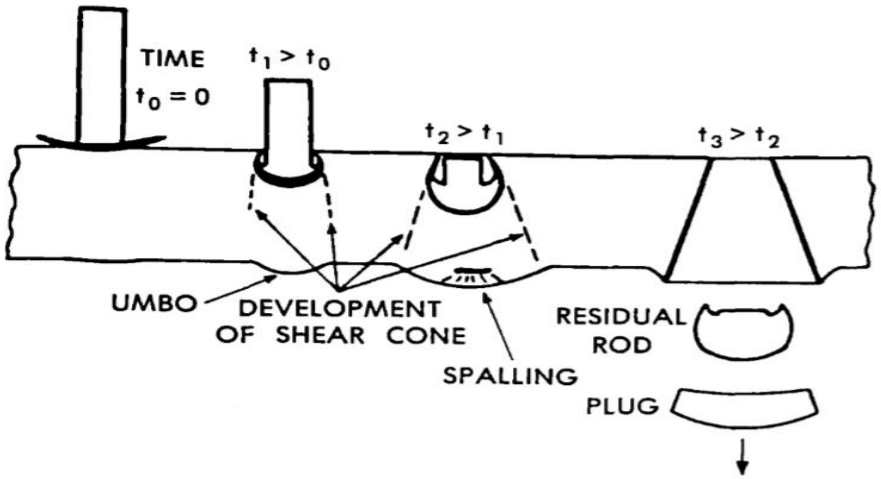

Figure 2.8. The impact behavior on the ballistic limit [70].

As a result of the ballistic impact, a series of damage mechanisms for bullets and armor materials are emerging. These damage mechanisms shown in figure 2.9 :

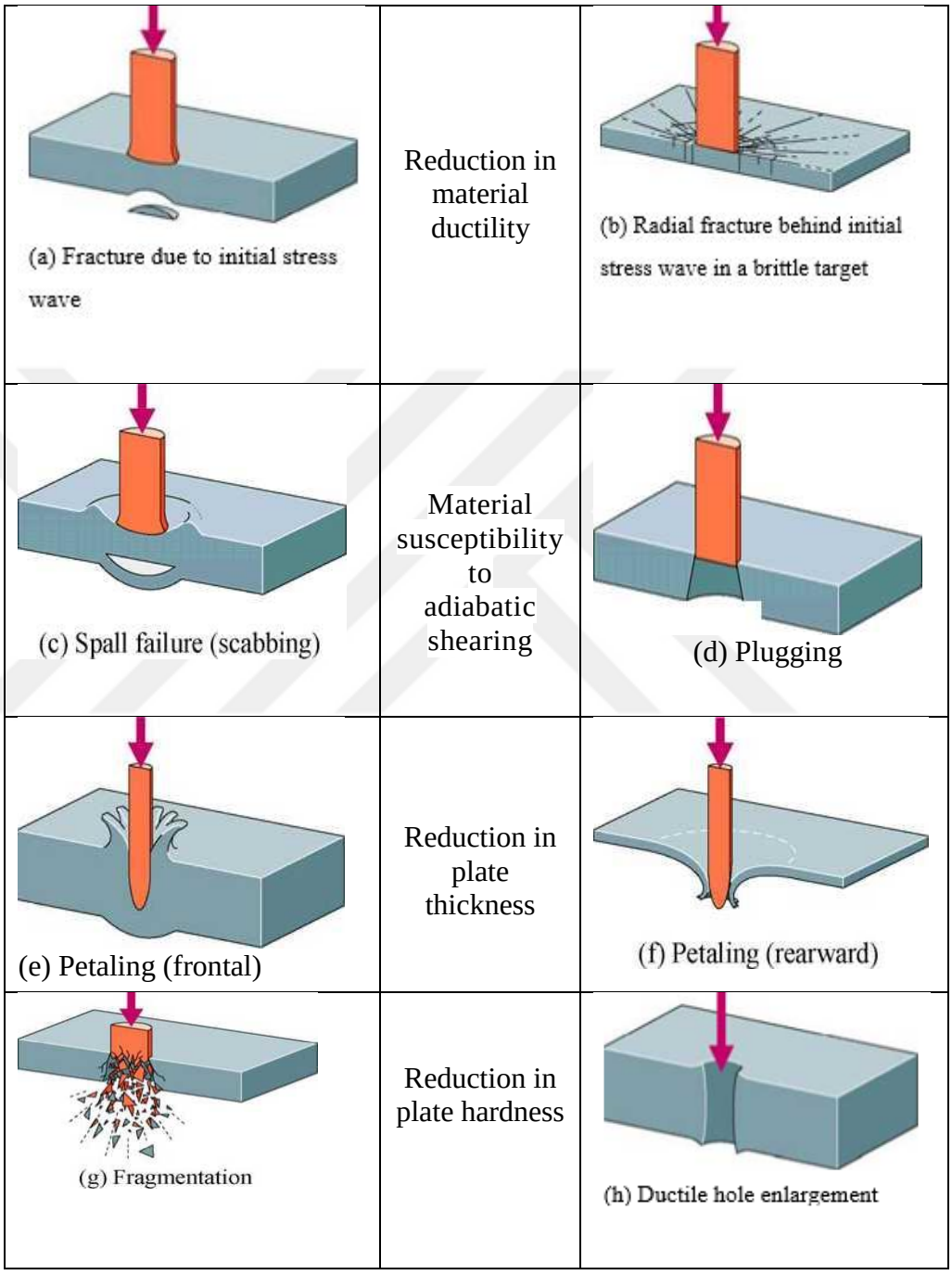

Figure 2.9. Damage mechanisms under ballistic impact [71].

Often, materials such as hard metals and ceramics have dynamic damage due to high pressure.

In ballistic impact analysis, the properties of the projectile or penetrator must be well known, as well as knowing the mechanical properties of the armor system. Because the effects of impacts are different according to the type of projectile. With the developing

technology, different types of bullets have been developed for different weapons such as speed, geometric shape, core structure. Therefore, the characteristics of the bullet, which will create a blow in the design of ballistic armor, must be considered . In armor design, the following are some of the essential features that should be followed:

- Bullet material (steel, copper, lead, etc.)

- Bullet tip geometry (pointed, bump , etc.)

- Core weight

- Bullet speed

The geometry of bullet affects the speed of penetration or puncture events at a considerable degree. In order to better understand the significance of these parameters, different bullet geometries are shown in Figure 2.10 [68, 72] .

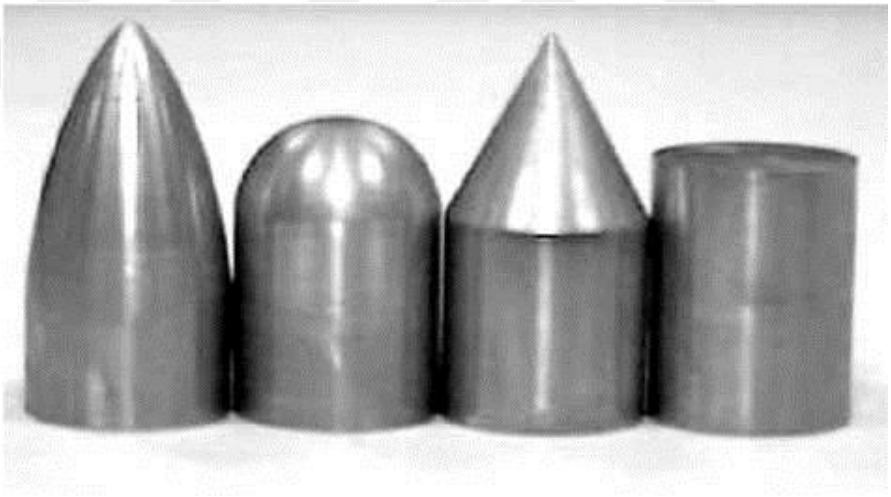

Figure 2.10. Bullets used in ballistic tests [72].

2.6. The Ballistic Limit

There are different approaches in the literature for the concept of ballistic limit and it is necessary to define these approaches. The ballistic limit velocity V_{BL} is defined as the velocity at which the bullet can not penetrate the target and the velocities below this velocity. Figure 2.11 shows different approaches to the concept of ballistic limit. The main difference between these approaches is the different criteria for defining the phenomenon of puncture [73].

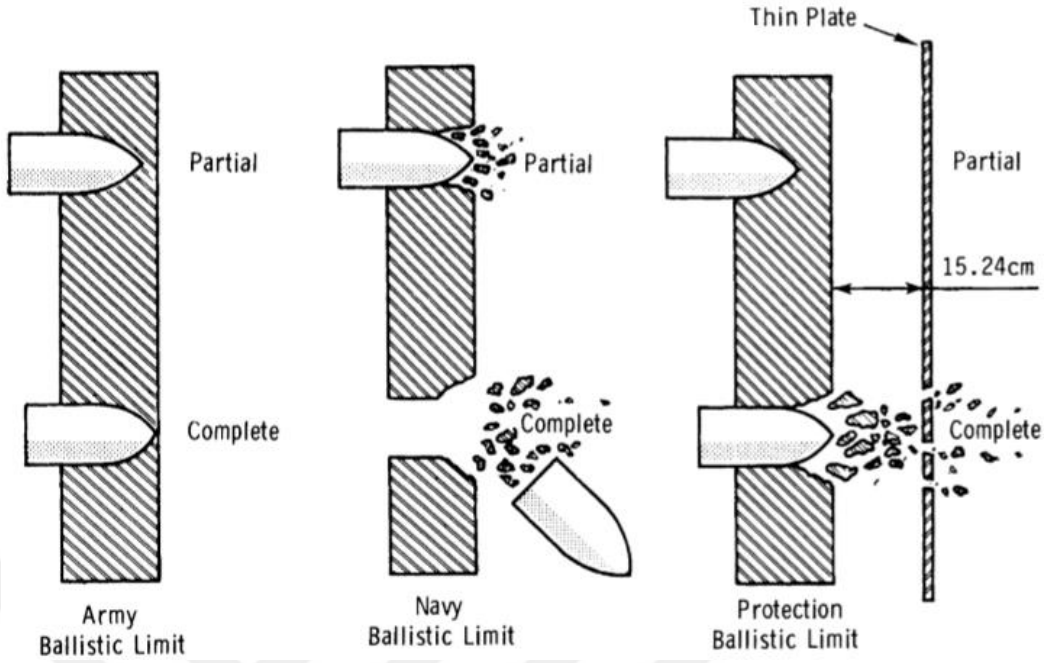

Figure 2.11. Different approaches to the concept of ballistic limit [73].

The actual assessment to determine the ballistic limit speed is made with tests based on statistical studies. The ballistic limit velocity is indicated by V_{50}, which is the speed at which the bullet has 50% of its post-impact target in perpendicular to the target. As mentioned, statistical approaches are used to determine the V_{50} velocity. Basically, the ballistic limit speed is determined by taking the average of the three highest speeds that cause full penetration and the lowest three speeds that cause partial penetration. The smaller the difference between the lowest speed that penetrates the target in the test results and the highest speed that does not penetrate, the higher the accuracy of the ballistic limit estimate. A typical V_{50} diagram for the ballistic pulse is shown in Figure 2.12 [70].

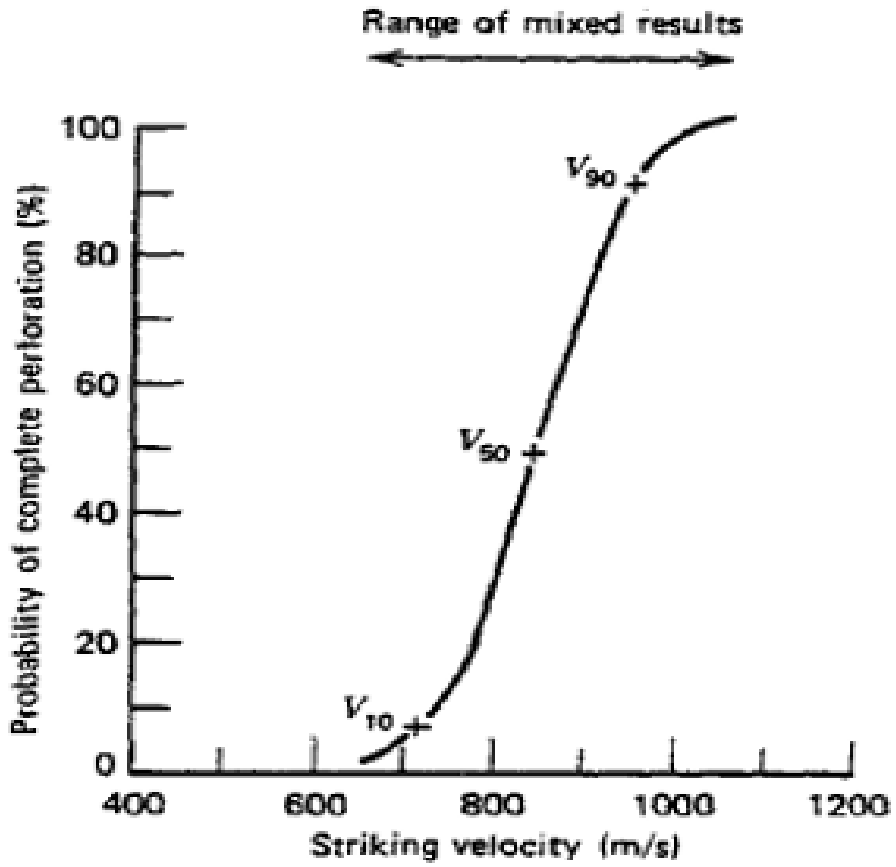

Figure 2.12. Ballistic limit curve [70].

Another approach to the concept of ballistic limit is the Lambert-Jonas approach. as show in the following equations:

$$V_{res} = a\,(V_{imp}^{p} - V_{bl}^{p})^{1/p} \quad \text{where} \quad V_{imp} > V_{bl} \tag{2.34}$$

Here, V_{imp} the collision velocity of the bullet, V_{res} the residual velocity of the bullet, and V_{bl} the ballistic limit velocity of the , a and P are the coefficients obtained from the experimental data, and when P = 2, the equation is named Recht-Ipson approach (Equation 2.35).

$$V_{res} = a\,(V_{imp}^{2} - V_{bl}^{2})^{1/2} \quad , \quad a = \frac{M}{(M+m)} \tag{2.35}$$

M is the mass of the ammunition used to find the coefficient a, and m is the mass of the crushed fragment from the collision. When the ballistic limit curve is plotted according to Lambert-Jonas equation, the horizontal axis indicates the multiplication rate and the vertical axis indicates the residual velocity. The horizontal axis of the curve gives the

ball point velocity limit. That is, when V_{res} = 0, the impact velocity V_{imp} is equal to the ballistic limit velocity V_{bl} [74].

The use of diagrams to illustrate the high-speed collision phenomenon is more helpful in understanding the system. When these diagrams are constructed, effects such as speed, target thickness, impact angle, impact kinetic energy, push, force and time are taken into consideration. The curves represent relationships between one dependent variable and one independent variable, Figure 2.13 is an example of the phase diagram portraying the behavior of a (6.35 mm) ogival-nosed projectile striking a aluminum target [75].

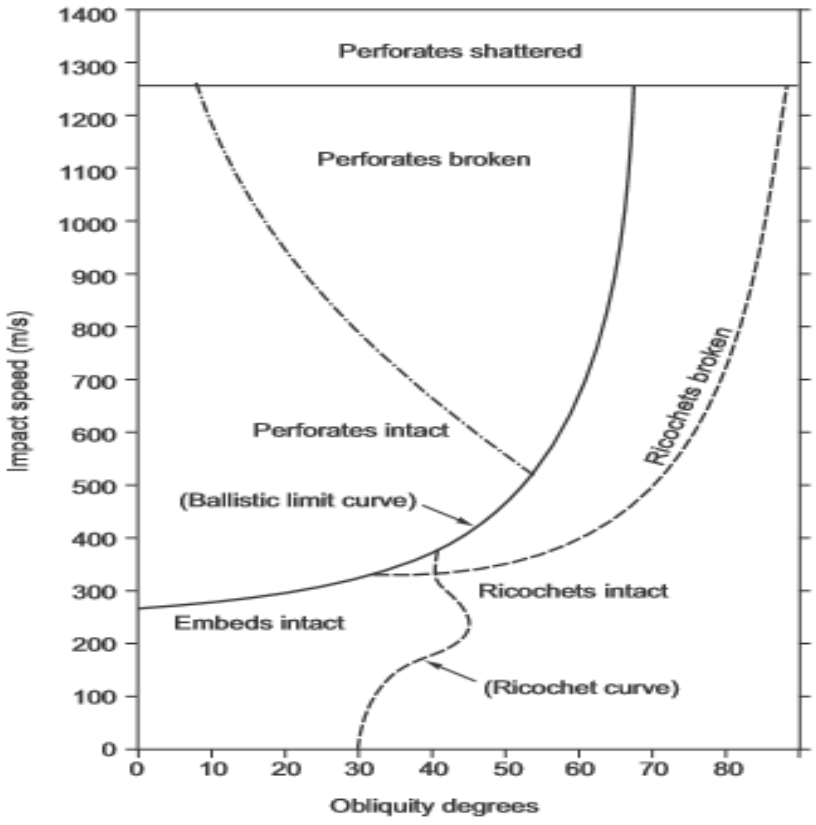

Figure 2.13. Ballistic phase diagram [75].

The diagram was built from both experimental and theoretical data based on a behavior model of ogival projectiles fired at plates. The variables are the impact velocity (v_0) and impact obliquity (θ). It has several curves for the boundaries of the phases. A ballistic curve is formed from points that represent perforation stages and richoet or embedement (the ballistic limits). This limit is used to evaluate both projectile and armor performance. The overall practice is known as ordnance science [75].

2.7. Standards Used in Ballistic Tests

Ballistic tests will be performed using single-stage gas gun system. 0.30 caliber FSPs *(Fragment Simulating Projectiles)* which is defined by STANAG 2920 [76] and MIL-DTL- 46593B (MR) [77] standards will be used in ballistic tests. The launcher of gas gun operates with sabot projectiles. AISI 4340H steel was used for the production of the FSPs and the schematic view and geometrical dimensions are demonstrated in Figure 2.14. The material properties of AISI 4340H steel are listed in Table 2.1 [78].

Ballistic tests will be carried out for three different fiber orientations of the thick and thin composite plates. Also, ballistic tests will be performed for three different FSP velocities in order to determine the impact energies on the damage mechanism of the thick and thin composites.

Table 2.1. Material properties of the AISI 4340H steel projectile [78].

Materials	Young's modulus (G Pa)	Poisson's ratio	Density (kg/m^3)	Yield stress (MPa)	Tangent modulus (MPa)	Failure strain
Steel AISI 4340	200	0.29	7850	970	470	0.77

Table 2.2. Features of 0.30 caliber FSP projectiles

Material	AISI 4340H-4337H
Weight (grain)	44±0.5
Hardness (RC)	30±2

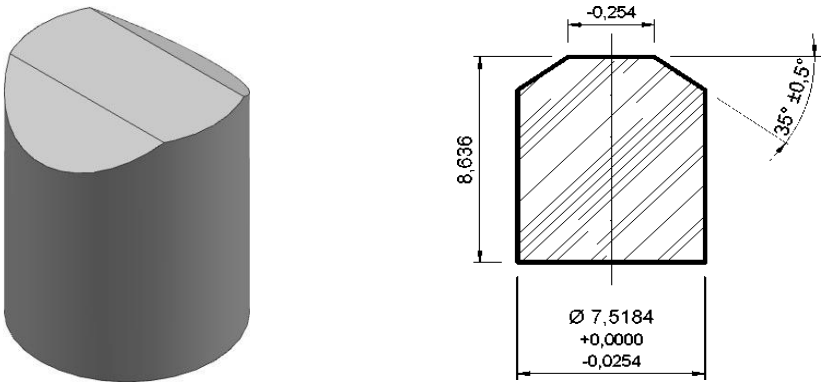

Figure 2.14. The geometrical details of 0.30 caliber FSP (dimensions in mm).

2.8. Specimens Preparation

The E-glass/epoxy composite material will be used in this study, and it will be produced in Mechanics Laboratory in Mechanical Engineering Department using Vacuum Assisted Resin Injection (VARI) method (Figure 2.15). Unidirectional E-glass fiber having a density of 600 g/m^2 will be using as reinforcing the material. Epoxy and hardener will be mixing and applied to the unidirectional E-glass fiber reinforcement, carrying out by using a vacuum with temperature and time control. A thin composite plate consists of 16 unidirectional layers and a thick composite plate consists of 50 unidirectional layers at the end of the manufacturing process, the final thickness of the composite plate will be measuring. The thin and thick composite plates will be produced antisymmetric layer stacking and three different fiber orientations such as 0/90, -45/+45 and 30/60.

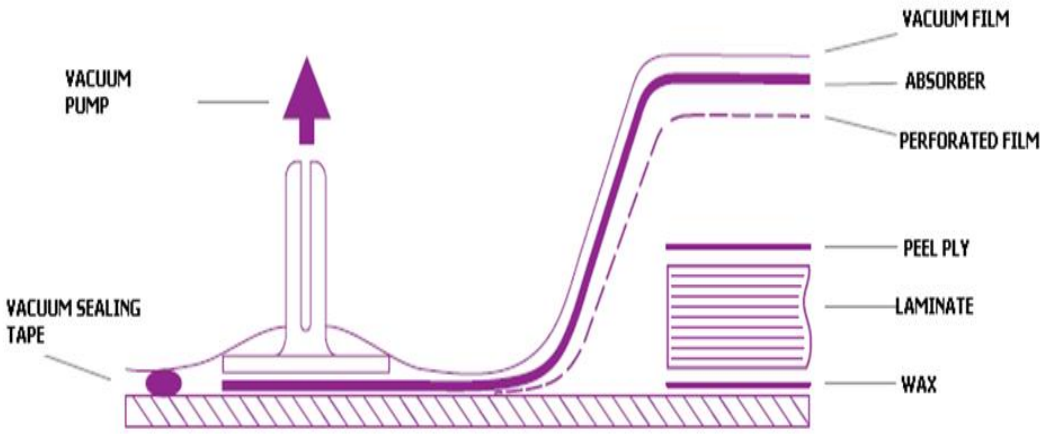

Figure 2.15. Vacuum Assisted Resin Injection (VARI) method [79]

Where all laminated composites produced in this chapter study were made from unidirectional E-glass fiber. The Table 2.3 below has described important materials for production fiber reinforced composites in the laboratory.

Table 2.3. Materials used in Mechanics Laboratory

Materials	Description
	unidirectional E-Glass Fiber.
 (A)  (B)	(A) Epoxy (MGS LH 160) (B) Hardener (MGS LH 160) (with mixing ratio 3/1)
 (A)  (B)	A. flow tank 1 liter B. Vacuum Pump 5m^3 / h The final vacuum level is 2 *m*bar.
 (A)  (B)	A. Fabric (peel ply) B. Infusion mesh
 (A)  (B)	A. Release film(G-lease 200 Y) B. Vacuum Nylon (G- bag 200)

Table 2.4. Properties of Materials

No	Materials	Weight gr/m^2	Weaving	Width cm	Warp /Weft
1	E-Glass fiber	600	unidirectional	127	EC – 0^0

No	Materials	Operation time 20 C^0	Mixing ratio		Duration of mold	Application temperature		
			Weight	volumetric		50 C^0	60 C^0	80 C^0
2	Epoxy	60 min	100/25	100/30	24 hours	70	87	92
3	Hardener	60 min	100/25	100/30	24 hours	70	87	92

No	Materials	color	Weight g/m^2	Width cm	Warp / weft
4	Fabric (peel ply)	Red	83	80 - 160	19 * 19

No	Materials	Color	Width	Temperature	Ingredient
5	Infusion mesh	green	120 cm	115 C^0	PE

No	Materials	color	Thickness µm	Tension %	Working temp. Max	Ingredient
6	Release film (G-lease 200 Y)	Yellow	30	500	153 C^0	PP

No	Materials	color	Thickness µm	Tension %	Working temp. Max	Description
7	Vacuum Nylon G- bag 200	Green	50	400	200 C^0	General,vacuum ,infusion

2.8.1. Production of composite laminates in laboratory

VARI method was used to produce the specimens. 16 and 50 plies of unidirectional E-glass fiber and epoxy resin are used, as described in the following steps:

A unidirectional E-glass fiber having density of 600 g/m^2 was used as reinforcing material as shown in Figure 2.16

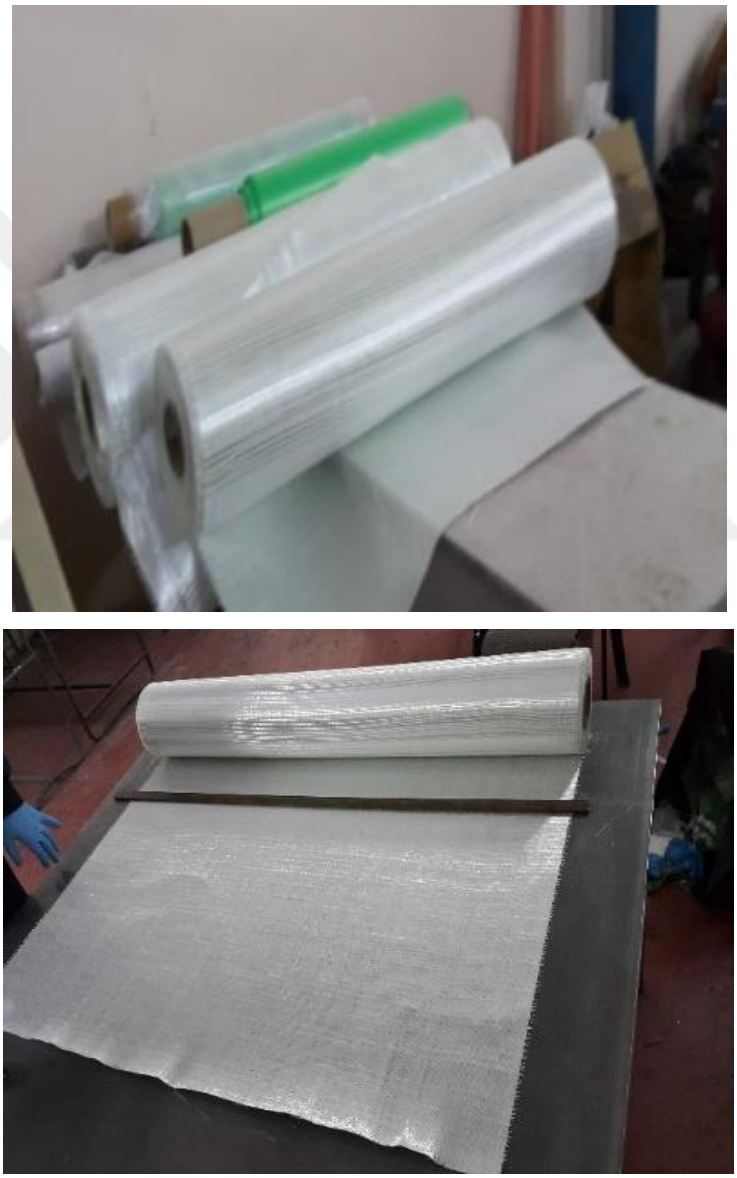

Figure 2.16. E-glass fiber roll

The table (heating mold) is coated with a release agent and 16 or 50 plies of fibers with [0°/90°], [30°/60°], [-45°/45°] orientations are placed on to the table for each plate, based to angle sequence, as shown in Figure 2.17.

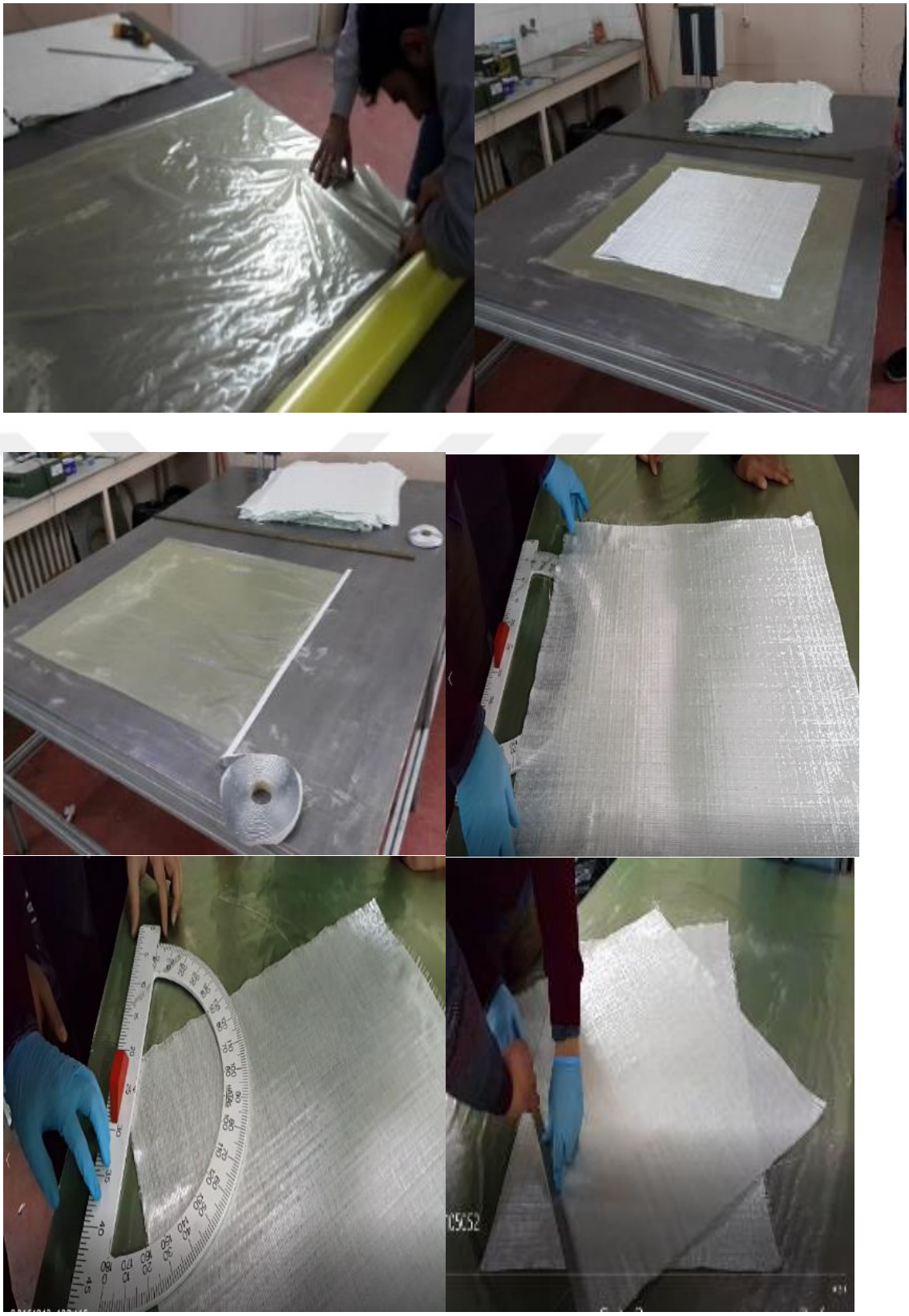

Figure 2.17. Heated table coated with release agent and fibers were placed

Peel ply is placed on the fiber plies and infusion mesh is placed on the peel ply, as shown in Figure 2.18.

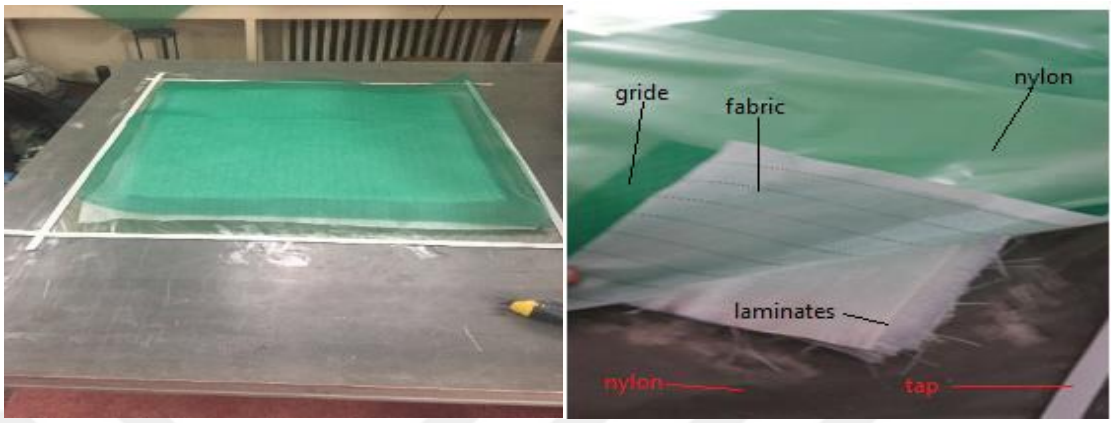

Figure 2.18. Peel ply and infusion mesh

Spiral hoses connected by a T pipe are along the right end of the resin distribution parts. Because of gaps between the hoses and the connecting pipe, tape is wrapped around the hose tips. The hoses are then put onto a teflon film of 5 cm from the fibers' left edge. Breather materials are used for continuity. The fibers and hoses have a distance between them so that no resin flows into the hose of the vacuum. After, this stack was covered with sealant tape. The result is shown in Figure 2.19.

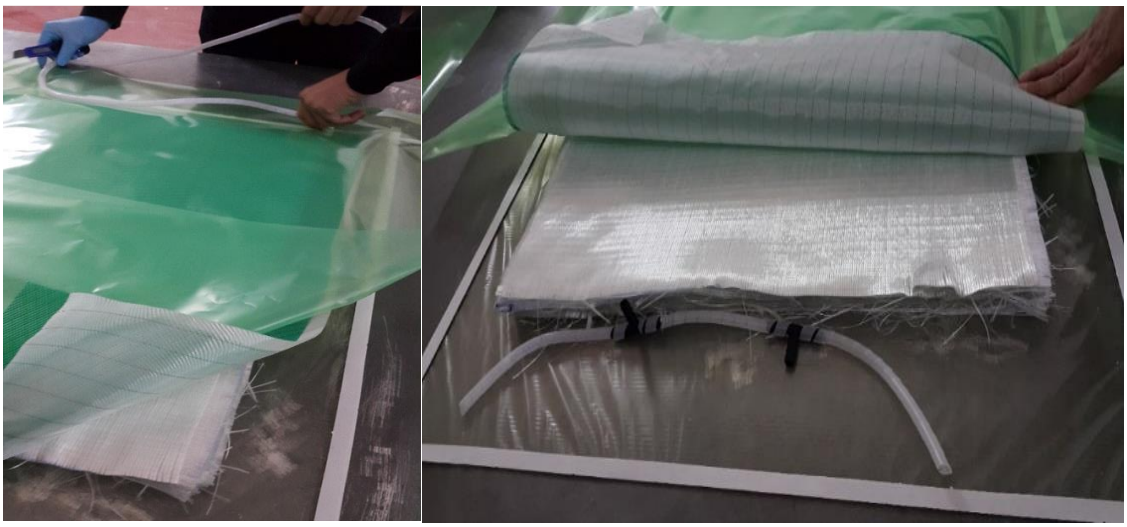

Figure 2.19. Spiral hoses and the T pipe

The vacuum bag is pasted carefully onto the tape once the top is removed. Two holes remain on the pipes to connect the vacuum and resin hoses. As such, the entirity was covered by a vacuum bag. This is shown in Figure 2.20.

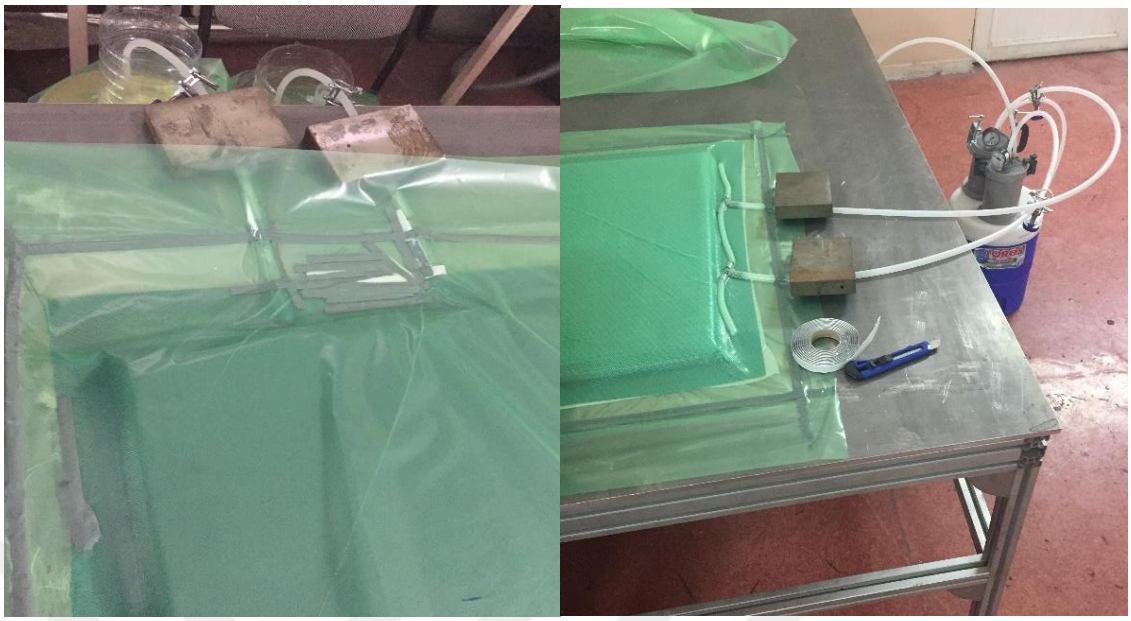

Figure 2.20. The sealant tape

Clamps were used to connect the pipes with the vacuum and hoses. Tape on the pipe and hoses stopped leakage from the vacuum. Sticky tape was then used to conect the security bar with the vacuum and hoses. A PLC touch panel was used to check for leakage after the procedure, as shown in Figure 2.21.

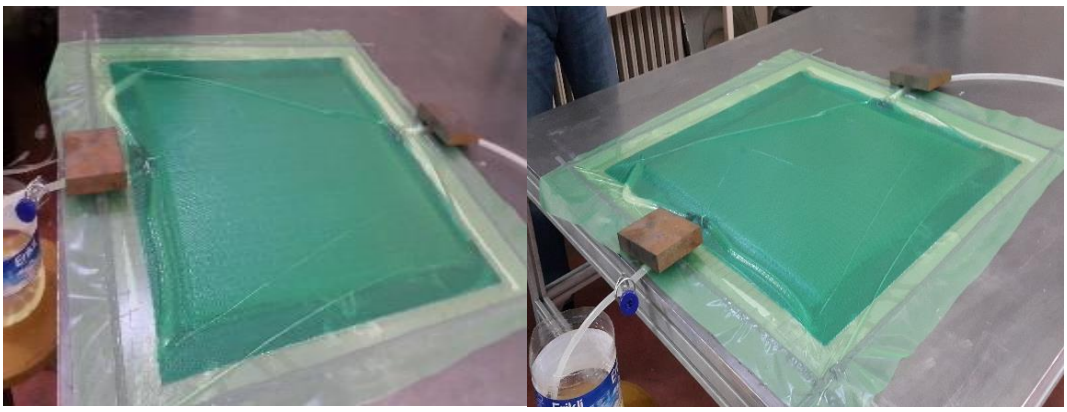

Figure 2.21. Checking vacuum

As the resistance temperature increased to 50°C, resin and hardner were placed in a container in a 3:1 ratio (MGS LH 160). The mixture was then mixed for five minutes until reaching 60°C. The resin infusion began after 50°C was reached as the resistance temperature. This process is shown in the following four pictures. The composite's thickness at the end was 8 mm for thin and 25 mm for thick composites. Curing took place for 24 hours at 20°C after the infusion. Then the last fiber ply is resined , as shown in Figure 2.22.

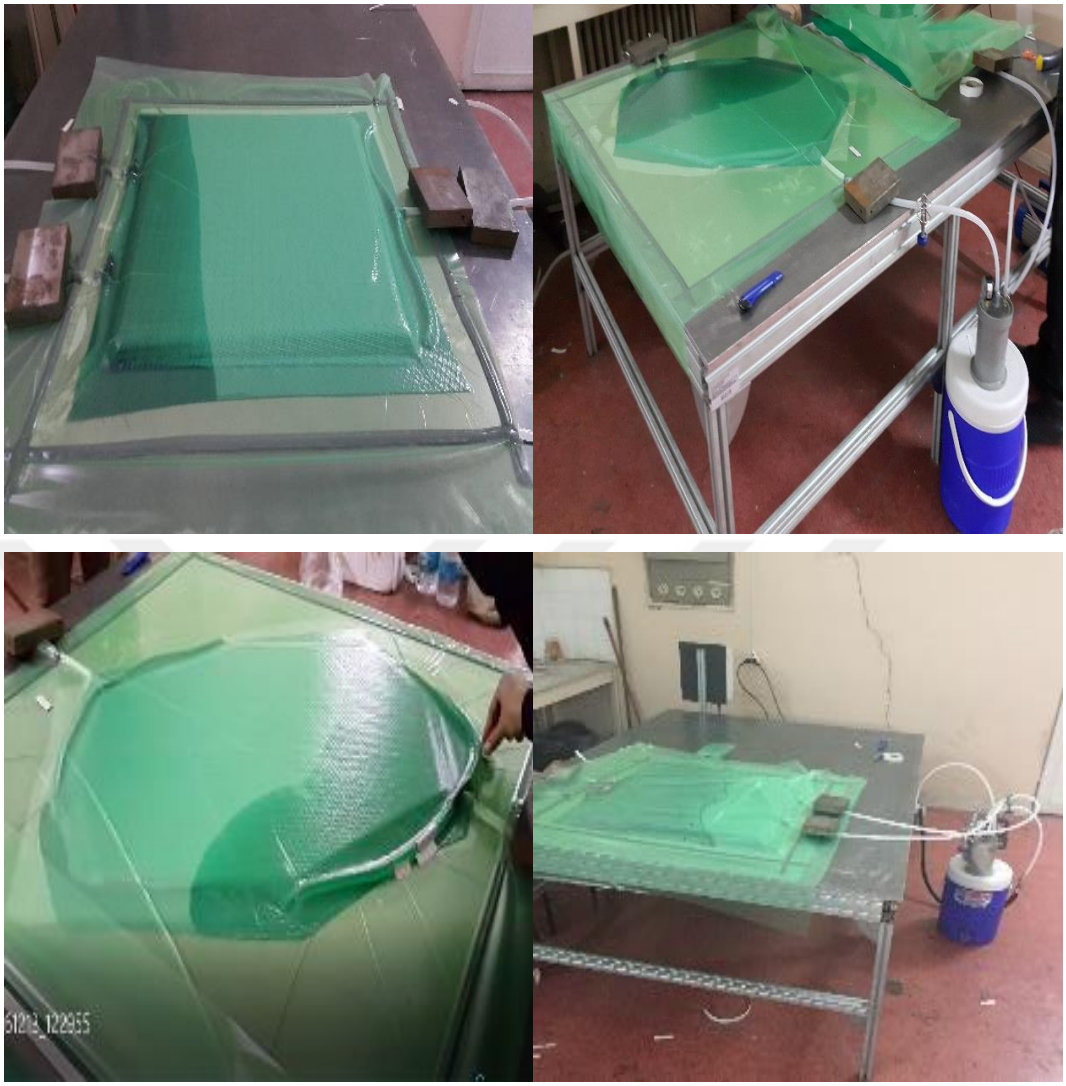

Figure 2.22. The resin infusion process is initiated

2.8.2. Specimens cutting process

After production process, excessive region of specimens was cut by the cutting machine is shown in the pictures below . The DAWALT cutting machine is a capable tool which is used for cutting variety of materials. While cutting is performed, tool uses pressure water for cooling, at cutting zone. This technique overcomes edge cracks and provide better finish quality. After cutting process is finished, the laminated composite were cut into squares shape of 100x100 mm as shown in Figure 2.23.

Figure 2.23. Cutting machine and specimens.

2.9. Ballistic Test System

The ballistic tests were carried out in the mechanics Laboratory Erciyes University by using the single -stage gas- gun (Figure 2.24).

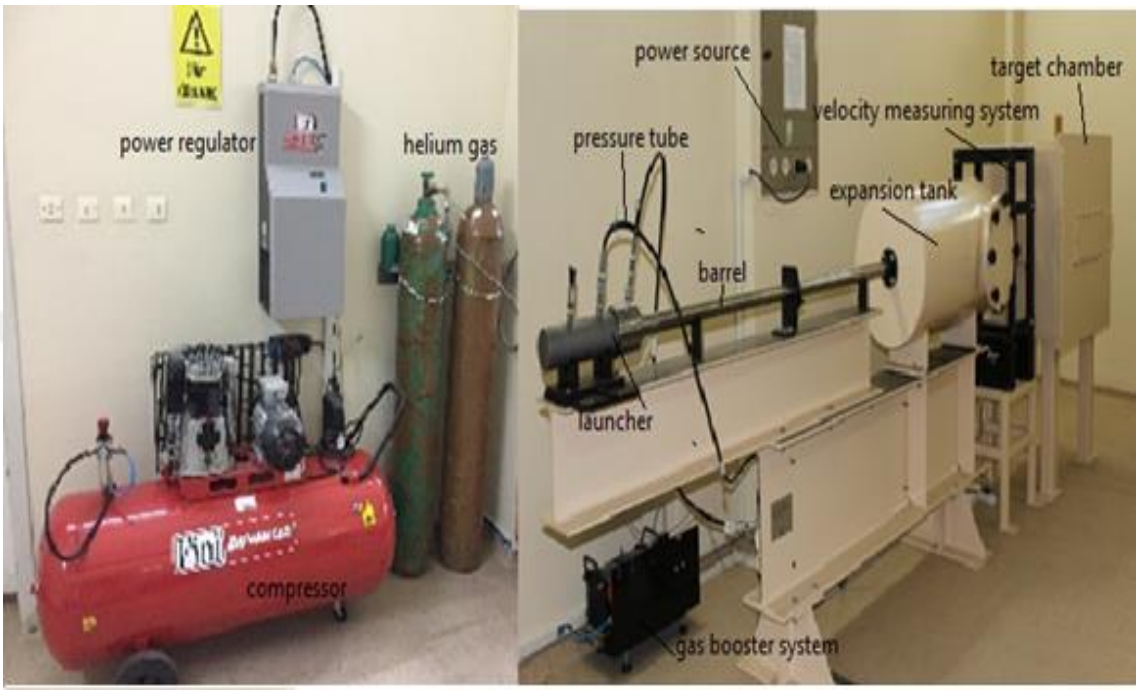

Figure 2.24. Ballistic testing system (Single- stage gas -gun).

In the gas weapon system, different types of gases such as air, nitrogen, and helium can be used to launch the bullet. The launcher system in the gas gun has a barrel of 12.7 mm in diameter and 1.8 m in length (Figure 2.25). The highest working pressure is 690 bar in the lancer system, different types of bullets can shoot at different velocities. Using different pressures and diaphragms, it can shoot with high sensitivity in the velocity range of 300 m/s to 1200 m/s.

The launcher system consists of three chambers separated by diaphragms made of metal or polymer material (Figure 2.26). The first chamber is pressurized with gas at a lower pressure than the diaphragm burst pressure, then the pressure in the first chamber is increased to two times after the second chamber is removed by the same pressure.

By suddenly discharging the gas in the secondary chamber, diaphragm burst and high-pressure gas pass the bullet in the last chamber. The bullet is placed in a sabot made from polymer, associated with the last chamber of the launcher system in the barrel.

Sabot is one of the most critical parts of the gas weapon system (Figure 2.27). Because it allows the bullet to steer and reach the target properly.

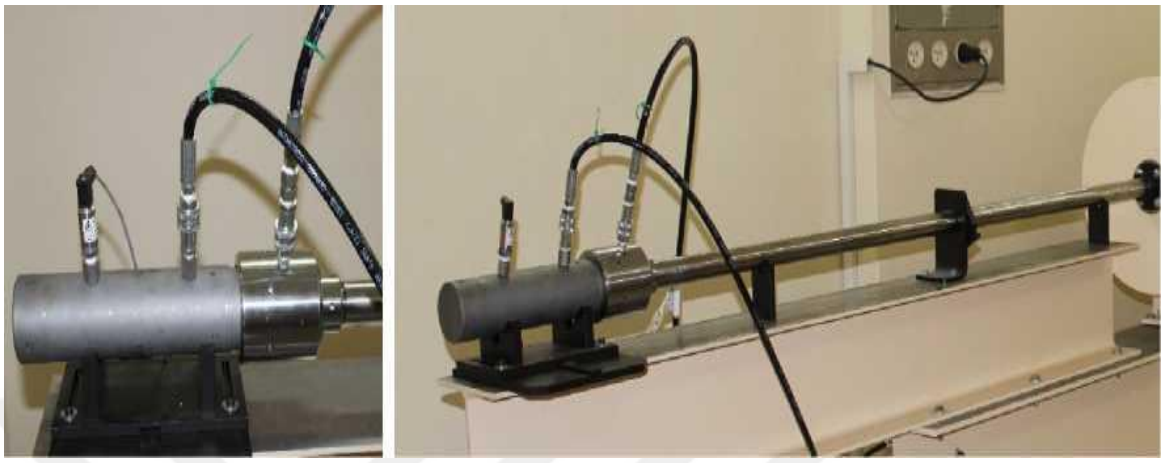

Figure 2.25. The launcher system.

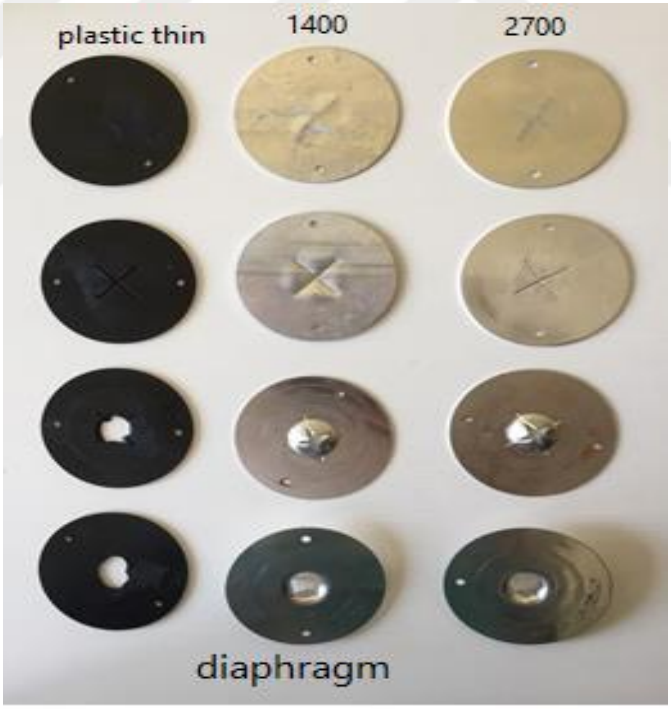

Figure 2.26. Diaphragms.

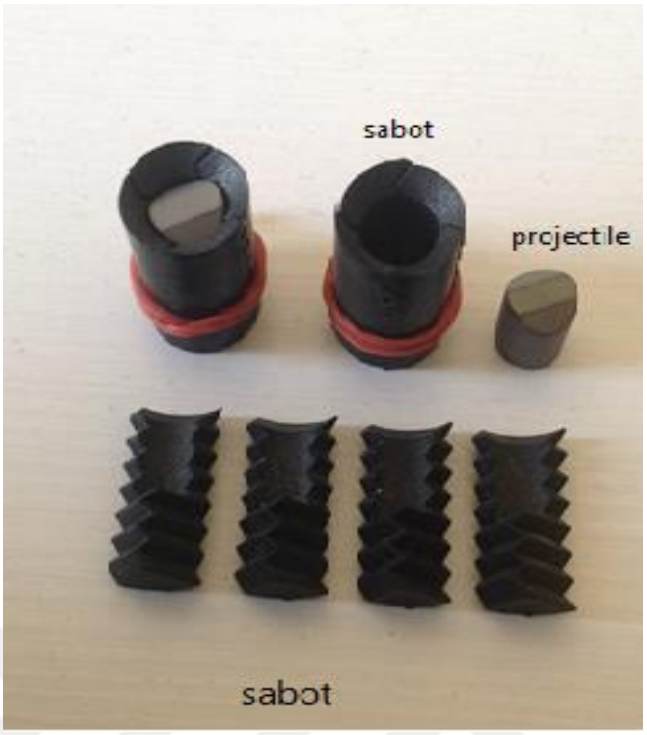

Figure 2.27. Sabot.

In the tests, the measurement of the bullet speeds is carried out with the velocity measurement system integrated into the gas gun system (Figure 2.28). The system works with the principle of finding the bullet speed by calculating the time taken to cut two beams having light curtain with a fixed distance between them.

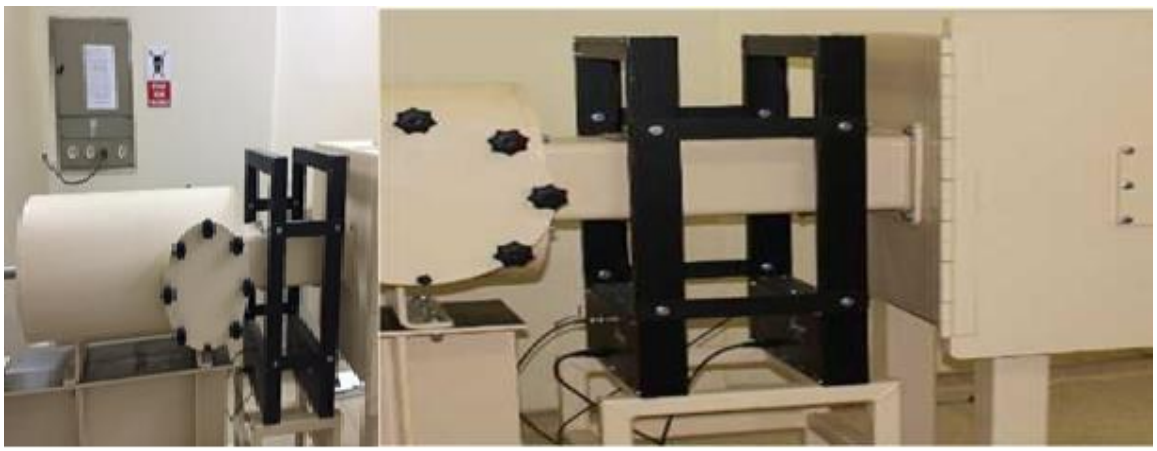

Figure 2.28. Velocity measurement system.

The pressurization and ignition mechanism of the gas weapons site is made by a computer controlled unit using software developed by the supplier company.

The apparatus is designed for the sample connection in accordance with the sample sizes and to form the boundary condition of the problem (Figure 2.29).

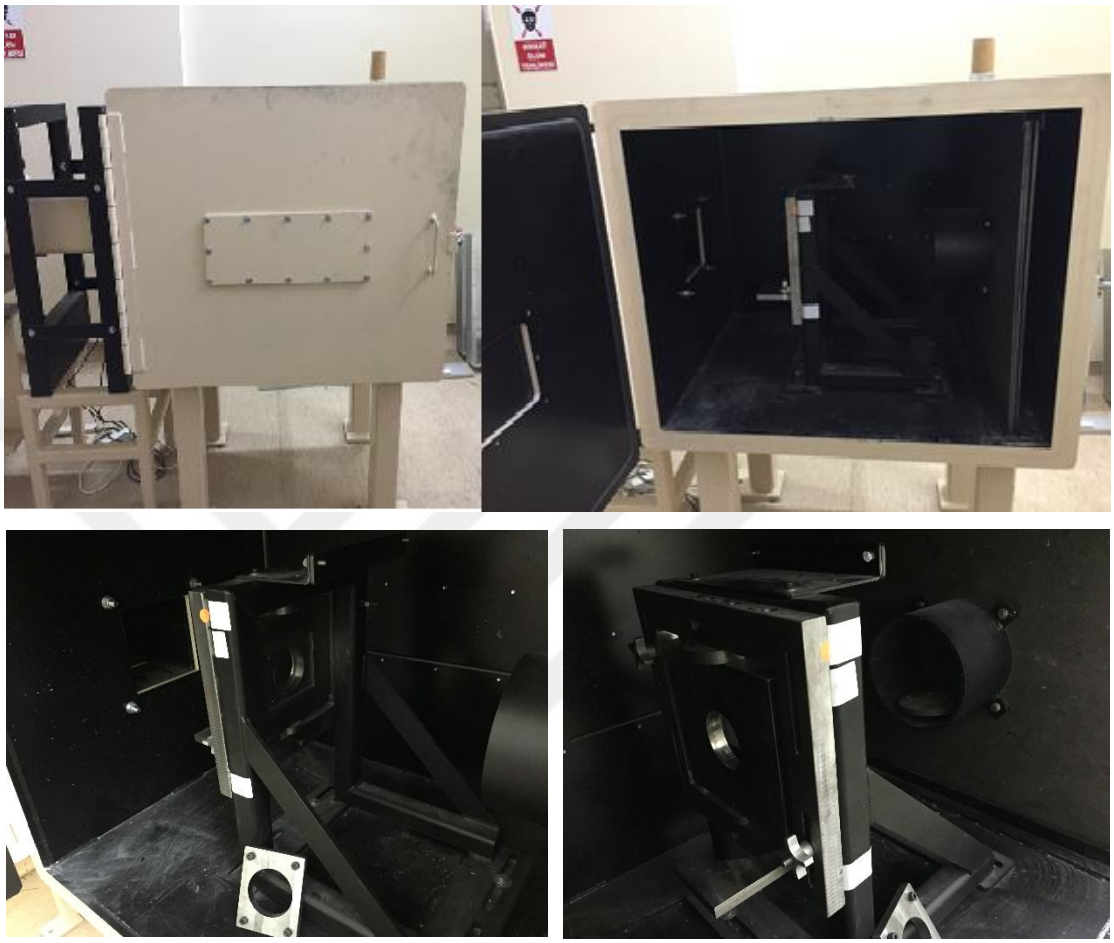

Figure 2.29. The chamber and target binding apparatus.

CHAPTER THREE

EXPERIMENTAL RESULTS AND DISCUSSIONS

3.1. Overview

This section is divided into two parts: first part has given information about results that have got from experimental by ballistic impact system and second part has given information about discussion of these results.

The ballistic behavior of two types of (E-glass /Epoxy) laminated composites, thick one with 25 mm thickness and thin with 8 mm thickness having different staking sequences of reinforcement's fiber orientation $[30^{\circ}/60^{\circ}]_{A}$, $[0^{\circ}/90^{\circ}]_{A}$, $[-45^{\circ}/+45^{\circ}]_{A}$ was investigated experimentally at room temperature under different bullet velocities.

Note that all of those thick and thin laminated composites were impacted by shooting one kind of projectile and all the damaged composites were visually inspected and photographed.

3.2. Experimental Schedule

Tables 3.1 – 3.6 shows the experimental schedules which are include experimental conditions. All experiments were performed using this scheme.

Table 3.1. The First Experiment

0.30 caliber FSP						
ID	Diaphragm (psi)	Pressure (bar)	Velocity (m/s)	Type	Angle (degree)	Thickness (mm)
Thin	Plastic thin	44	447.6	Glass fiber	(0,90)	8
Thin	1400	160	743.6	Glass fiber	(0,90)	8

Table 3.2. The Second Experiment

0.30 caliber FSP						
ID	Diaphragm (psi)	Pressure (bar)	Velocity (m/s)	Type	Angle (degree)	Thickness (mm)
Thick	Plastic thin	44	461.4	Glass fiber	(0,90)	25
Thick	1400	160	760.1	Glass fiber	(0,90)	25
Thick	2700	220	861.4	Glass fiber	(0,90)	25

Table 3.3. The Third Experiment

0.30 caliber FSP						
ID	Diaphragm (psi)	Pressure (bar)	Velocity (m/s)	Type	Angle (degree)	Thickness (mm)
Thin	Plastic thin	44	450.3	Glass fiber	(-45,+45]	8
Thin	1400	160	764.8	Glass fiber	(-45,+45)	8

Table 3.4. The Fourth Experiment

0.30 caliber FSP						
ID	Diaphragm (psi)	Pressure (bar)	Velocity (m/s)	Type	Angle (degree)	Thickness (mm)
Thick	Plastic thin	44	450	Glass fiber	(-45,+45)	25
Thick	1400	160	762.7	Glass fiber	(-45,+45)	25
Thick	2700	220	844.8	Glass fiber	(-45,+45)	25

Table 3.5. The Fifth Experiment

0.30 caliber FSP						
ID	Diaphragm (psi)	Pressure (bar)	Velocity (m/s)	Type	Angle (degree)	Thickness (mm)
Thin	Plastic thin	44	455	Glass fiber	(30,60)	8
Thin	1400	160	750.1	Glass fiber	(30,60)	8

Table 3.6. The Sixth Experiment

0.30 caliber FSP						
ID	Diaphragm (psi)	Pressure (bar)	Velocity (m/s)	Type	Angle (degree)	Thickness (mm)
Thick	Plastic thin	44	447.1	Glass fiber	(30,60)	25
Thick	1400	160	763.4	Glass fiber	(30,60)	25
Thick	2700	220	844	Glass fiber	(30,60)	25

3.3. Experimental Results and Discussion

The following experiments were carried out in order to determine the ballistic impact damages on thick and thin laminate composites. A total of 15 composite plates were produced from E-glass/Epoxy unidirectional laminate for each thin (16 plies) and thick (50 plies) specimens. Three anti-symmetric stacking sequences of reinforcements fiber orientation [30˚/60˚], [0˚/90˚], [-45˚/+45˚] were chosen for this study. The samples were tested at three different velocities, where the average of the first velocity was approximately 452 m/s, the average of the second velocity is approximately 758 m/s and the average of the third velocity is approximately 850 m/s for each types of thin and thick plates.

Each plate was fired by the same type of bullet. The bullets have the same shape, however the impact velocities and fiber stacking were varied during the experiments. It is difficult to model every event in ballistic impact, but this section presents one based on delamination from inter-laminar shear stress that occur from penetration of the projectile into the plate. When the bullet connects with the laminate, the sequence is:

1. Initial contact after bullet connects with surface
2. Bullet starts deforming
3. A plug is made from the shear deformation of the composite
4. Plate bends because of bullet pressure
5. The plate has a stress wave as the bullet pushes the plug to move within the plate
6. Because of friction, there are forces in the plate near the bullet diameter and shear stresses begin in the plate’s inter-laminar areas from the penetration

The following discussions obtained from the result depending on the effect of angle orientation, effect of bullet velocity level and layer number effect (thickness effect).

3.3.1. Effect of layer number (thickness effect)

1(a). The stacking sequnce of $[0^{\circ}/90^{\circ}]_A$ at the first velocity

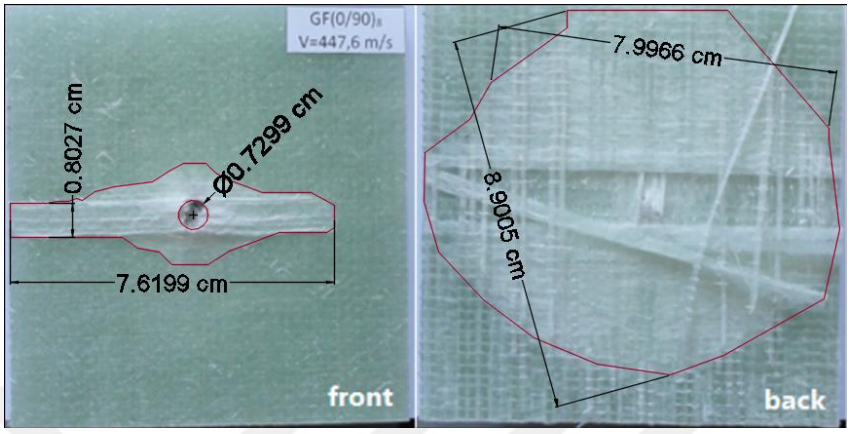

a) Damages on the front and back surface of the thin specimen after ballistic impact (V= 447.6 m/s) (perforation case).

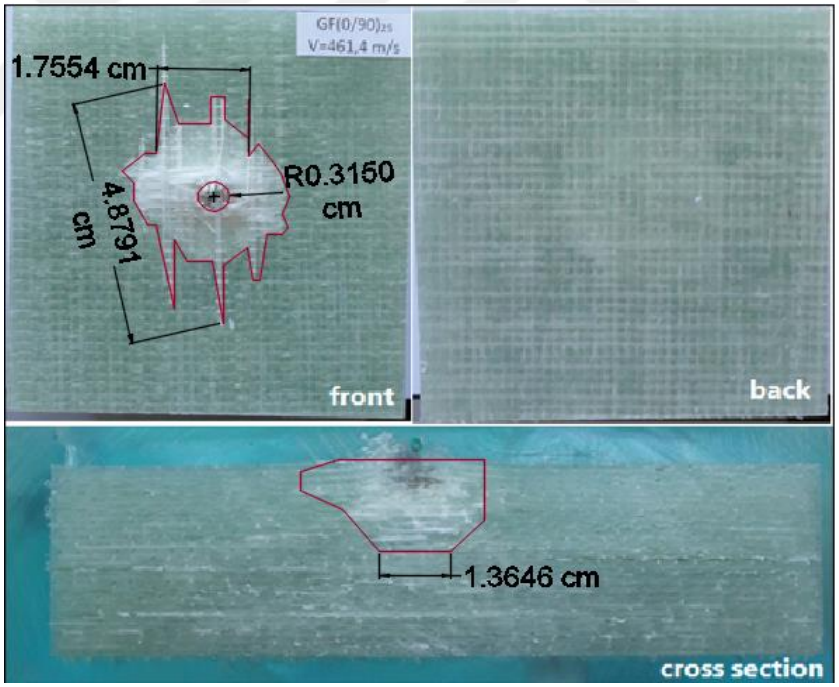

b) Damages on the front and back surface and cross-section through of the thick specimen after ballistic impact (V= 461.4 m/s) (partial penetration case).

Figure 3.1.Visual inspection of damages on thin and thick composite plates.

Figure 3.1 shows the damages on thin and thick composite plates after ballistic impact. Damages area of the thin plate was measured as 9.91 cm^2 on the front face and 62.30 cm^2 on the back face. For thick plate, the frontal area of damage was 9.95 cm^2 which no

damage was observed on the back face. The area of delamination in the cross-section of the thick plate is 4.93 cm^2.

1(b). The stacking sequnce of $[0^{\circ}/90^{\circ}]_A$ at the second velocity

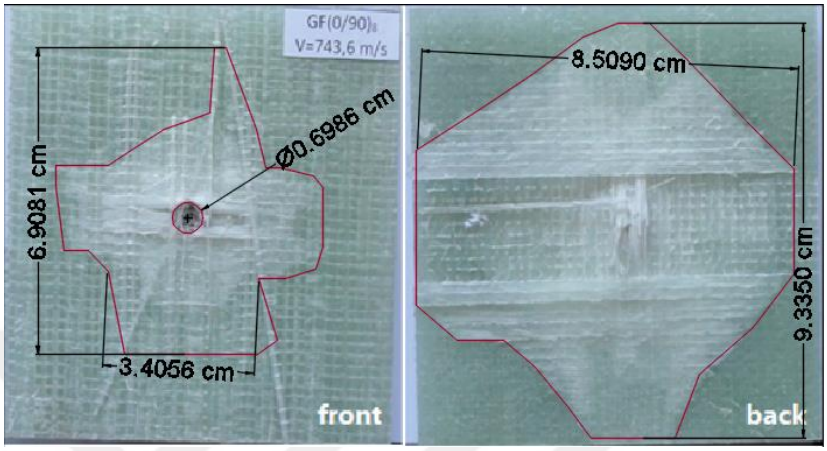

a) Damages on the front and back surface of the thin specimen after ballistic impact (V= 743.6 m/s) (perforation case).

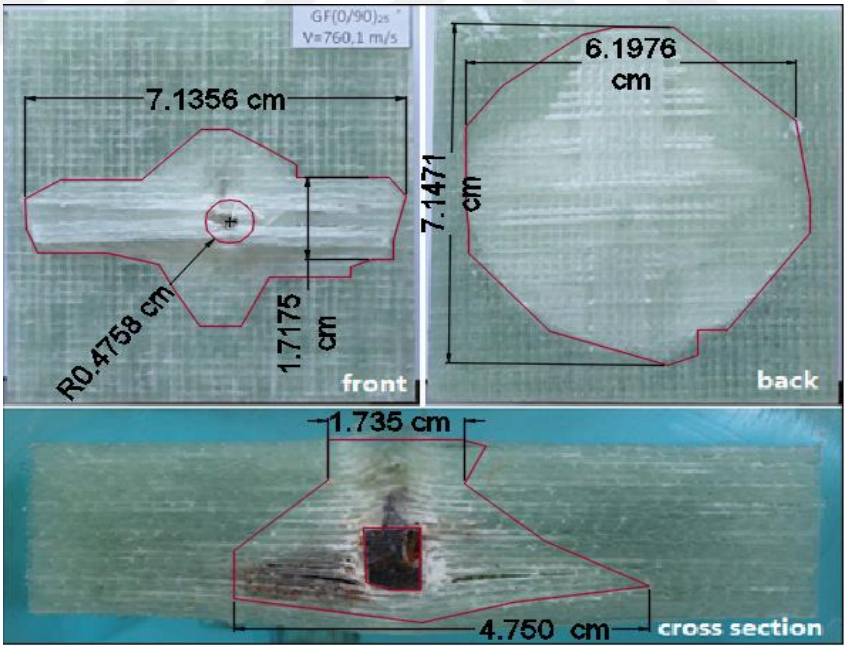

b) Damages on the front and back surface and cross-section through of the thick specimen after ballistic impact (V= 760.1 m/s) (penetration case).

Figure 3.2. Visual inspection of damages on thin and thick composite plates.

Figure 3.2 shows the damages on thin and thick composite plates after ballistic impact. Damages area of the thin plate was measured as 23.75 cm^2 on the front face and 55.27

cm^2 on the back face. For thick plate, the frontal area of damage was 16.20 cm^2 and 34.32 cm^2 on the back face. The area of delamination in the cross-section of the thick plate is 16.31 cm^2. This impact velocity leads to delamination, shear plugging and breakage fiber especially in back face and cross section while in front face for each samples limited deformation compared with back face.

1(c). The stacking sequnce of $[0^{\circ}/90^{\circ}]_A$ at the third velocity

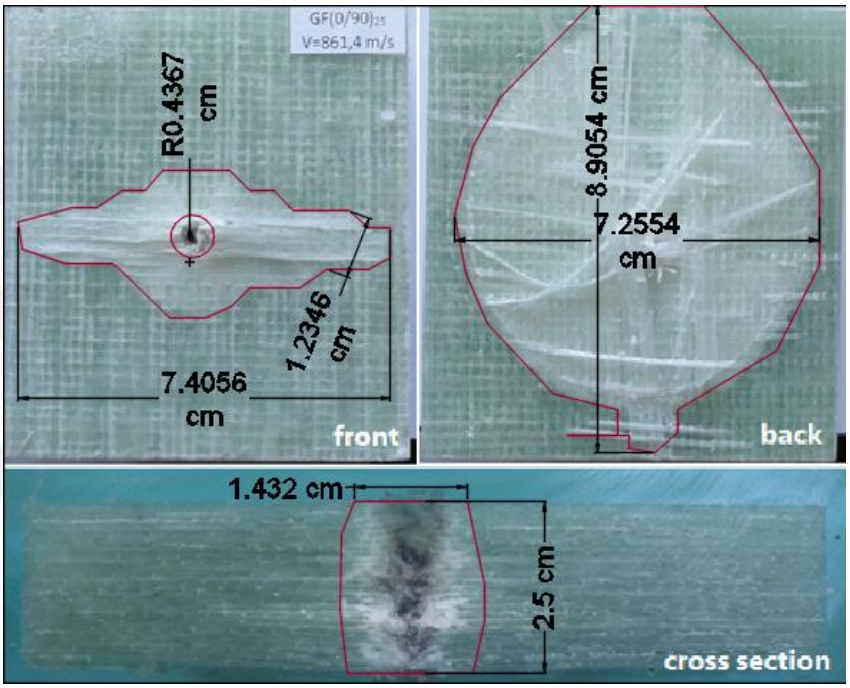

Figure 3.3. Visual inspection of damages on thick composite plates (V= 861.4 m/s) (penetration case).

Figure 3.3 shows the damages on thick composite plates after ballistic impact. Damaged area of the thick plate was measured as 12.37 cm^2 on the front face and 45.63 cm^2 on the back face. The area of delamination in the cross-section of the thick plate is 9.18 cm^2. This impact velocity leads to little delamination area surrounding by the bullet penetrating area, and increased hole depth because of high velocity of the bullet, and larger damage on the back face (matrix crushing and breakage fiber) compared with the front face.

2(a). The stacking sequnce of $[-45^{\circ}/+45^{\circ}]_A$ at the first velocity

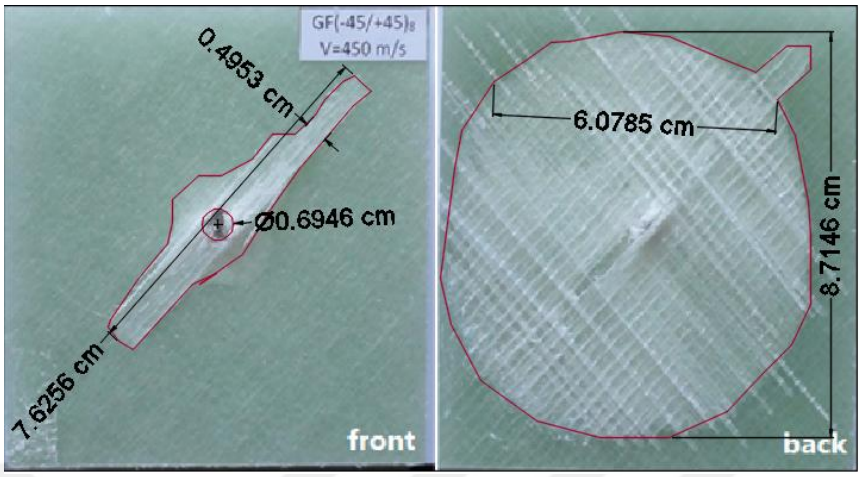

a) Damages on the front and back surface of the thin specimen after ballistic impact (V= 450 m/s) (perforation case).

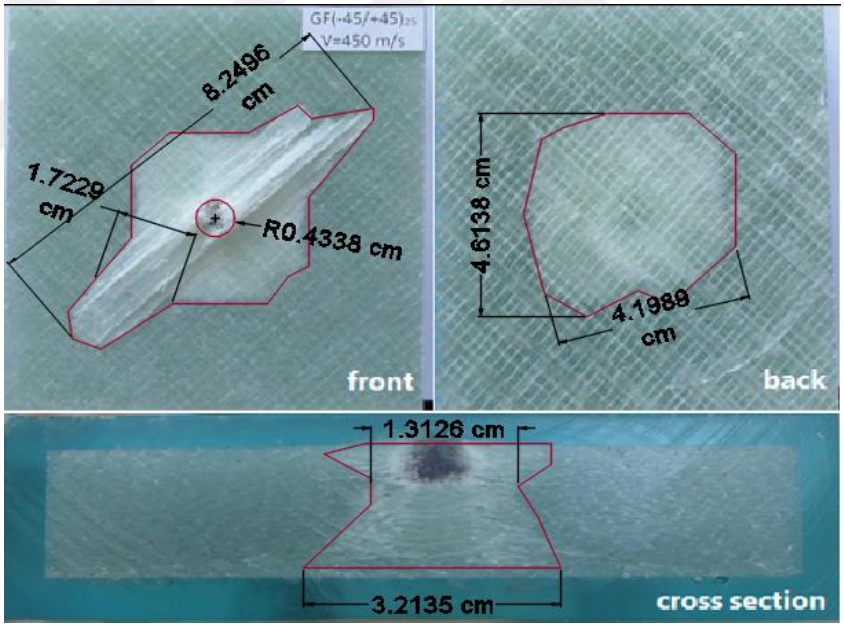

b) Damages on the front and back surface and cross-section through of the thick specimen after ballistic impact (V= 450 m/s) (partial penetration case).

Figure 3.4. Visual inspection of damages on thin and thick composite plates.

Figure 3.4 shows the damages on thin and thick composite plates after ballistic impact. Damages area of the thin plate was measured as 8.21 cm^2 on the front face and 56.81 cm^2 on the back face. For thick plate, the frontal area of damage was 17.89 cm^2 which damage was observed 16.62 cm^2 on the back face. The area of delamination in the cross-section of the thick plate is 11.64 cm^2. It is observed that damage sizes in the thin

plate are bigger than those of thick plate in which the thin specimen absorbed the shock of the bullet by its more flexible structure.

2(b). The stacking sequnce of $[-45^{\circ}/+45^{\circ}]_A$ at the second velocity

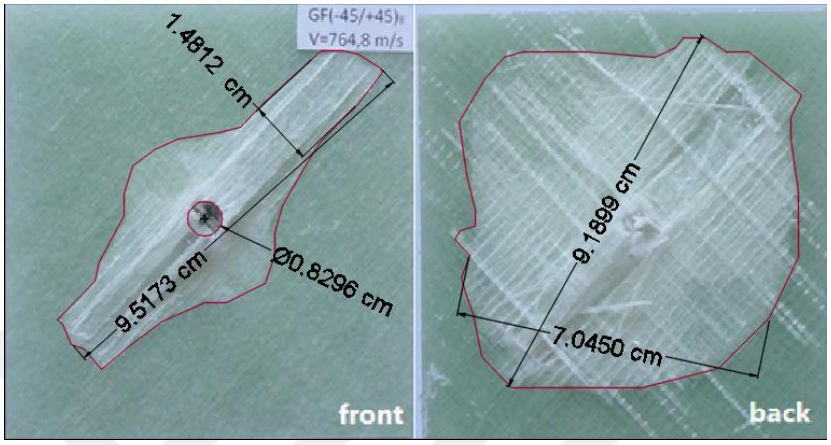

a) Damages on the front and back surface of the thin specimen after ballistic impact (V= 764.8 m/s) (perforation case).

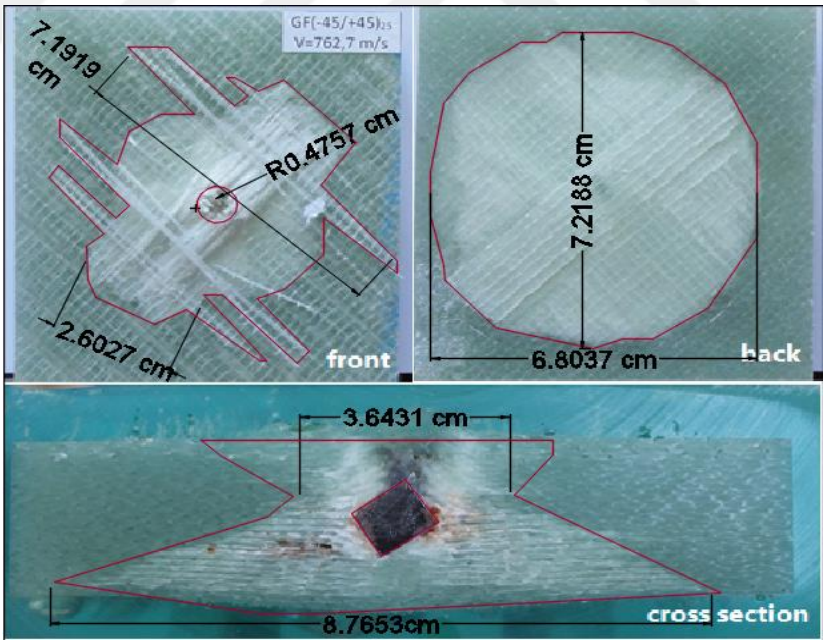

b) Damages on the front and back surface and cross-section through of the thick specimen after ballistic impact (V= 762.7 m/s) (penetration case).

Figure 3.5. Visual inspection of damages on thin and thick composite plates.

Figure 3.5 shows the damages on thin and thick composite plates after ballistic impact. Damages area of the thin plate was measured as 20.76 cm^2 on the front face and 53.85 cm^2 on the back face. For thick plate, the frontal area of damage was 22.29 cm^2 which

damage was observed 39.92 cm^2 on the back face. The area of delamination in the cross-section of the thick plate is 26.53 cm^2. It is observed damage sizes in the thin plate are bigger than those of thick plate. However, occurred delamination, which is form through the cross-section of thick composite. Beside that fiber breakage and matrix crushing damages are observed on the front and back surfaces.

2(c). The stacking sequnce of $[-45^{\circ}/+45^{\circ}]_{A}$ at the third velocity

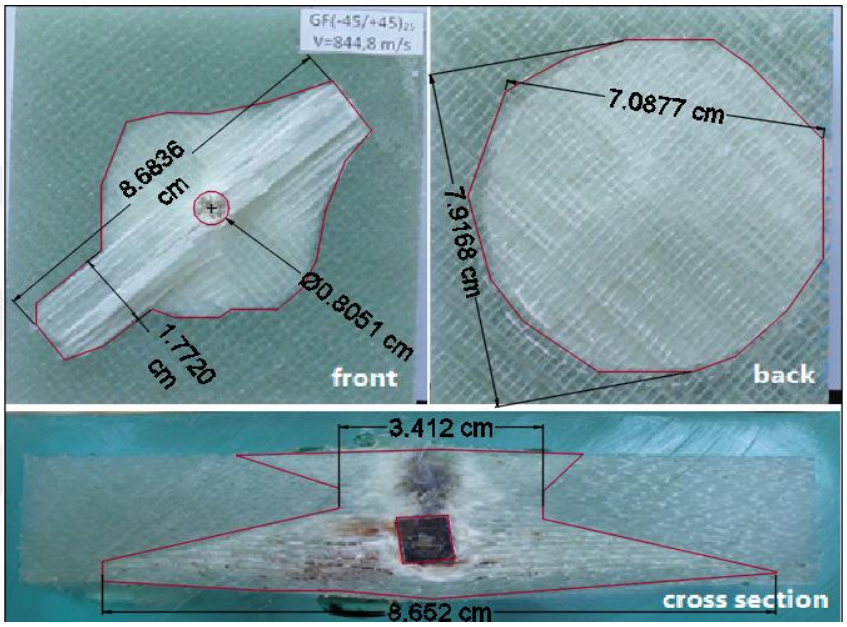

Figure 3.6. Visual inspection of damages on thick composite plates (V= 844.8 m/s) (penetration case).

Figure 3.6 shows the damages on thick composite plates after ballistic impact. Damaged area of the thick plate was measured as 26.69 cm^2 on the front face and 48.38 cm^2 on the back face. The area of delamination in the cross-section of the thick plate is 27.22 cm^2. This impact velocity leads to large delamination area surrounding by the bullet penetrating area due to the bullet held by the thick plate having $[-45^{\circ}/+45^{\circ}]_{A25}$ stacking sequence. Moreover, increased damaged area on the back face can be characterized by bulge formation compared with the front face damage (matrix crushing and breakage fiber).

3(a). The stacking sequnce of $[30^{\circ}/60^{\circ}]_{A}$ at the first velocity

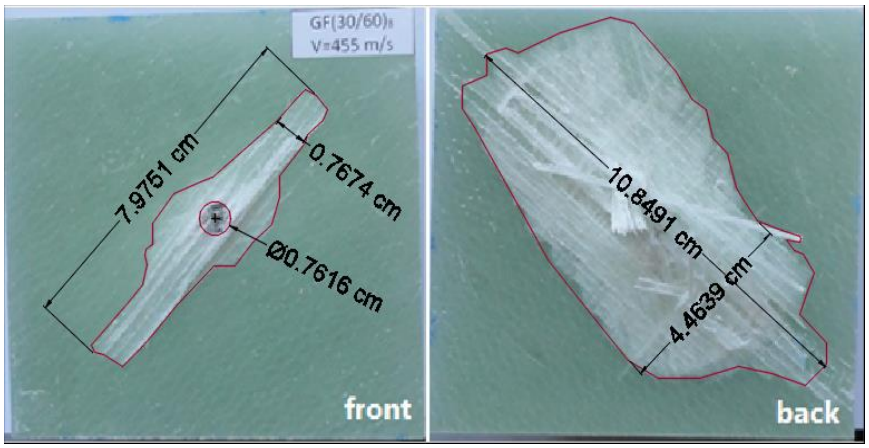

a) Damages on the front and back faces of the thin specimen after ballistic impact (V= 455 m/s) (perforation case).

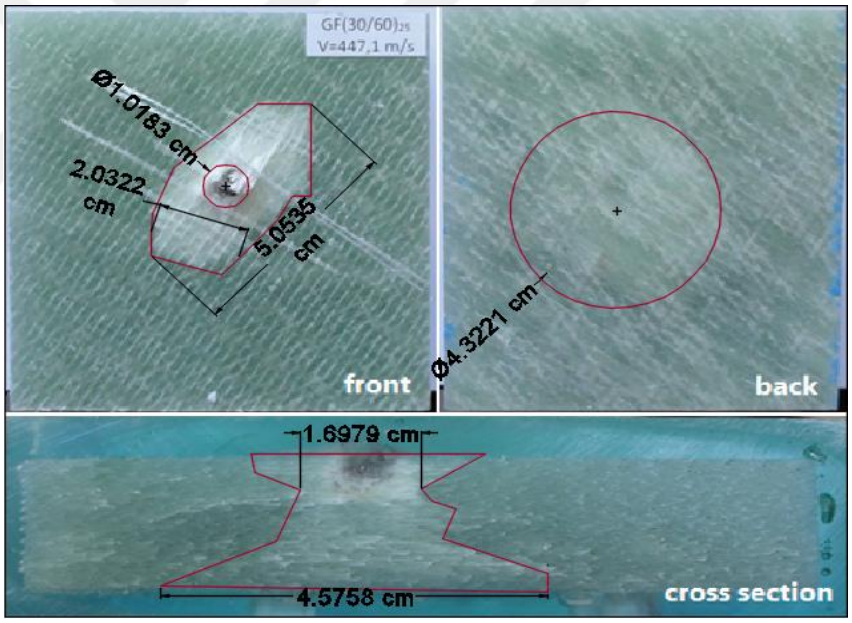

b) Damages on the front and back surface and cross-section through of the thick specimen after ballistic impact (V= 447.1 m/s) (partial penetration case).

Figure 3.7. Visual inspection of damages on thin and thick composite plates.

Figure 3.7 shows the damages on thin and thick composite plates after ballistic impact. Damages area of the thin plate was measured as 9.98 cm^2 on the front face and 41.86 cm^2 on the back face. For thick plate, the frontal area of damage was 9.46 cm^2 which damage was observed 14.67 cm^2 on the back face. The area of delamination in the cross-section of the thick plate is 15.25 cm^2. It is observed that damage sizes in the thin

plate are bigger than those of thick plate in which the thin specimen absorbed the shock of the bullet by its more flexible structure. It is also observed that through the cross section of thick composite more less delamination was observed the composite stacking sequence of $[30^{\circ}/60^{\circ}]_{A25}$.

3(b). The stacking sequnce of $[30^{\circ}/60^{\circ}]_{A}$ at the second velocity

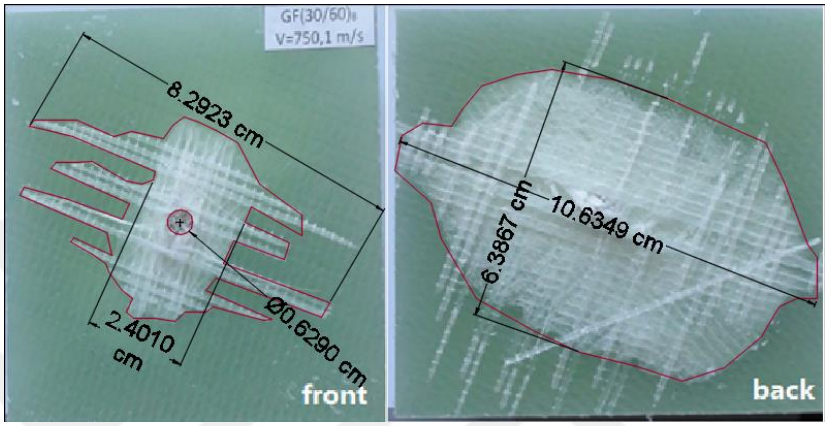

a) Damages on the front and back faces of the thin specimen after ballistic impact (V= 750.1 m/s) (perforation case).

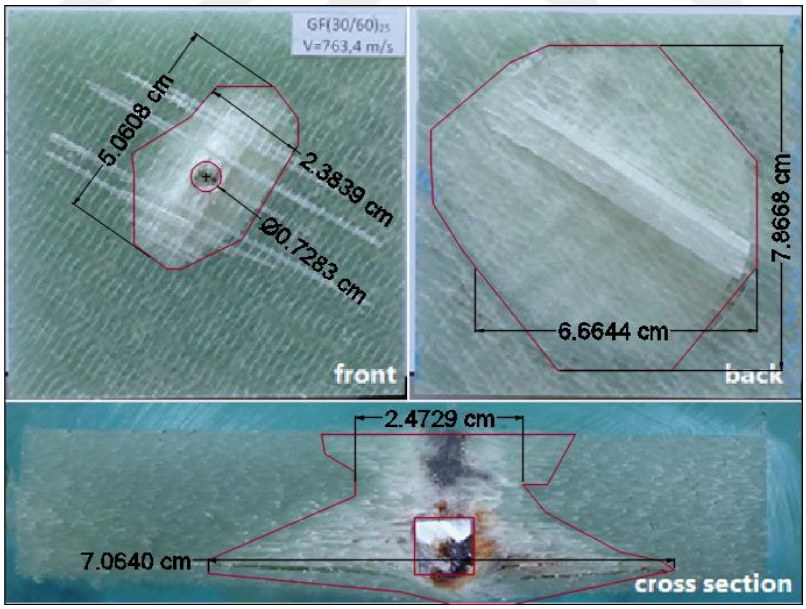

b) Damages on the front and back surface and cross-section through of the thick specimen after ballistic impact (V= 447.1 m/s) (penetration case).

Figure 3.8. Visual inspection of damages on thin and thick composite plates.

Figure 3.8 shows the damages on thin and thick composite plates after ballistic impact. Damages area of the thin plate was measured as 16.92 cm^2 on the front face and 49.97 cm^2 on the back face. For thick plate, the frontal area of damage was 12.01 cm^2 which

damage was observed 46.51 cm^2 on the back face. The area of delamination in the cross-section of the thick plate is 15.25 cm^2. It is observed that damage sizes in the thin plate are bigger than those of thick plate due to its flexible structure. However, in the thick plate is observed delamination which is bulge form through the cross section. However, Fiber breakage and matrix crushing damages are also observed on the front and back faces.

3(c). The stacking sequnce of $[30^{\circ}/60^{\circ}]_A$ at the third velocity

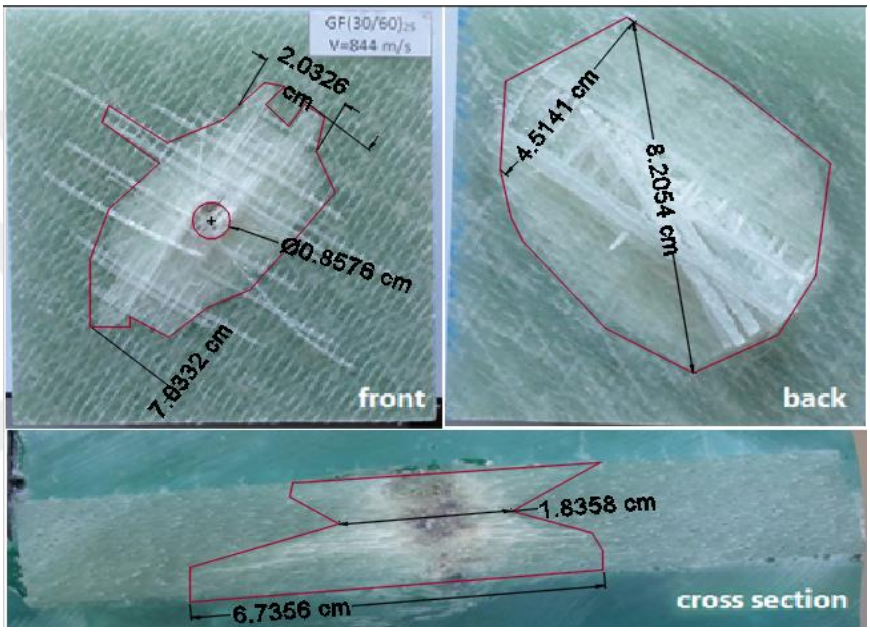

Figure 3.9. Visual inspection of damages on thick composite plates (V= 844 m/s) (perforation case).

Figure 3.9 shows the damages on thick composite plates after ballistic impact. Damaged area of the thick plate was measured as 19.28 cm^2 on the front face and 40.88 cm^2 on the back face. The area of delamination in the cross-section of the thick plate is 17.49 cm^2. Also, it is observed that the bullet can perforate the thick plate having $[30^{\circ}/60^{\circ}]_{A25}$ stacking sequence.

Comparison:

For Thin Laminates;

These observations were noted while studying thin laminates:

1. Size of damage depends more on the bullet size and shape than impact energy.
2. The stacking sequence of the laminated composite considerably affect the damage.
3. Damage is not always what is seen. For thin plates, the damage was also more at the back surface that at the front surface.

For Thick Laminates;

These observations were noted while studying thick laminates:

1. Damage is more related to bullet speed. Thus, slower bullets caused more damage than those of faster. Also, the damage relates to the laminate stacking sequence, with cross and angle-ply receiving more damage.
2. There is more damage at the point of exit than the point of entry.
3. Real damage is much more than what is seen.
4. Shear stresses cause failure, and this was seen by a model of the bullet penetration. The outer-ply is the first to fail. Delamination is caused by shear stress between the laminates.

It is concluded from the experiments on the thin and thick specimens that the greater the thickness of the sample the less the damage. The thin composites contain more damage than the thick composites at the same bullet velocity, due to their elastic structures.

3.3.2. Effect of bullet velocity level

1(a). The stacking sequnce of $[0^{\circ}/90^{\circ}]_{A8}$

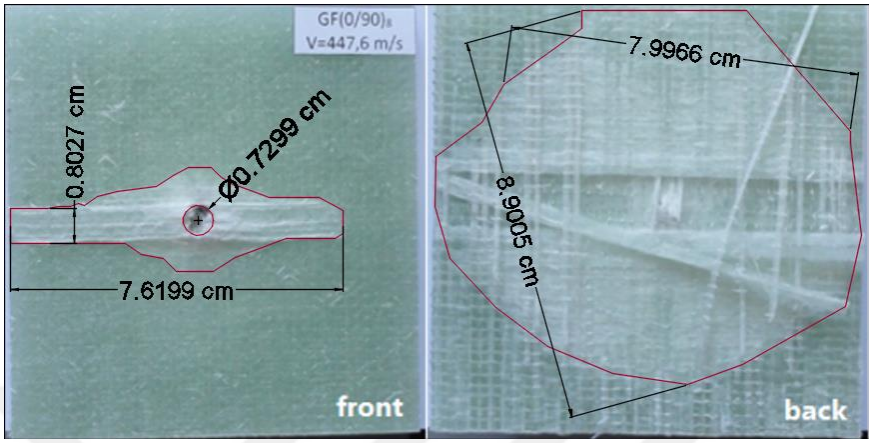

a) Thin plate at V_1=447.6 m/s, E_k= 286.5 J, A_{df} = 9.91 cm^2, A_{db} = 62.30 cm^2

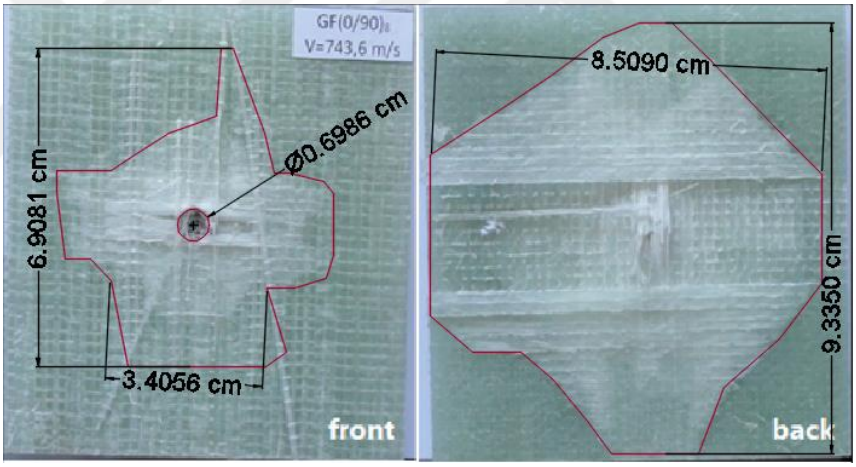

b) Thin plate at V_2=743.6 m/s, E_k= 790.7 J, A_{df} = 23.75 cm^2, A_{db} = 55.27 cm^2

Figure 3.10. Thin plate with $[0^{\circ}/90^{\circ}]_{A8}$ stacking sequence.

Figure 3.10 shows the front and back damages of the thin plates with $[0\circ/90\circ]_{A8}$ stacking sequence, subjected to tow different velocities of bullet when the velocity of projectile is equal to 447.6 m/s, the area of front damage (A_{df}) is 9.91 cm^2, the area of back damage (A_{db}) is 62.30 cm^2. However, when the velocity is increased to 743.6 m/s, the front surface damage area become 23.75 cm^2, the size of back surface damage become 55.27 cm^2 the plates were perforated both of two bullet velocities. Increased bullet velocity causes the area of damage on the front surface of the composite plate increases, while the area of damage on its back surface decreases. Matrix crush damage crush was

observed on the front of surfaces of the plates, while damage to the back surface was in the form of fiber breakage.

2. The stacking sequnce of $[0^{\circ}/90^{\circ}]_{A25}$

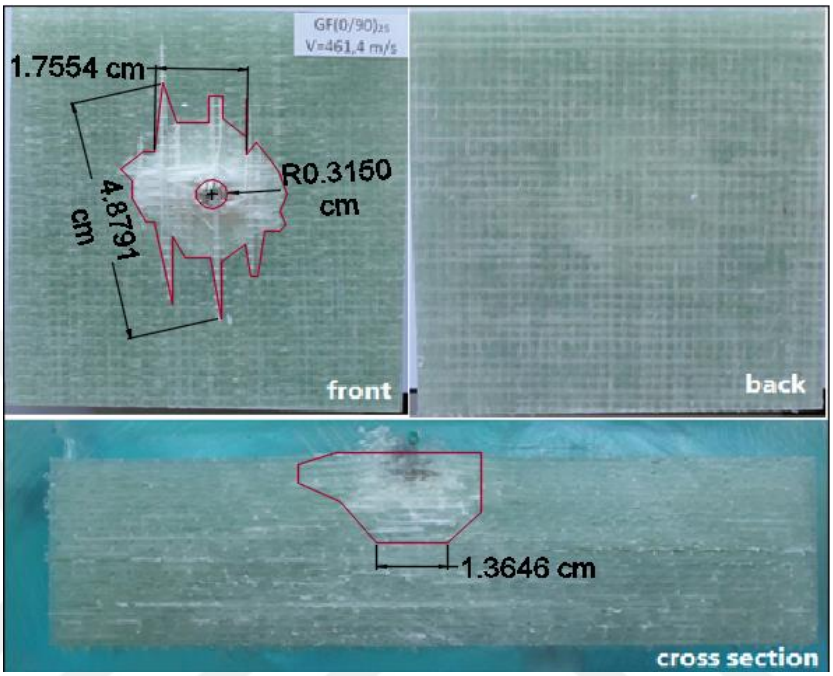

(a) Thick plate at V_1= 461.4 m/s, E_k= 304.4 J.

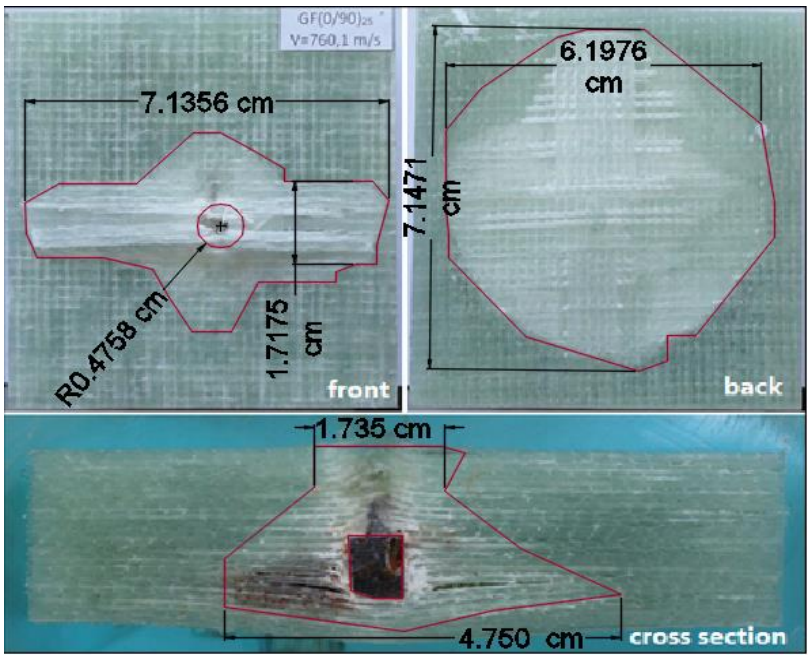

(b) Thick plate at V_2=760.1 m/s, E_k= 826.2 J.

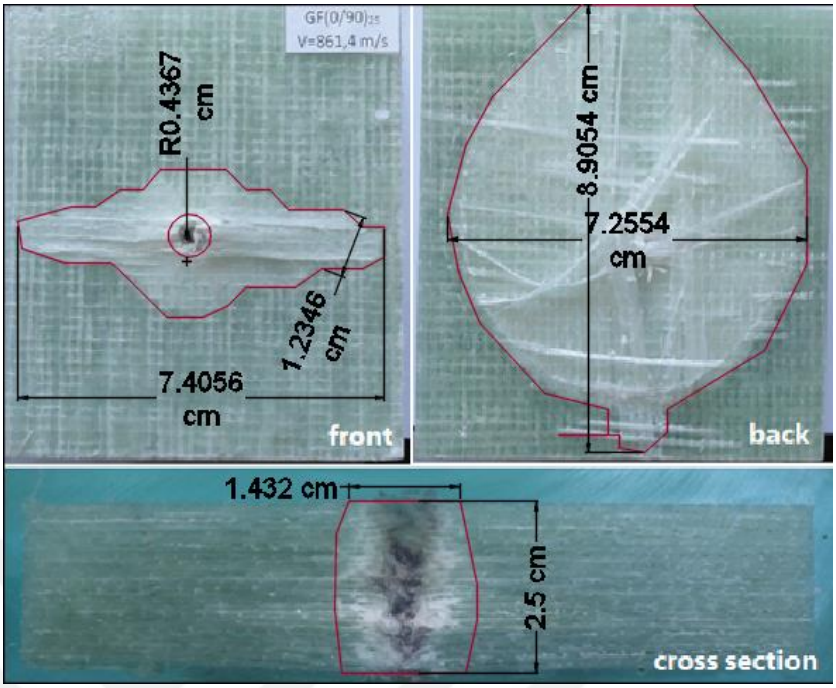

(c) Thick plate at V_3= 861.4 m/s, E_k= 1061.1 J.

Figure 3.11. Thick plate with $[0^{\circ}/90^{\circ}]_{A25}$ stacking sequence.

Figure 3.11 shows the damages that occur on the front and back surfaces and a cross-sectional area of the thick laminated composites subjected to three different velocities of bullet. it is observed that when the velocity of projectile is equal to 461.4 m/s, the damage area of the front surface (A_{df}) is 9.95 cm^2 and no damage was observed on the back surface of the plate. The bullet was rebounded after several layers have been damaged from the top surface of the plate (Figure 3.11 (a)). For figure (b), the bullet velocity is V_2=760.1 m/s which was penetrated through the plate. It is observed the matrix crushing and fiber breakage on the back surface of the plate, whereas, delamination and swelling through the cross-section of the plate. For figure 3.11 (c), the bullet velocity is V_3= 861.4 m/s which perforation case and damage area on the back surface is bigger than those of Figures (a) and (b).

3. The stacking sequnce of $[-45^{\circ}/+45^{\circ}]_{A8}$

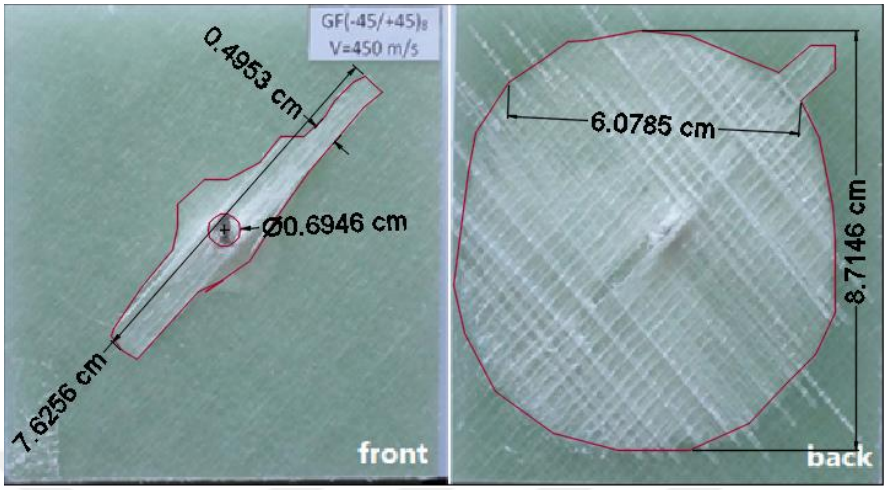

(a) Thin plate at V_1= 450 m/s, Ek= 290.6 J.

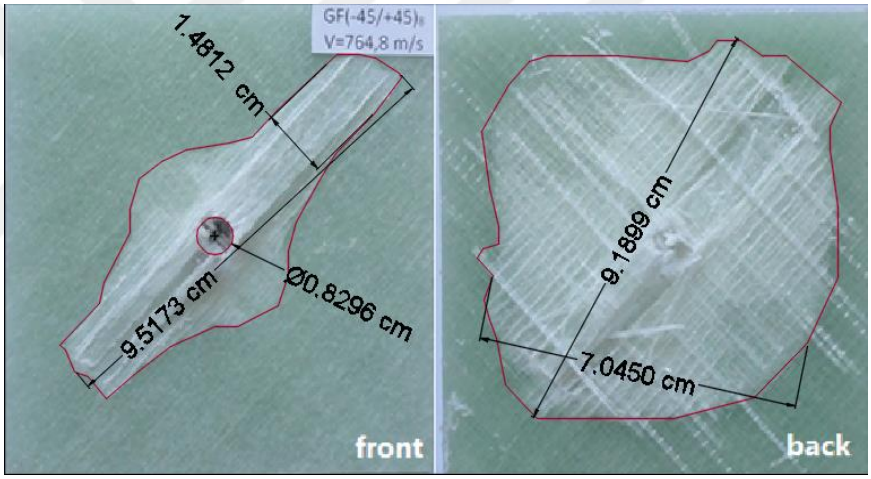

(b) Thin plate at V_2= 764.8 m/s, Ek= 836.4 J.

Figure 3.12. Thin plate with $[-45^{\circ}/+45^{\circ}]_{A8}$, stacking sequence.

Figure 3.12 Shows the front and back damages of the thin plates with $[-45^{\circ}/+45^{\circ}]_{A8}$ stacking sequence, subjected to two different velocities of bullet. When the velocity of projectile is equal to 450 m/s the area of front damage is 8.21 cm^2, the area of back damage is 20.76 cm^2. However, when the velocity is increased to 764.8 m/s, the front surface damage area become 56.81 cm^2, the size of back surface damage become 53.85 cm^2 the plates were perforated both of two bullet velocities. Increased bullet velocity causes the area of damage on the front surface of the composite plate increases, while the area of damage on its back surface decreases. Matrix crush damage crush was observed on the front of surfaces of the plates, while damage to the back surface was in

the form of fiber breakage. In particular, the directions of fiber breakage are the same as the direction of stacking sequence of the laminate.

4. The stacking sequnce of $[-45^{\circ}/+45^{\circ}]_{A25}$

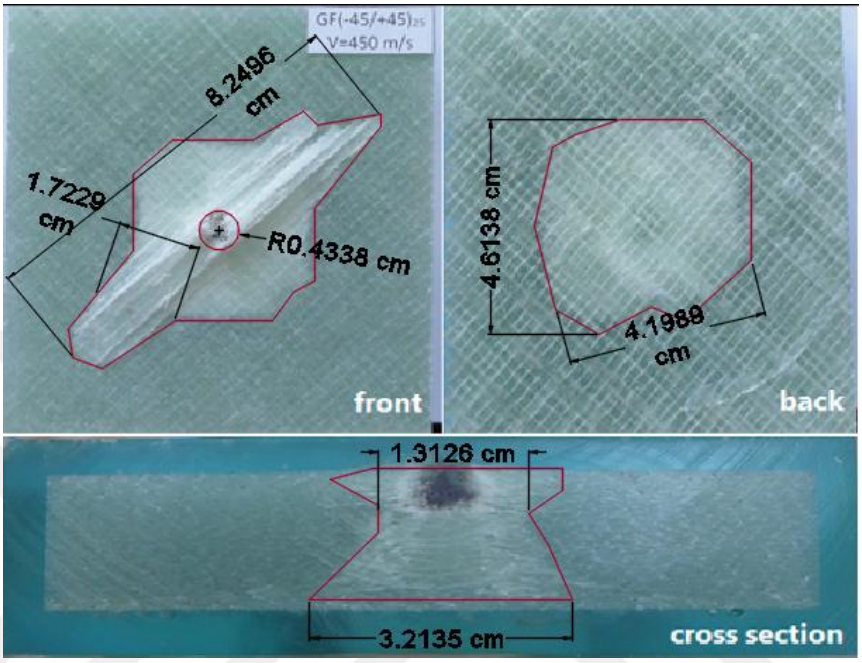

(a) Thick plate at V_1= 450 m/s, E_k = 289.6 J.

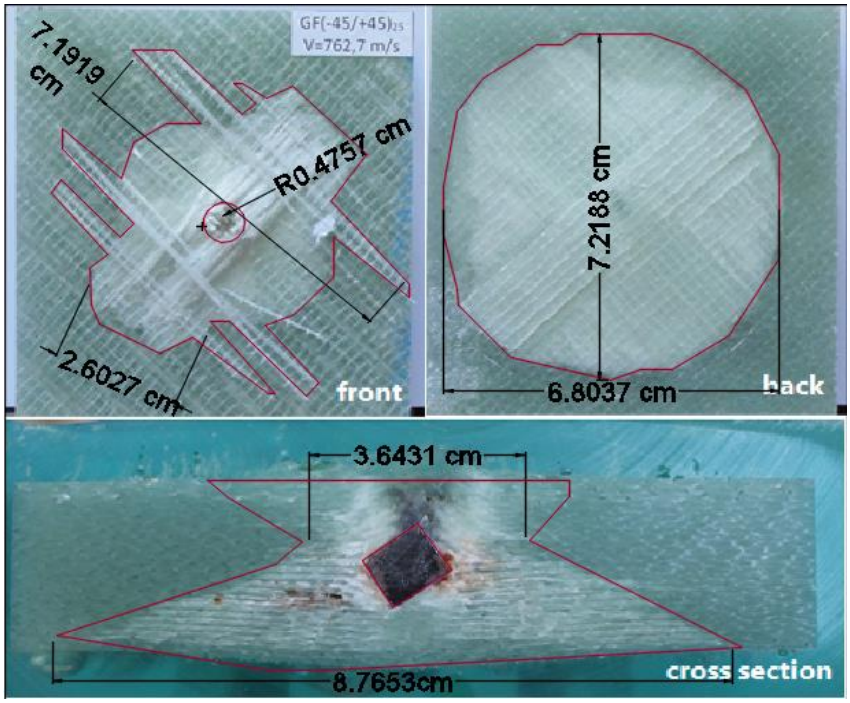

(b) Thick plate at V_2= 762.7 m/s, E_k=831.8 J.

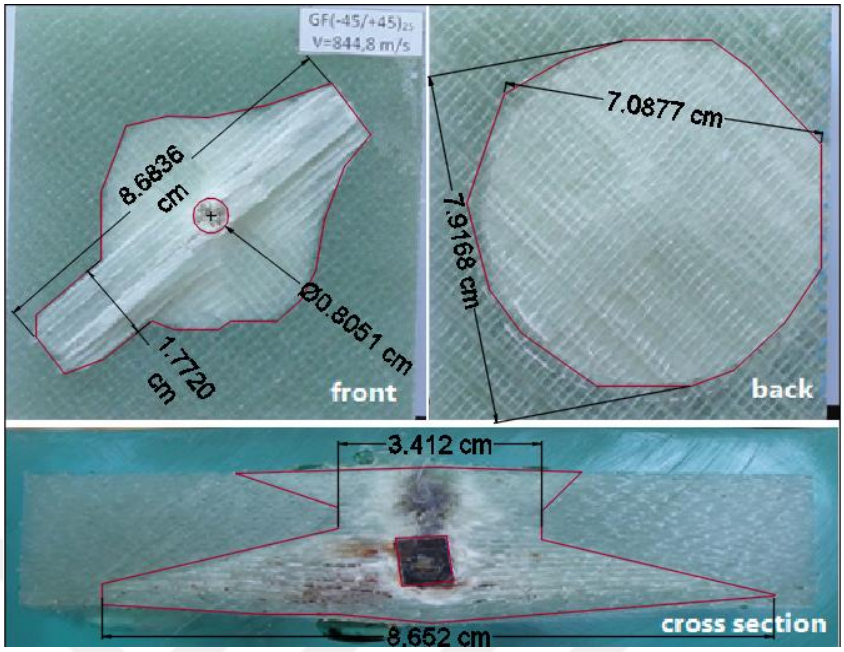

c) Thick plate at V_3= 844.8 m/s, E_k= 1020.6 J.

Figure 3.13. Thick plate with $[-45^{\circ}/+45^{\circ}]_{A25}$ stacking sequence.

Figure 3.13 shows the damage that occur on the front and back surface and a cross-sectional area of the thick laminated composites, subjected to three different velocities of bullet. The damage areas at the front and back surfaces of the plate are; A_{df} = 17.89 cm^2, A_{db}= 16.23 cm^2 for V_1= 450 m/s, A_{df}= 24.93 cm^2, A_{db}= 39.92 cm^2 for V_2= 762.7 m/s and finally, A_{df} = 26.69 cm^2, A_{db}= 48.38 cm^2 for V_3= 844.8 m/s, respectively. these values indicated that the area of damage occurring on the composite plate increases slightly with increasing bullet velocity (matrix crushing, fiber breakage, delamination). It was found for all cases at the above velocities that the bullet penetrated through the thick composite plate, and observed that an increased delamination and swelling through the cross-section of the plate with increasing bullet velocity. At this stacking sequence, the thick plate was not perforated by for all velocities of the bullet.

5. The stacking sequence of $[30^{\circ}/60^{\circ}]_{A8}$

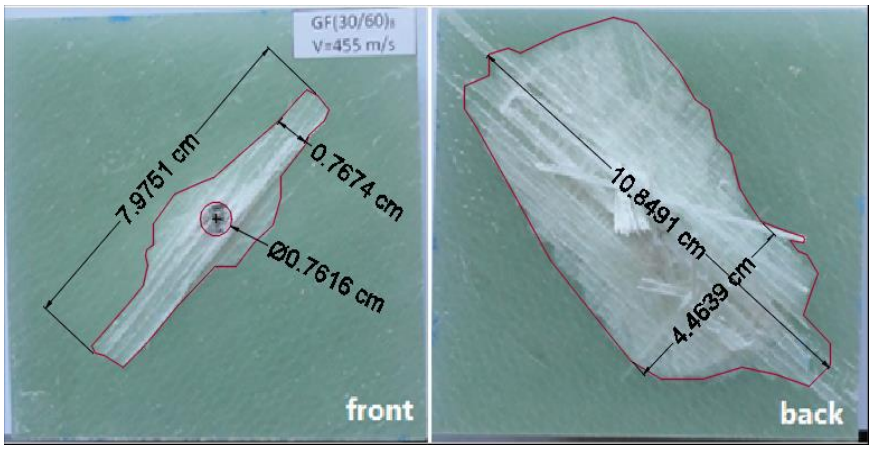

a) Thin plate at V_1 = 455 m/s, E_k= 296 J.

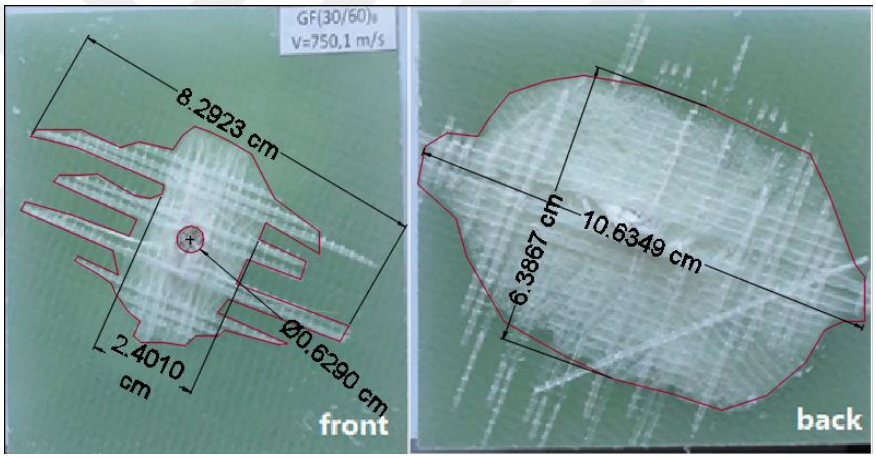

b) Thin plate at V_2 = 750.1 m/s, E_k = 804.6 J.

Figure 3.14. Thin plate with $[30^{\circ}/60^{\circ}]_{A8}$ stacking sequence.

Figure 3.14 Shows the front and back damages of the thin plates with $[30^{\circ}/60^{\circ}]_{A8}$ stacking sequence, subjected to tow different velocities of bullet when the velocity of projectile is equal to 455 m/s , the area of front damage is 9.98 cm^2, the area of back damage is 41.86 cm^2. However, when the velocity is increased to 750.1 m/s, the front surface damage area become 16.92 cm^2, the size of back surface damage become 49.97 cm^2 the plates were perforated both of two bullet velocities. Increased bullet velocity causes the area of damage on the front surface of the composite plate increases, while the area of damage on its back surface decreases. Matrix crush damage crush was observed on the front of surfaces of the plates, while damage to the back surface was in the form of fiber breakage. Especially, the direction of fiber breakage is the same with direction of stacking sequence of the laminate.

6. The stacking sequence of $[30^{\circ}/60^{\circ}]_{A25}$:

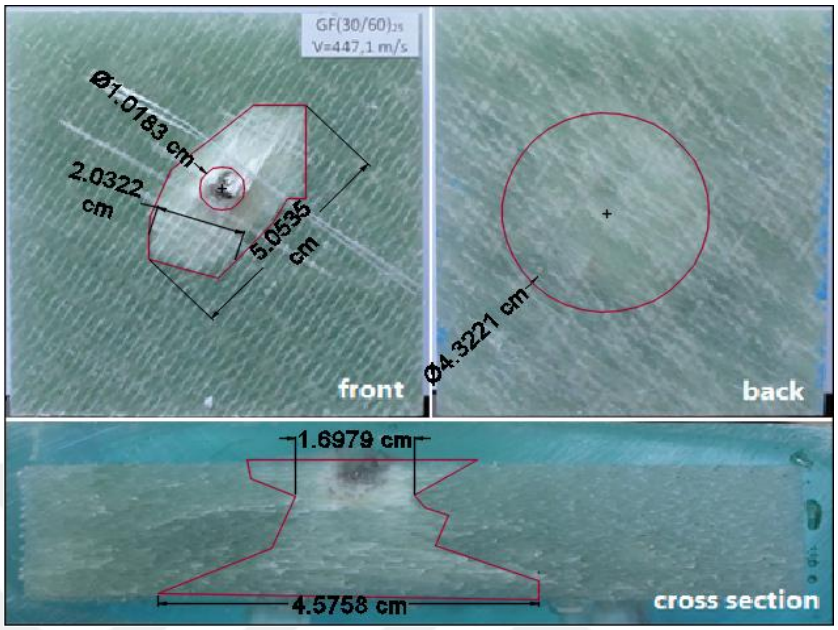

a) Thick plate at V_1= 447.1 m/s, E_k = 285.9 J.

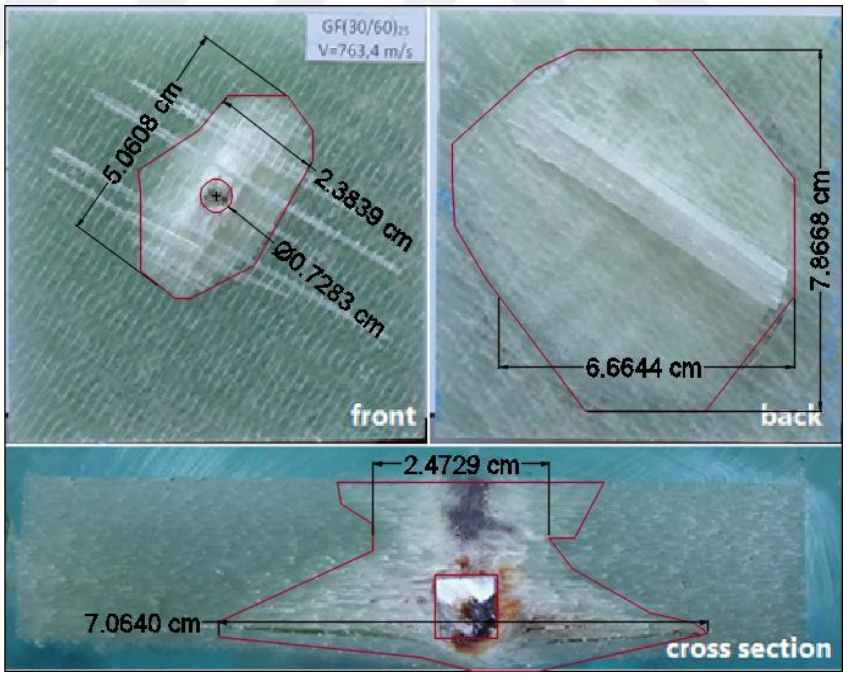

b) Thick plate at V_2= 763.4 m/s, E_k = 833.4 J.

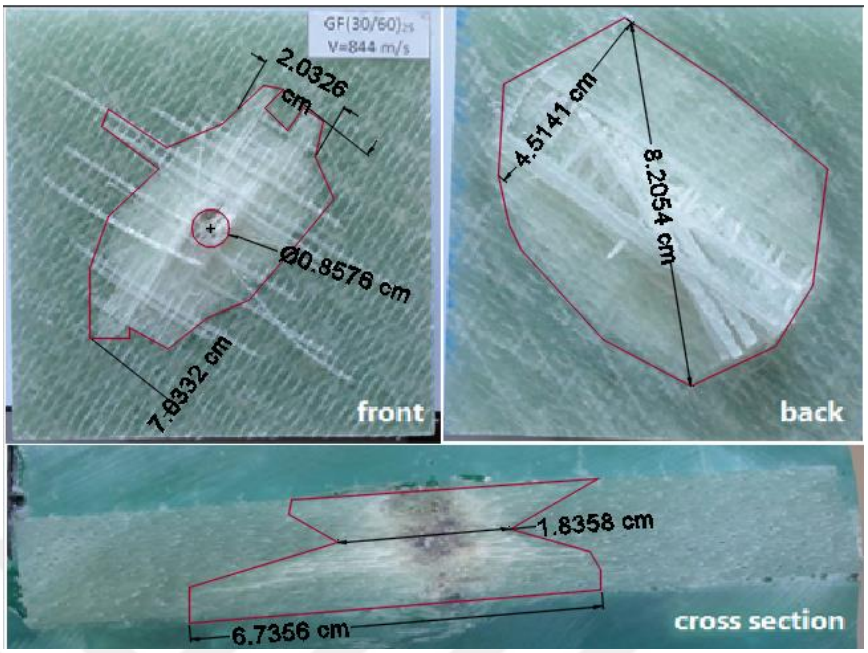

c) Thick plate at V_3= 844 m/s, E_k = 1018.6 J.

Figure 3.15. Thick plate with $[30^{\circ}/60^{\circ}]_{A25}$ stacking sequence.

Figure 3.15 shows the damages that occur on the front and back surfaces and a cross-sectional area of the thick laminated composites subjected to three different velocities of bullet. it is observed that when the velocity of projectile is equal to 447.1 m/s, the damage area of the front surface (A_{df}) is 9.46 cm^2 and no damage was observed on the back surface of the plate. The bullet was rebounded after several layers have been damaged from the top surface of the plate (Figure 3.15 (a)). For figure (b), the bullet velocity is V_2=763.4 m/s which was penetrated through the plate. It is observed the matrix crushing and fiber breakage on the back surface of the plate, whereas, delamination and swelling through the cross-section of the plate. For figure 3.15 (c), the bullet velocity is V_3= 844 m/s which perforation case and damage area on the back surface is bigger than those of Figures (a) and (b).

Evaluation

It was observed the following points that during the experimental studies on thin and thick composite plates under different velocities:

A. In thin and thick composite plates, increased bullet velocity causes increased damage areas on the front surfaces.

B. In all thin composite plates were occurred perforation because of this high velocity effect that exceeds the ballistic limit velocity.

C. From the Figure 3.16, in the first velocity all specimens were occurred rebounding with a small damage area from the top surface, in the second velocity all specimens were penetrated by the bullet which caused along the thickness delamination and burn type damaged areas surrounding bullet enter, in the third velocity all specimens were perforated except the stacking sequence of $[-45^{\circ}/+45^{\circ}]_{A25}$. In this penetration case, observed delamination and swelling similar with its second velocity case.

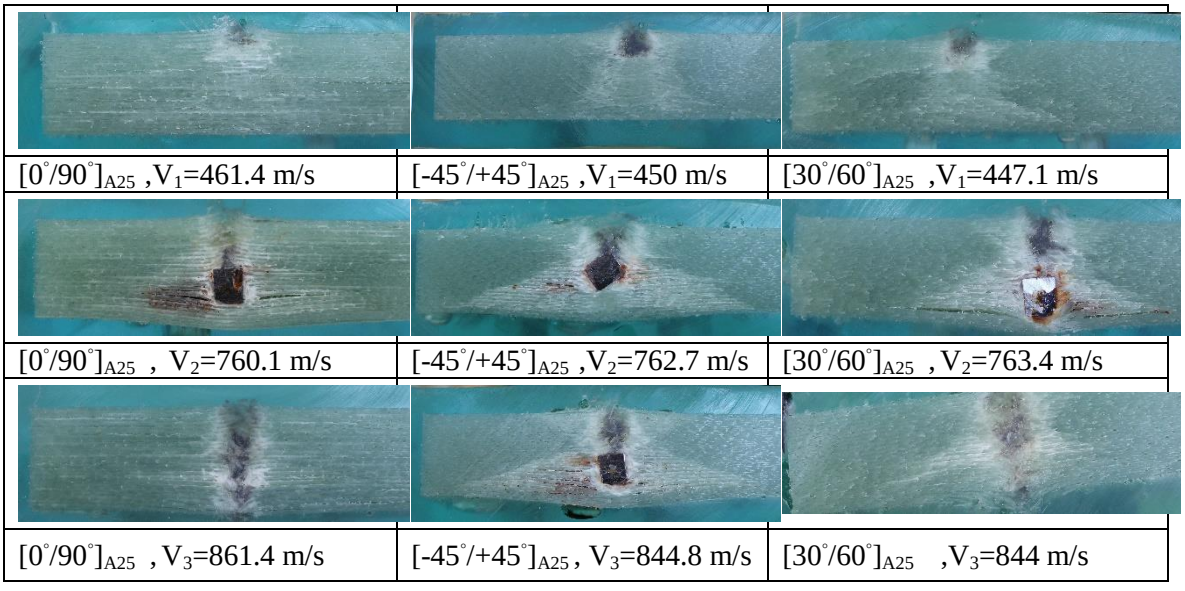

Figure 3.16. Damages across the cross-sectional area of all thick composite plates having different staking sequences.

3.3.3. Effect of fiber angle orientation

1(a). Thin plates at the first velocities

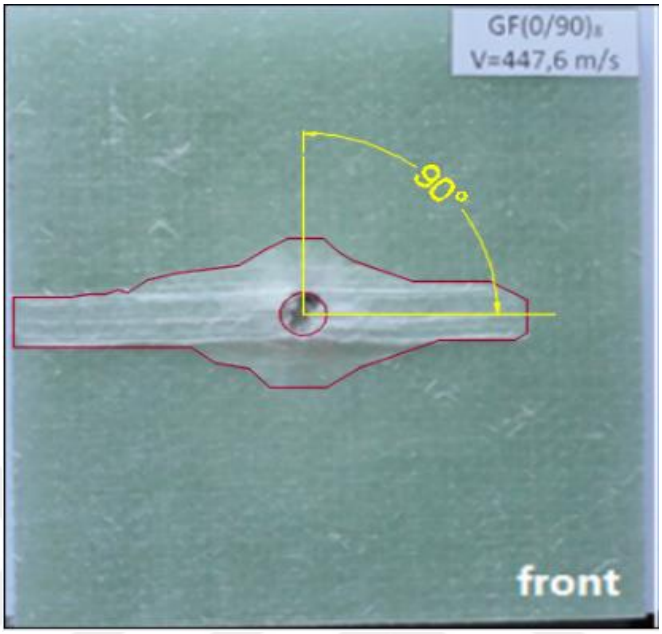

a) stacking sequence of $[0^{\circ}/90^{\circ}]_{A8}$, V_1= 447.6 m/s

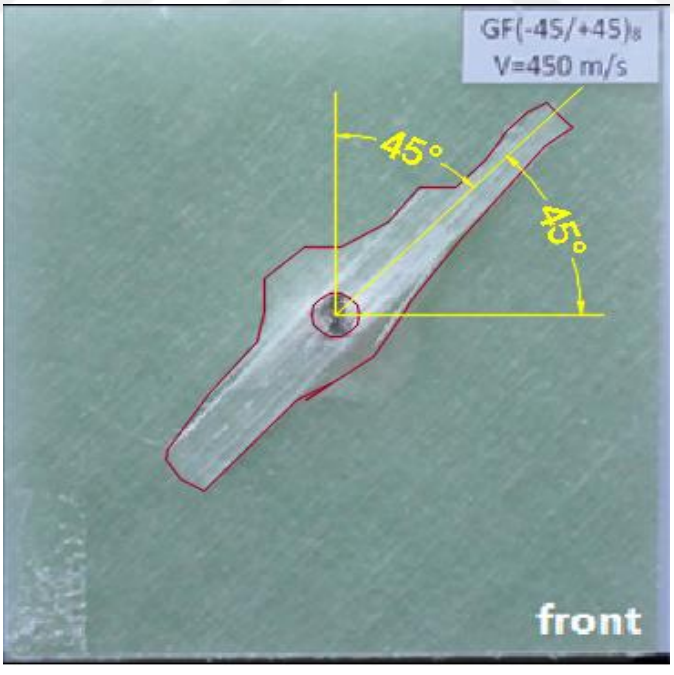

b) stacking sequence of $[-45^{\circ}/+45^{\circ}]_{A8}$, V_1 = 450 m/s

c) stacking sequence of $[30^{\circ}/60^{\circ}]_{A8}$, V_1 = 455 m/s

Figure 3.17. Damages on the front surfaces of thin composite plates at the first velocities.

Figure 3.17 shows the damages on the front surfaces of thin composite plates having stacking sequenced of $[0^{\circ}/90^{\circ}]_{A8}$, $[-45^{\circ}/+45^{\circ}]_{A8}$, $[30^{\circ}/60^{\circ}]_{A8}$, at the first velocities of V_1. It was observed that the directions of damages are the same with orientations of fibers.

1(b). Thick plate at the first velocities

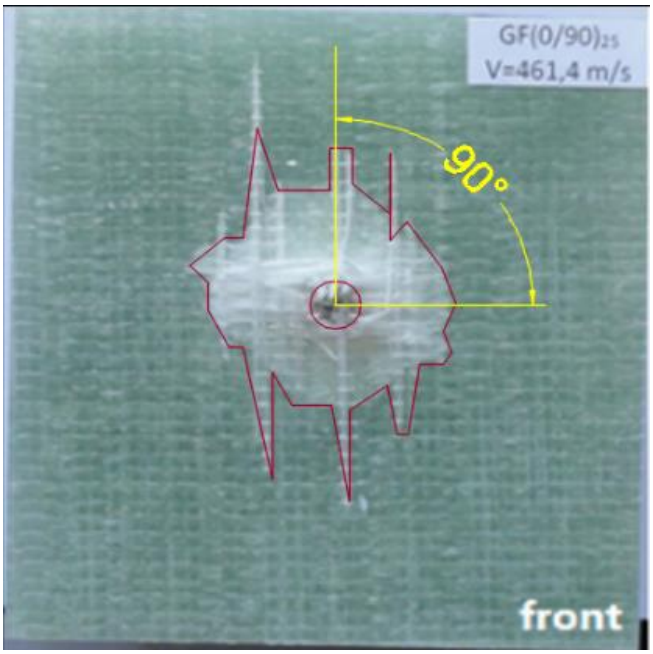

a) stacking sequence of $[0^{\circ}/90^{\circ}]_{A25}$, V_1 = 461.4 m/s

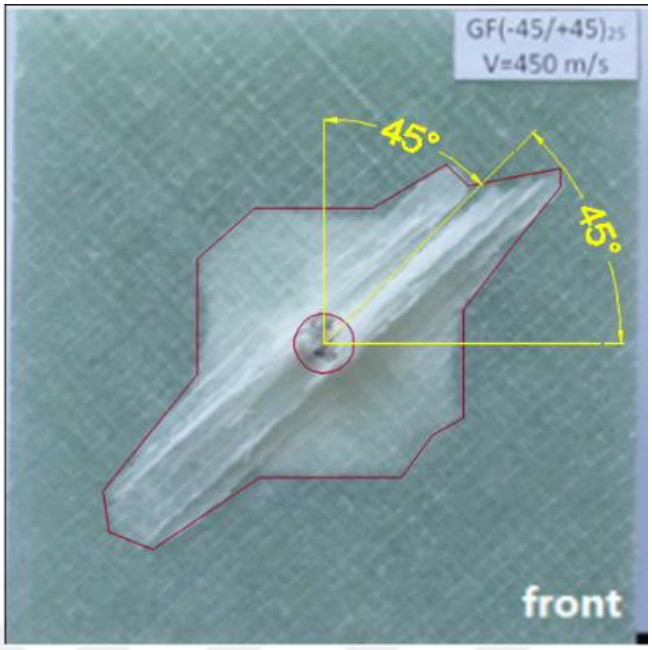

b) stacking sequence of $[-45^{\circ}/+45^{\circ}]_{A25}$, V_1 = 450 m/s

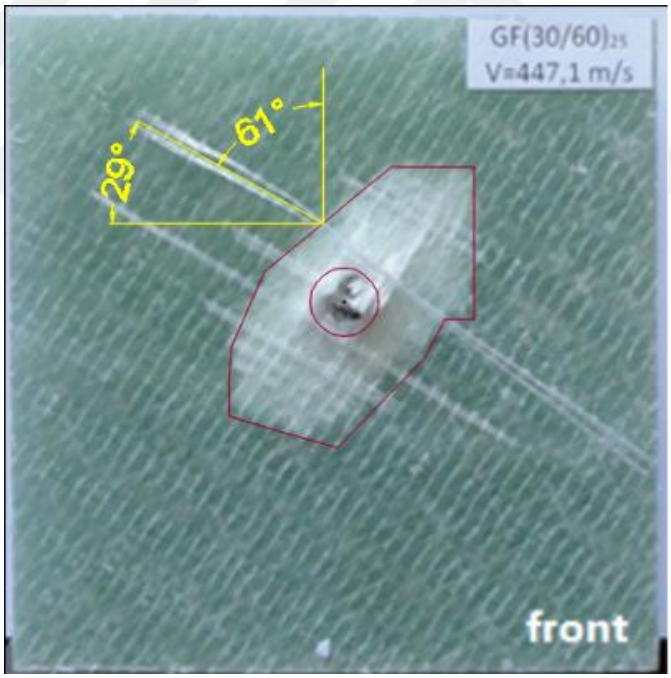

c) stacking sequence of $[30^{\circ}/60^{\circ}]_{A25}$, V_1 = 447.1 m/s

Figure 3.18. Damages on the front surfaces of thick composite plates at the first velocities.

Figure 3.18 shows the damages on the front surfaces of thick composite plates having stacking sequenced of $[0^{\circ}/90^{\circ}]_{A25}$, $[-45^{\circ}/+45^{\circ}]_{A25}$, $[30^{\circ}/60^{\circ}]_{A25}$, at the first velocities of V_1. It was observed that the directions of damages are the same with orientations of fibers.

2(a). Thin plates at the second velocities

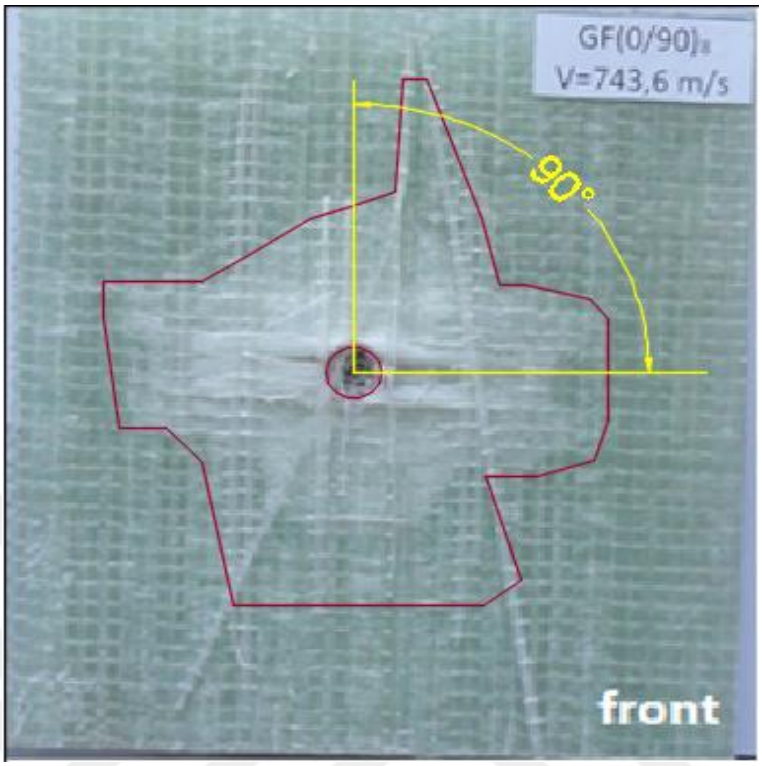

a) stacking sequence of $[0\circ/90^{\circ}]_{A8}$, V_2 = 743.6 m/s

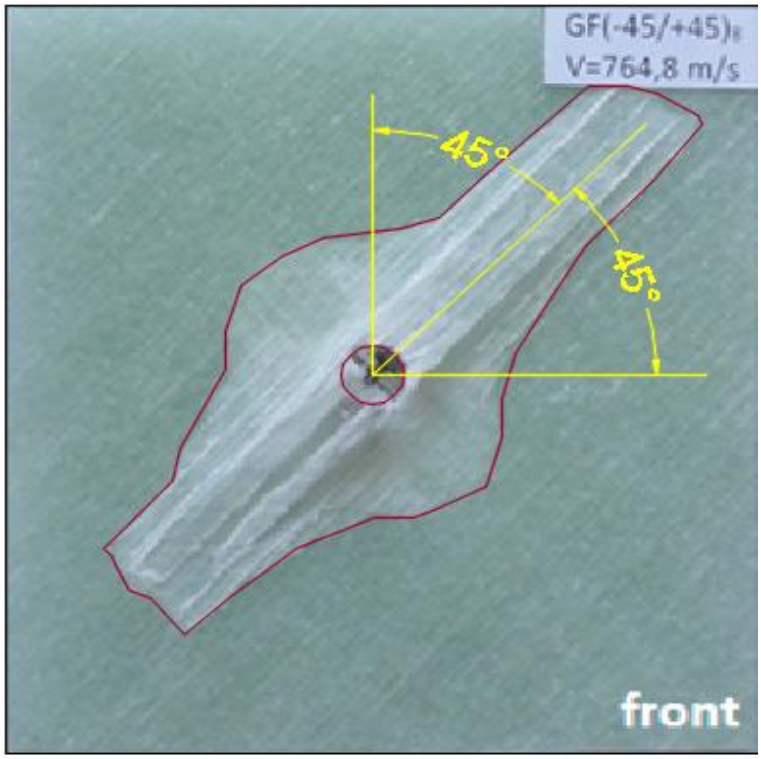

b) stacking sequence of $[-45^{\circ}/+45^{\circ}]_{A8}$, V_2 = 764.8 m/s

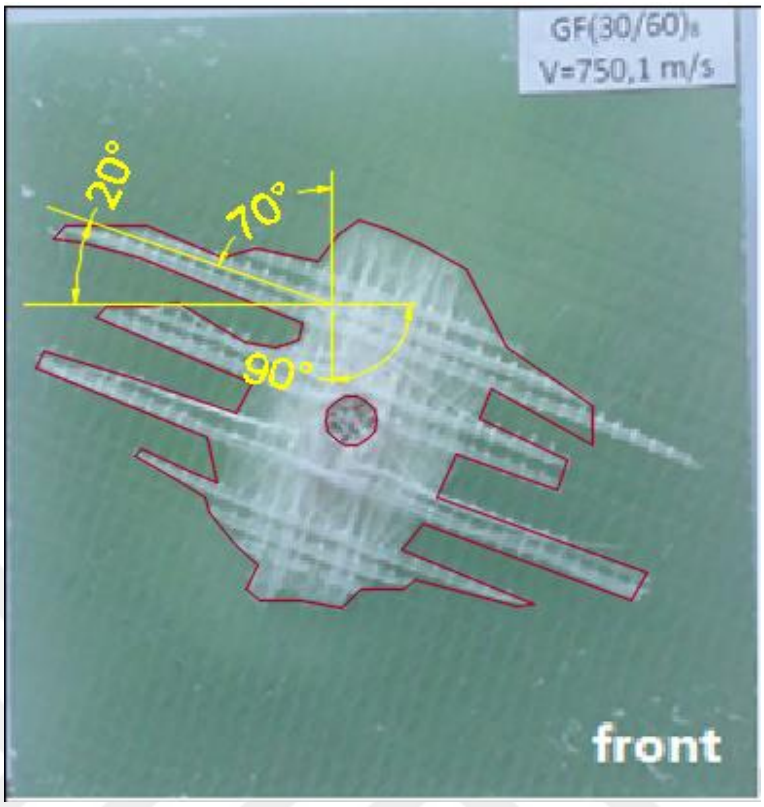

c) stacking sequence of $[30^{\circ}/60^{\circ}]_{A8}$, V_2 = 750.1 m/s

Figure 3.19. Damages on the front surfaces of thin composite plates at the second velocities.

Figure 3.19 shows the damages on the front surfaces of thin composite plates having stacking sequenced of $[0^{\circ}/90^{\circ}]_{A8}$, $[-45^{\circ}/+45^{\circ}]_{A8}$, $[30^{\circ}/60^{\circ}]_{A8}$, at the velocities of V_2. It was observed that the directions of damages are related to the orientation of fibers. For the second velocities, large damages were aggregated around the bullet entry center than those of the first velocities.

2(b). Thick plates at second velocities

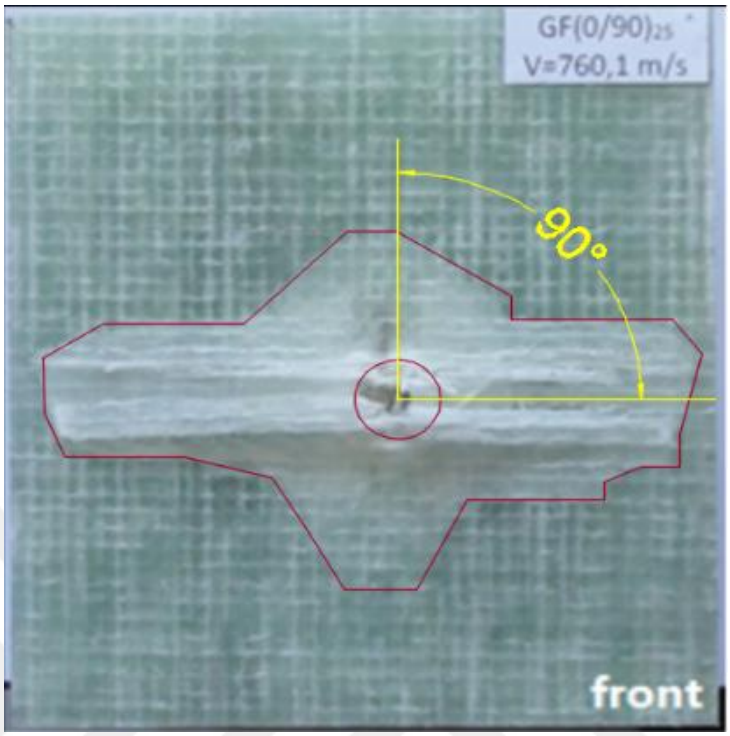

a) stacking sequence of $[0^{\circ}/90^{\circ}]_{A25}$, V_2 = 760.1 m/s

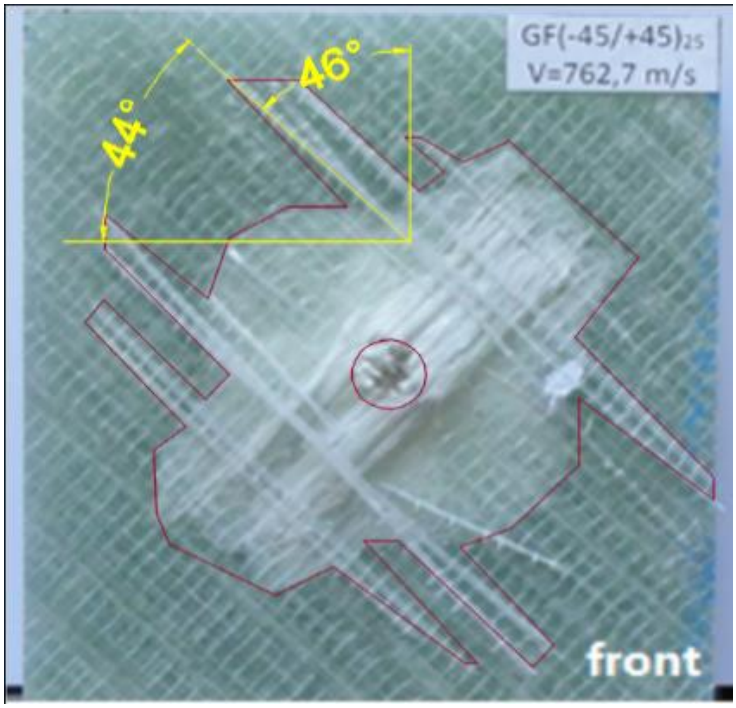

b) stacking sequence of $[-45^{\circ}/+45^{\circ}]_{A25}$, V_2 = 762.7 m/s

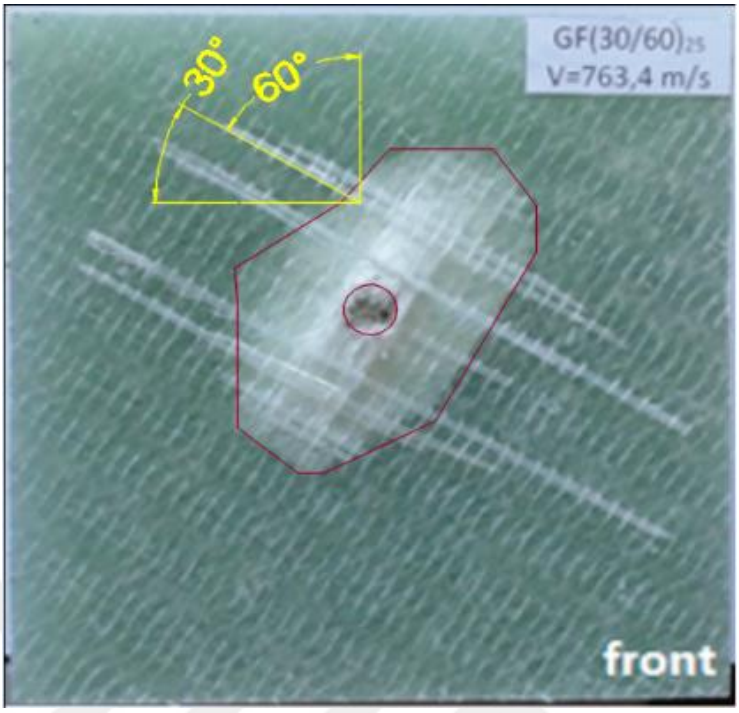

c) stacking sequence of $[30^{\circ}/60^{\circ}]_{A25}$, V_2 = 763.4 m/s

Figure 3.20. Damages on the front surfaces of thin composite plates at the second velocities.

Figure 3.20 shows the damages on the front surfaces of thick composite plates having stacking sequenced of $[0^{\circ}/90^{\circ}]_{A25}$, $[-45^{\circ}/+45^{\circ}]_{A25}$, $[30^{\circ}/60^{\circ}]_{A25}$, at the velocities of V_2. It was observed that the directions of damages are related to the orientations of fibers. For the second velocities, large damages were aggregated around the bullet entry center than those of the first velocities.

.

3(a). Thick plates at the third velocities.

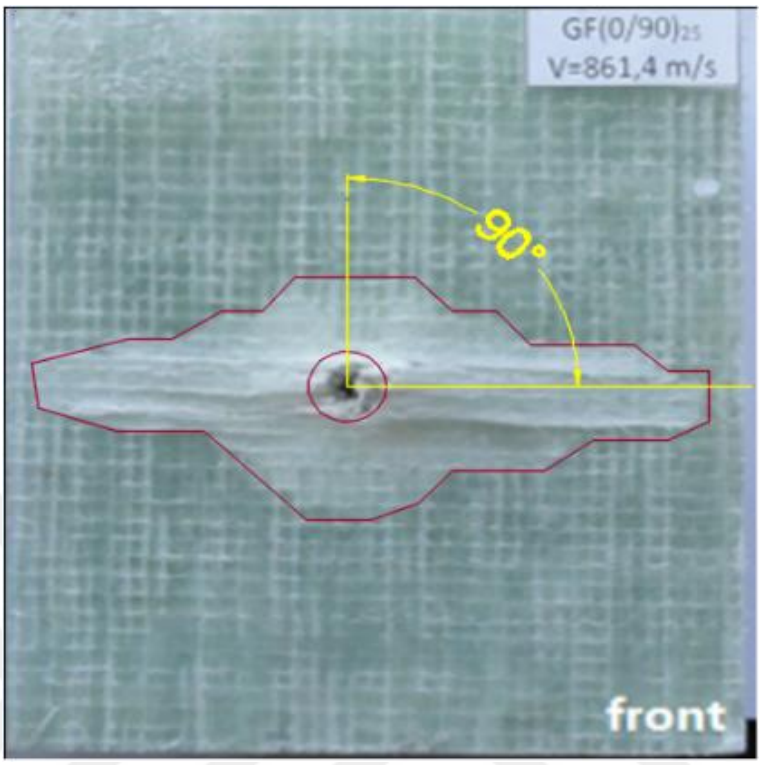

a) stacking sequence of $[0^{\circ}/90^{\circ}]_{A25}$, V_3= 861.4 m/s

b) stacking sequence of $[-45^{\circ}/+45^{\circ}]_{A25}$, V_3 = 844.8 m/s

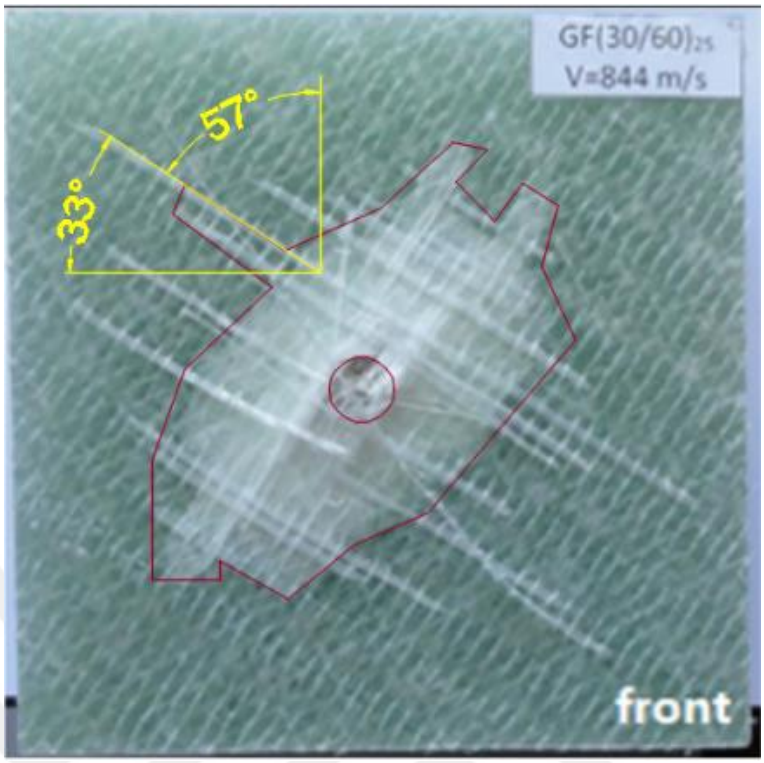

c) stacking sequence of $[30^{\circ}/60^{\circ}]_{A25}$, V_3 = 844 m/s

Figure 3.21. Damages on the front surfaces of thick composite plates at the third velocities.

Figure 3.21 shows the damages on the front surfaces of thick composite plates having stacking sequenced of $[0^{\circ}/90^{\circ}]_{A25}$, $[-45^{\circ}/+45^{\circ}]_{A25}$, $[30^{\circ}/60^{\circ}]_{A25}$, at the velocities of V_2. It was observed that the directions of damages are related to the orientations of fibers. For the third velocities, slightly large damages were aggregated around the bullet entry center than those of the second velocities.

The direction of damage in thin specimens is more pronounced and regular than those of thick specimens. The influence of the fiber angle on the behavior of the damage in thick composite plates under high velocities is that the damages are more clear and regular for the stacking sequences of $[-45^{\circ}/+45^{\circ}]_{A25}$ at the first velocities (Fig. 3.18), the damages are more clear for the stacking sequences of $[0^{\circ}/90^{\circ}]_{A25}$ at the second velocities, and at the third velocities, the damages are evident for the stacking sequences of $[-45^{\circ}/+45^{\circ}]_{A25}$ and $[0^{\circ}/90^{\circ}]_{A25}$, however , the damage was aggregated around the bullet entry point for the stacking sequence of $[30^{\circ}/60^{\circ}]_{A25}$ (Fig. 3.21). The difference between these samples is that the thin specimens have higher elasticity than the thick plates at the same time. It was also demonstrated that inter-laminar shear stresses increased gradually as the

number of effective plies in the laminate decrease because of failure. This increasing in inter-laminar shear stresses is based on also the stacking sequences of the composites.

Now generally, it has been mentioned about the damage that occurs during the ballistic event as follows as seen in the thin and the thick specimens:

1. Swelling can form at the front of the target because of initial compression and material flow moving to the front. The swelling can also be effected by delamination and matrix crushing, as well as heat during the first impact.

2. Compressive and shear waves are made along the thickness during impact. Tensile and shear waves are also formed along the layers' radial direction. Damage is formed during this stage when stress going beyond the threshold. Damage is either delamination or the crushing of the matrix. Delamination can also come from swelling at the target's back.

3. Fiber breakage occurs due to shear plugging, tension, or both during impact. Because of this, the face of the bullet gets plugged. If the bullet's kinetic energy is not absorbed before the plug is formed, the bullet moves towards the back along with the plug and the target will absorb some of the bullet's kinetic energy. The bullet can become lodged in the target when there is enough kinetic energy to break the fibers but not enough to overcome resistance from friction. Resistance is different based on the fit that is formed between the bullet and target. Fiber breakage is the main cause of a hole being formed. Temperatures are also increased as the bullet moves inside the target and creates resistance. Then, some energy is absorbed as heat.

CHAPTER FOUR

CONCLUSIONS AND FUTURE WORKS

4.1. Conclusions

Impact damages under high velocity in aircraft structures from laminated composites are very complex and the most common are delamination, matrix crushing and fiber breakage as in the samples discussed in the previous chapter. The ability to expect the initiation and growth of damage is crucial for expecting performance and developing dependable and safe designs of composites.

The relevant finding resulting from the present study are presented below:

- In both thin and thick composites, bullet velocity was important. Lower speed bullets cause more damage than higher speed ones because they interact longer with the plate and cause damage. The opposite is true for higher speed bullets.
- All thin composites are perforated with increasing all three velocities (V_1, V_2, V_3).
- All thick composites are divided into three groups; the first group is the case of bullet rebounding under the first velocity (V_1), the second group is the case of penetration under the second velocity (V_2) and the third group is the case of perforation except stacking sequence of $[-45^{\circ}/+45^{\circ}]_{A25}$ under the third velocity (V_3).
- For thin laminates, the size of damage depends on the bullet velocity and kinetic energy at impact. This is because, the first area of contact has more area and faces more impact by the bullet, damaging the plate more.
- For both thin and thick composites, damage at the exit side was more than the entry side. This is because, when a bullet connects with the plate and moves to the back, there is a wave that causes delamination.

- In all the cases, damage in cross-ply laminates $[0^{\circ}/90^{\circ}]_A$ and angle-ply laminates $[-45^{\circ}/+45^{\circ}]_A$ suggests that damage is dependent on the stacking sequence of the laminate but anti-symmetric laminate $[30^{\circ}/60^{\circ}]_A$ slightly different because of the concentration of damage near the entry point of the bullet.

4.2. Future Works and Recommendations

- Determining the ballistic limit in ballistic performance studies is an important issue and to further investigate the problem of ballistic impact damage, it is recommended that bullets of different shape and size are used, hence different impact energies.
- After initial impact, bullets should be retrieved to measure deformation and calculate energy lost during deformation. Once this information is found, it is possible to learn exactly how much energy is absorbed by the plates during impact.
- Impact damage analysis of composite laminates to the high accurately by commercial softwares, ABAQUS, LS-DYNA and ANSYS, can be analyzed by using it in some circumstances (geometry, boundary conditions, mesh, load etc.) distribution of damage, stress, strain, deformations can be analyzed and presented. Also can calculate actual damage to samples and secondary damage. Then the results obtained through the above programs can be compared to the practical results obtained in the laboratory.

REFERENCES

1. Teti, R., 2002. Machining of Composite Materials. **CIRP Annals - Manufacturing Technology**, **51** (2): 611–634.

2. Erbil, E., 2008. Impact loading in laminated composites. M.Sc. Thesis, 9 september university. Izmir**.** pp.118.

3. Chung, D. D. L., 2004. **C**omposite **M**aterials. 683–700 pp., in Kirk-Othmer Encyclopedia of Chemical Technology. Dickey, J.R., John Wiley and Sons, **15**.

4. Kaw, A. K., 2006. **M**echanics **o**f **C**omposite **M**aterials. Taylor & Francis Group, **LLC 29,**(1-59): pp. 473**.**

5. Tsai, S. W., 1964. Strcutural Behavior of Composite Materials. philco corporation. NASA, Langley. California .

6. Balasubramanian, M., 2014. **C**omposite **M**aterials **A**nd **P**rocessing. CRC Press, Taylor AND Francis Group, **19** (26): 622 .

7. Barbero, E. J., 1999. **I**ntroduction **t**o **C**omposite **M**aterials **D**esign. Taylor & Francis Group, pp.562.

8. MIL-HDBK. -17-3F, 2002. Composite materials handbook, **Department of Defense (USA), 3** (5): pp. 693.

9. Leblanc, J., 2011. Dynamic Response and Damage Evolution of Composite Materials Subjected To Underwater Explosive Loading : an Experimental and Computational Study. Ph.D. Thesis, University of Rhode Island.

10. Navarro, C., Martinez, M. A., CORTES, R., Sanchez-Galvez V., 1993. Some observations on the normal impact on ceramic faced armours backed by composite plates. **International Jornal of Impact Engineering, 13** (1)**:** 145–156.

11. Hetherington, J. G., Rajagopalan, B. P., 1991. An investigation into the energy absorbed during ballistic perforation of composite armours, **International Jornal of Impact Engineering**, **11**: 33–40.

12. Leech, C., Mansell, J., 1977. Some aspects of wave propagation in orthogonal nets. **International Journal of Mechanical Sciences,** 19 (2): 93–102.

13. Field, J. E., Sun, Q., 1990. A high speed photographic study of impact on fibres and woven fabrics. *19th International Congress on High-Speed Photography and Photonics*, 1358**:** 703–712.

14. Ravid, M., Bodner, S. R., 1983. Dynamic perforation of viscoplastic plates by rigid projectiles. **International Journal of Engineering Sciences, 21**(6)**:** 577–591.

15. Joshi, S. P., Sun, C. T., 1985. Impact Induced Fracture in Laminated Composite. **Journal of Composite Materials, 19** (1)**:** 51–66.

16. Wu , Hsi-yung, T., Springer, G., S.,1988, Impact induced stresses, strains, and delaminations in composite plates. **Journal of Composite Materials, 22:** 533–560.

17. Govaert, L. E., Peijs, T., 1995. Tensile strength and work of fracture of oriented polyethylene fibre**. Polymer, 36 (23):** 4425–4431.

18. Peijs, T., Smets, E. A. M., Govaert, L. E., 1994. Strain rate and temperature effects on energy absorption of polyethylene fibres and composites, **Applied Composite Materials, 1**(1): 35–54.

19. Smith, T. L., 1958. Dependence of the ultimate properties of a GR-S rubber on strain rate and temperature, **Journal of Polymer Science, 32**(124)**:** 99–113.

20. Duell, J. M., 2004. **I**mpact **T**esting **o**f **A**dvanced **C**omposites. 97–112., Advanced Topics in Characterization of Composites. Kessler, M.R., 2004. Trafford Publishing.

21. Razali, N., Sultan, M. T. H., Mustapha, F., Yidris, N., Ishak, M. R., 2014. Impact Damage on Composite Structures–A Review, **The International Journal of Engineering And Science 3** (7), 8–20.

22. Dash, K., Sukumaran, S., Ray, B.C., 2014. Effect of loading speed on deformation of composite materials: a critical review. **Journal of Advanced Research in Manufacturing, Material Science and Metallurgical Engineering, 1**(M): 1-22.

23. Kazemahvazi, S., 2010. **I**mpact **L**oading of **C**omposite and **S**andwich **S**tructures. Ph.D. Thesis , Kungliga Tekniska Hogskolan University , Stockholm, Sweden. pp 147.

24. Menna, C., Asprone, D., Caprino, G., Lopresto, V., Prota, A., 2011. Numerical simulation of impact tests on GFRP composite laminates. **International Jornal of Impact Engineering** , **38:** 677–685.

25. Tanay Topac, O., Gozluklu, B., Gurses, E., Coker, D., 2016. Experimental and Computational Study of the Damage Process in CFRP Composite Beams under Low-Velocity Impact. **Composite: Part A, 92:** 167–182.

26. Hassan, M. A., Naderi, S., Bushroa, A. R., 2014. Low-velocity impact damage of woven fabric composites: Finite element simulation and experimental verification. **Journal of Materials and Design**, **53:** 706–718.

27. Gunes, R., Arslan, K., 2016. Development of numerical realistic model for predicting low-velocity impact response of aluminium honeycomb sandwich structures. **Journal of Sandwich Structures and Materials**, **18**(1): 95–112.

28. Iqbal, Z., 1997. **E**ffects of **B**allistic **I**mpact **D**amage on **T**hin and **T**hick **C**omposites. Ph.D. Thesis .Iowa State University, 127.

29. Ahmed, A., Wei, L., 2015. the Low-Velocity Impact Damage Resistance of the Composite Structures - a Review. **Reviews on Advanced Materials Science**, **40** (2)**:** 127–145.

30. Feli, S., Namdari, Pour, M. H., 2012. An analytical model for composite sandwich panels with honeycomb core subjected to high-velocity impact. **Composite: Part B** , **43**(5)**:** 2439–2447.

31. Fras, T., Colard, L., Lach, E., Rusinek, A., Reck, B., 2015. Thick AA7020-T651 plates under ballistic impact of fragment-simulating projectiles. **International Jornal of Impact Engineering**. **86,** 336–353.

32. Pandya, K. S., Pothnis, J. R., Ravikumar, G., Naik, N. K., 2013. Ballistic impact behavior of hybrid composites. **Journal of Materials and Design**, **44:** 128–135.

33. Buitrago, B. L., Santiuste, C., Sánchez-Sáez, S., Barbero, E., Navarro, C., 2010. Modelling of composite sandwich structures with honeycomb core subjected to high-velocity impact. **Composite Structures, 92** (9)**:** 2090–2096.

34. Ivañez, I., Santiuste, C., Barbero, E., Sanchez-Saez, S., 2011. Numerical modelling of foam-cored sandwich plates under high-velocity impact. **Composite Structures, 93:** 2392–2399.

35. Hazell, P. J., Appleby-Thomas, G. J., Kister, G., 2010. Impact, penetration, and perforation of a bonded carbon-fibre-reinforced plastic composite panel by a high-velocity steel sphere: An experimental study. **The Journal of Strain Analysis for Engineering Design**, **45** (6)**:** 439–450.

36. Azrin Hani, A.R., Azman, N.S., Ahmad, R., Mariatti, M., Roslan, M.N., Marsi, N., 2016. Ballistic impact response of woven hybrid coir / kevlar laminated composites. in *IConGDM* ,**78:** 1048

37. Terra, C., Pasquali, M., Gaudenzi, P., 2015. High-velocity impacts on aerospace thin composite laminates**.** in *7th ECCOMAS Thematic Conference on Smart Structures and Materials SMART*.

38. Chen, X., Sun, D., Wang, Y., Zhou, Y., 2012. 2D / 3D Woven fabrics for ballistic protection. in *4th World Conference on 3D Fabrics and Their Applications* 1–12.

39. Liaghat, G. H., Shanazari, H., Hadavinia, H., Aboutorabi, A., 2015. Analytical investigation of high-velocity impact on hybrid unidirectional / woven composite panels. **Journal of Thermoplastic composite materials**, **30**(4): 545-563.

40. Yen, C. F., 2012. A ballistic material model for continuous-fiber reinforced composites. **International Jornal of Impact Engineering**, **46:** 11–22.

41. Feli, S., Asgari, M. R., 2011. Finite element simulation of ceramic/composite armor under ballistic impact. **Composites: Part B, 42** (4): 771-780.

42. García-Castillo, S. K., Sánchez-Sáez, S., Barbero, E., 2012. Nondimensional analysis of ballistic impact on thin woven laminate plates. **International Jornal of Impact Engineering, 39** (1)**:** 8–15.

43. Sudhir Sastry, Y. B., Budarapu, P. R., Krishna, Y., Devaraj, S., 2014. Studies on ballistic impact of the composite panels.**Theoretical and Applied Fracture Mechanics**, **72** (1): 2–12.

44. Wang, J., Callinan, R., 2014. Residual strengths of composite structures subjected to ballistic impact. **Composite Structures**, **117** (1)**:** 423–432.

45. Luan, K., Sun, B., Gu, B., 2013. Ballistic impact damages of 3-D angle-interlock woven composites based on high strain rate constitutive equation of fiber tows. **International Jornal of Impact Engineering, 57:** 145–158.

46. Mohan, S., Velu, S., 2014. Ballistic impact behaviour of unidirectional fibre reinforced composites. **International Jornal of Impact Engineering**, **63:** 164–176.

47. Tasdemirci, A., Tunusoglu, G., Güden, M., 2012. The effect of the interlayer on the ballistic performance of ceramic/composite armors: Experimental and numerical study. **International Jornal of Impact Engineering, 44:** 1–9.

48. Chi, R., Serjouei, A., Sridhar, I., Tan, G. E. B., 2013. Ballistic impact on bi-layer alumina/aluminium armor: A semi-analytical approach. **International Jornal of Impact Engineering, 52:** 37–46.

49. Alankaya, V., Senyilmaz, H. K., Türker, M., 2013. Inspection of failure caused by ballistic impact on body armors composed of laminated dyneema^{TM}. **Gazi University Journal of Science, 26** (2)**:** 253–259.

50. Omidvar, H., Azari, K. K., Taheri, A. M., Saghafi, A. A., 2013. Impact and Ballistic Behavior Optimization of Kevlar-Epoxy Composites by Taguchi Method. **Arabian Journal for Science and Engineering, 38** (5)**:** 1161–1167.

51. Reddy, P. R. S., Reddy, T. S., Madhu, V., Gogia, A. K., Rao, K. V., 2015. Behavior of E-glass composite laminates under ballistic impact. **Materials and Design, 84:** 79–86.

52. Long, D., 2015. Simulation of Ballistic Impact on Polymer Matrix Composite Panels. **Journal of Theoretical and Applied Mechanics, 53** (2)**:** 263–272.

53. Zhang, D., Sun, Y., Chen, L., Zhang, S., Pan, N., 2014. Influence of fabric structure and thickness on the ballistic impact behavior of Ultrahigh molecular weight polyethylene composite laminate. **Materials and Design, 54:** 315–322.

54. McWilliams, B., Yu, J., Pankow, M., Yen, C. F., 2015. Ballistic impact behavior of woven ceramic fabric reinforced metal matrix composites. **International Jornal of Impact Engineering, 86:** 57–66.

55. Aydin, M., Apalak, M. K., 2016. Experimental damage analysis of Al/SiC functionally graded sandwich plates under ballistic impact. **Materials Science and Engineering: A, 671:** 107–117.

56. Gunes, R., Arslan, K., Apalak, M. K., Reddy, J. N., 2017. Ballistic performance of honeycomb sandwich structures reinforced by functionally graded face plates. **Journal of Sandwich Structures and Materials, 0 (00):** 1–19.

57. Gunes, R., Arslan, K., Apalak, M. K., Reddy, J. N., 2014. Numerical investigations on the ballistic performance of honeycomb sandwich structures reinforced by functionally graded plates. in *Blucher Material Science Proceedings* **1** (1)**:** 95–112.

58. Sharma, P., Chandel, P., Bhardwaj, V., Singh, M., Mahajan, P., 2017. Ballistic impact response of high strength aluminium alloy 2014-T652 subjected to rigid and deformable projectiles. **Thin-Walled Structures**, pp. 1–15.

59. Pach, J., Pyka, D., Jamroziak, K., Mayer, P., 2017. The experimental and numerical analysis of the ballistic resistance of polymer composites. **Composite Part B**, **113:** 24–30.

60. Holmen, J. K., Hopperstad, O. S., Børvik, T., 2017. Influence of yield-surface shape in simulation of ballistic impact. **International Journal of Impact Engineering**, pp. 1–11.

61. Yang, Y., Chen, X., 2017. Investigation of failure modes and influence on ballistic performance of Ultra- High Molecular Weight Polyethylene (UHMWPE) uni-directional laminatefor hybrid design. **Composite Structure, 174:** 233–243.

62. Naik, N. K., Doshi, A. V., 2008. Ballistic impact behaviour of thick composites: Parametric studies. **Composite Structure**, **82:** 447–464.

63. Reddy, J. N., 2003, **M**echanics **o**f **l**aminated **c**omposite **p**lates **a**nd **s**hells: theory and analysis. pp 840.

64. Jones, R. M., 1998. **M**echanics **o**f **C**omposite **M**aterials. CRC press. pp. 519.

65. Özşahin, E., 2008. **R**esponse of **A**luminum **P**lates **S**ubjected To **H**igh **V**elocity **I**mpact **L**oads. istanbul techincal Üniversitesi, Ph.D. Thesis, Istanbul, pp. 139.

66. Deniz, T., 2010. **B**allistic **P**enetration of **H**ardened **S**teel **P**lates. M.Sc. Thesis, Middle East Technical university. Ankara, pp 133.

67. Rosenberg, Z., Dekel, E., 2016. **T**erminal **B**allistics**.** Springer Science, 363 pp.

68. Kamal, A., 2014. Investigations on Ballistic Performance of Honeycomb Sandwich Structures Reinforced By Functionally Graded Plates. M.Sc. Thesis, erciyes university, kayseri, pp. 137.

69. ÖZER, İ., 2015. **I**nvestigation of **B**allistic **I**mpact **E**ffect **W**ith **F**inite **E**lements **M**ethod. M.Sc. Thesis, Mustafa Kemal University. Hatay, pp.67

70. Zukas, J. A., 1990. **H**igh **V**elocity **I**mpact **D**ynamics. John Wiley and Sons Inc., USA, pp. 960.

71. Wetzel, J. J., 2009. **T**he **I**mpulse **R**esponse of **E**xtruded **C**orrugated **C**ore **A**luminum **S**andwich **S**tructures. M.Sc. Thesis, University of Virginia, School of Engineering and Applied Science, ABD, pp. 180.

72. Tan, V. B. C., Khoo, K. J. L., 2004. Perforation of flexible laminates by projectiles of different geometry. **International Journal of Impact Engineering**, **31** (7)**:** 793–810.

73. Laible, R., 2012. **B**allistic **M**aterials **a**nd **P**enetration **M**echanics**.** Elsevier Scientific Publishing Company, The Netherlands, 5: pp. 306.

74. Ben-Dor, G., Dubinsky, A., Elperin, T., 2002. On the Lambert-Jonas approximation for ballistic impact. **Mechanics Research Communications, 29 (2-3):** 137–139.

75. Backman, M. E., Goldsmith, W., 1978. The mechanics of penetration of projectiles into targets. **International Journal of Engineering Science, 16** (1)**:** 1–99.

76. NATO STANAG 2920, 2003. Ballistic Test Method for Personal Armour Materials and Combat Clothing.

77. MIL-DTL-46593B (MR) w/AMENDMENT 1, 2008. Detail Specification, Projectile Calibers .22, .30, .50 and 20 mm Fragment-Simulating, ASME Int.

78. Nechitailo, N. V., Batra, R. C., 1998. penetration / perforation of aluminum , steel and tungsten plataes by ceramic rods. **Computers and Structures, 66** (5)**:** 571–583.

79. **https://www.dostkimya.com/en/products/vacuum-technology.**

CURRICULUM VITAE

Name and Surname : DAWOOD SALEEM HUWIASH AL BEHADILI

Nationality **:** IRAQ

Birth Date and Place **:** 19 – 12- 1976 / BAGHDAD

Marital Status : MARRIED

Cell Phone : 05352910123

E-mail : saleem_david835@yahoo.com, 4013531608@erciyes.edu.tr

Correspondence address: Kayseri- Talas- Mevlana Mah. Mehmet Tumcin cad. Ilkadim apt. 30/36.

EDUCATION

DEGREE	INSTITUTION	DATE OF GRADUATION
MSc	Erciyes University	
Undergraduate	University of Technology	1999-2000
High school	Al JMHOREA Secondary School	1994-1995

FOREIGN LANGUAGE

English B2 level

Turkish A1 level